6-2022

Leveraging single cell technologies for the characterization and treatment of refractory pancreatic cancer

Maria Monberg

Leveraging single cell technologies for the characterization and treatment of refractory

pancreatic cancer

by

Maria E. Monberg, BS

APPROVED:

_____
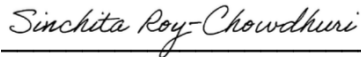
Anirban Maitra, MBBS.
Advisory Professor

_____
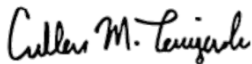
Ken Chen, Ph.D.

_____

Chad Huff, Ph.D.

_____

Sinchita Roy-Chowdhuri, M.D., Ph.D.

_____

Cullen Taniguchi, M.D., Ph.D.

Paul Scheet   Digitally signed by Paul Scheet
Date: 2022.06.20 15:53:47 -05'00'
_____

Paul Scheet, Ph.D.

APPROVED:

_____

Dean, The University of Texas
MD Anderson Cancer Center UTHealth Graduate School of Biomedical Science

Leveraging single cell technologies for the characterization and treatment of refractory

pancreatic cancer

A

Dissertation

Presented to the Faculty of

The University of Texas

MD Anderson Cancer Center UTHealth

Graduate School of Biomedical Sciences

in Partial Fulfillment

of the Requirements

for the Degree of

Doctor of Philosophy

by

Maria E. Monberg, BS

Houston, Texas

August, 2022

I had to do this for myself.

Acknowledgements

This is the beginning of an End, the journey to which has taken the efforts, kindness, care, support, and love of many incredible people in my life to make possible. In no particular order, and certainly not in one that indicates a hierarchy of importance, I will do my best to express my gratitude.

To Mom and Dad- The number of things I have to thank you both for is exhaustive, so I will limit this to the Graduate School Specific Line Items only. Houston would never have been on my map if not for you. I'd never heard of MD Anderson Cancer Center and had even less interest in Texas (both as a political entity and a region I could ever imagine myself living in). Because of you, I came to graduate school here. Because of me, you two stayed in Houston. On the days I'd worked "too late" and was "too tired", you were there with warm dinner, consolation, good advice, and big hugs. I think back to the days of the Pandemic's beginning, and I know with certainty that I would not have been able to thrive in Houston if we hadn't been here as a family. The Monbergs have always been on The Move, but I'm just glad that for a little while, we were all rooted someplace together.

To Jess- light of my life, my baby sister, my polar opposite, thank goodness for you. Every day, you help me keep my peace. Every day, you make me beam with pride while annoying the living hell out of me. Every day, I am so glad that you are patient and rational with my chaos, and always answer the phone when I call. There's no Me without You, thank you all the time.

To Lakin, Nathan, and Peter- for almost a decade, you've been the best big brothers a gal could ever hope for. From Michigan biochemistry studying sessions to Boston, from the Chicago Bordello Days to Ski Trips, and to Boston back again (and the million moments in between), you've loved, supported, and looked out for me. Thank goodness y'all have got my

back, I never would have believed in myself enough to apply for graduate school if you hadn't believed in me first.

To Michelle- for almost a decade, you've been my second sister. London's lucky to have you, and I'm jealous of that city every day for all the time it's gotten to spend with you while we're an ocean apart. You know me so well, and have ushered me through my lowest lows and happiest highs with your absolute brilliance. You've always been able to see what's best for me before I recognize it myself, be it orientation smoothies or Zola's wine or a very specific book reference or a good cry over a bad week in lab. Thank you for visiting me in Houston when I needed you, thank you for hosting me in New York when I didn't know I needed it.

To Babydog Porter, the second light of my life- you can't read, but I know mom will lovingly read this to you. The last two years of graduate school have been so very stressful, but you've made my heart so very full. Watching you grow up into the darling, delightful little doggy you are has been my favorite and sweetest "extracurricular activity". May you always have big hugs, ducks to chase, big fields to run through, and cheese cubes for snackies- it's the very least you deserve as Thanks for your role in my becoming Dr Monberg.

To Cail- for three years, we've lived together and weathered so much.. You've helped me build a lovely home and important friendships, and have been a source of so many laughs and comforts and honest conversations and good food and freshcut flowers and etc. on this wild grad school ride. Houston would be so lonely without you.

To Dylan, Edgar, Pagna, Drew, Barb, and Adam- goodness gracious am I glad to have made friends with y'all here in Texas. I would have lost my whole mind from culture shock, boredom, PhD Stress, or worse, if each of you hadn't provided such a balancing presence in my life. In some capacity- you've all celebrated with me, been there to catch my falls, encouraged me, made me laugh, welcomed me into your families, traveled with me, made space for me vent to you- God, I can't sum it all up and I hope each of you knows how thankful

I am for the impacts you've had. You've made my world so much bigger, brighter, and more fun, and this PhD would not have gotten done if not for you.

To Marta & Oscar, Vittorio & Andrea, Vahid & Dahlia- you all are wonderful. I divide my time in the Maitra Lab into 2 very distinct chapters, the pre-pandemic time without you all, and the post-pandemic time where each of you has enriched my life so much. As coworkers, you push me to do better science, help me work through challenging problems, and provide endless laughs and entertainment in the lab. You help glue my brain back together when I'm in shambles, and help me to reel in my frustrations when I've convinced myself that everything's falling apart. You've become such dear friends to me and I'll miss our dinners, nights out, beach vacations, and brunches very very much. I so look forward to these next chapters in our lives as we change and grow and move on to different things. I know you will all continue to inspire me with all the Good that you'll accomplish.

To Alex, Vince, Dan, Jaewon, and Bret- you guys took Lab Baby Maria by the hand as I crawled, then toddled, then eventually learned to walk in your footsteps. Everything foundational about the Maitra Lab, Single Cell Sequencing, Pancreatic Cancer, and how to cultivate a phenomenal lab environment, I first learned from you. I don't know how you found the patience to guide me in those early days and to impart your knowledge and skills to me, but I am deeply thankful that you did. As each of you departed from the lab and the pandemic began, I truly believe that I was only able to stay motivated in those (indeed, dark) months because of the legacies you'd left, and the motivation I had to somehow make you guys proud. Thank you for everything.

To Fredrik- in teaching me to slow down and be more thoughtful, you've helped me to design better experiments and interpret results far beyond what I would have come up with on my own. You are a friend and confidant to me in the lab, and a calm and collaborative leader for many other lab members. When I was all alone at my first AACR conference in Boston, you

took me under your wing and have helped me along ever since. It's been a joy to work with you.

To Kimal- for always lending a helping hand with my Data Problems included but not limited to patiently advising my analysis plans, advising me when I couldn't figure out how to run a script, and uploading files for paper submissions; you've made my work possible. Thanks for all of this, and for always laughing at my jokes.

To Doug Jones- thank you for being my friend. You outfitted me with the best possible computers, granted me all sorts of special IT permissions and privileges, and were always available to help me overcome any institutional tech barrier that MD Anderson threw my way. You made my life so much easier, and I was able to do my analysis work because of your help.

To Carolina Garcia Garcia- what would I do without you! We publish together, write together, think together, and laugh together. You've helped me find my voice and uplifted me in so many ways, you're a rockstar.

To Paola- I've joked that you've been my Lab Mom for these past four years, and I truly commend you for seeing me through my scientific growing pains as I've navigated graduate school. You've kept me focused, you've challenged me to be a better scientist, and you've taught me so much. I often hear people complain that they lack strong female role models in science, and because of you, and I look forward to my career knowing that I can never share those lamentations. In my first years of graduate school, I looked up to you as I tried to figure out how to speak to collaborators, ask technical experts for help, and clearly explain the goals I wanted to achieve. You've not only set an example for me, but invested innumerable hours of your time into developing me into the scientist I've become. You've had such a profound impact on the trajectory of my life and education, and words will always fall short.

To my advisory committee- from our very first committee meeting, you've given me support and encouragement, even when my ideas were barely half-baked and my data was Not Good. Instead of being nervous and dreading committee meetings, as so many graduate

students do, I instead always looked forward to ours and only wish we could have had more of them. Especially towards the end of my degree, as these meetings truly became such fun spaces for me to be able to talk out my projects with all of you. Dr Scheet, thank you for allowing me to rotate in your lab and learn how to work with genomic data so early on in my graduate schooling. Dr Huff, in my candidacy exam and "regular" advisory meetings, you always asked the best questions. Dr Roy-Chowdhuri, thank you for being a balancing presence, contributing clinical insight to my translational biology, and for being willing to help me progress in my work. Drs Chen and Taniguchi, you've been such helpful mentors and co-authors, and have created spaces for me to refine my analytic skills and apply them more appropriately to complicated biology. You've recommended me for opportunities that have entirely changed the trajectory of my life and my appreciation for each of you goes far beyond the scope of this degree.

And, finally, to Anirban- I wish every graduate student could have you as their mentor. The lengths you've gone to in order to help me are truly immeasurable. You've somehow managed to strike the perfect balance between keeping projects on track and giving me plenty of trust and room to grow ideas- a balance that has taught me so much, and empowered me to confidently and fearlessly carry out my work. When things have gone wrong, and they most certainly have, you've been there not to reprimand but to remind me that failure is part of science, I've got to express grace through gritted teeth, always be realistic and honest about my results, and move forward in the direction of a best possible outcome. From my first day in the lab, you made me feel like you'd always have my back, and I've come to learn how absolutely true that is. Leaving your laboratory environment will be one of the most difficult transitions I'll ever make, but I cannot wait to sing your praises to anyone who will listen for the rest of my career. Thank you for training me. Thank you for trusting me. Thank you for building a laboratory of people who have taught me the most amazing things. Everything I've become is because of who you are as a leader- thank you for helping me achieve my dreams.

Leveraging integrated single cell technologies for the characterization and treatment of refractory pancreatic cancer.

Maria E. Monberg, BS

Advisory Professor: Anirban Maitra, MBBS

Heterogeneity is a hallmark of cancer, and the advent of multimodal single-cell technologies has helped uncover heterogeneity in a high-throughput manner in different cancers across varied contexts at an unprecedented resolution. In an effort to improve precision medicine approaches in pancreatic ductal adenocarcinoma (PDAC), a highly lethal malignancy with a mere 11% 5-year survival rate, this dissertation focuses on first questioning the assumptions of the most basic models used to study PDAC via multimodal single-cell characterization methods at multiple levels of biological organization (scCNVseq and snATACseq for DNA assays, scRNAseq for transcriptomics, and paired protein assays such as multiplexed immunofluorescence and fluorescence in situ hybridization for validation methods) to reveal inherent heterogeneity in assumptively isogenic pancreatic cancer (PDAC) cell lines, patient-derived organoids (PDOs), and patient tissue samples that contribute to the proliferation of resistant cell phenotypes and, ultimately, treatment failures in the clinic. I then apply single-cell characterization methods to a panel of PDO samples to explore adaptive resistance mechanisms of PDAC lesions following administration of epigenetically-modifying therapeutic agents (HDAC inhibitors). I describe a novel HDACi resistance mechanism of AP1 activation, which can be intercepted by using an AP1 inhibitor in combination with an HDAC inhibitor to achieve tumor cell death. Finally, in an effort to explore and characterize the molecular consequences of newly-developed KRAS inhibitors in PDAC samples, I present a series to studies illustrating differential PDO sensitivity to KRAS inhibitors with different mechanisms of action, induce KRASi-resistance in select G12C-mutant PDO samples, and suggest avenues for future study to achieve maximal clinical benefit for PDAC patients on KRAS-inhibitory therapies.

Table of Contents

List of Figures

List of Tables

Dissertation Introduction

The #1 rule of surgery is "don't touch the pancreas". This is for good reason, as this bizarre, medium-sized (avg. 6-inches in length), temperamental organ with both endocrine and exocrine functions has a long and complicated history with human health. Pancreatic dysfunction, at its mildest, results in diseases such as Type 2 Diabetes or acute pancreatitis. Pancreatic dysfunction, at its worst, results in pancreatic ductal adenocarcinoma (PDAC), a lethal malignancy with a 5-year survival rate ranging from 5-11%, depending on whom you ask[1],[2]. PDAC represents approximately 90% of all pancreatic cancer cases, with the other ~7-10% comprised of neuroendocrine-derived tumors[3]. With no reliable, preventative, early-detection or screening methods currently available, the far majority of PDAC patients present in the clinic with locally advanced or already-metastasized disease[4], making surgical resection (via pancreaticoduodenectomy for tumors in the head of the pancreas, laparoscopic surgery for tail tumors[5]) an impossibility for many patients. While there are few effective therapeutic regimens for the treatment of PDAC, patients with various stages of disease progression have historically been stratified to one of two treatment regimens: FOLFIRINOX (or a variation thereof[6]), or Gemzar + Abraxane[7],[8]. Despite recent clinical trials and valiant efforts on the part of researchers and oncologists alike to improve treatment strategies in both the adjuvant and neoadjuvant settings, the incidence of PDAC is increasing both globally and in the United States. With 60,000+ new cases annually in the US alone (and approximately 400,000 new diagnoses globally each year[9]), PDAC is projected to be the second leading cause of cancer-associated death by 2030[4]. Given the limited state of current therapeutic options for this rapidly burgeoning patient population, there is a critical need to develop effective ways to detect, characterize, and treat this malignancy.

PDAC initiation and progression.

While this dissertation does not focus on PDAC precursor lesions, a nod to the stepwise developmental progression of this malignancy is nonetheless warranted. Broadly speaking, PDAC tumors arise from so-called precursor lesions that develop as a function of pancreatic injury, genetic predisposition, or a variety of other factors ("environmental insults", if you will). Precursor lesions include but are not limited to intraductal papillary mucinous lesions (IPMNs), pancreatic intraepithelial neoplasias (PanINs), and, rarely, mucinous cysts (MCNs)[10], and originate from either pancreatic ductal or acinar cells, which follow distinctly different modes of progression into PDAC tumors (e.g. in a study of acinar-to-ductal metaplasia [ADM], the acquisition of an activating AGR2 mutation in ductal cells led to high AGR2 expression in ductally-derived precursor lesions, whereas acinar-derived lesions exhibited low AGR2 expression)[11]. Canonically, the initiating mutation for PDAC progression from precursor lesions is KRAS[12], with over 90% of PanINs and 40-65% of IPMNs[13] harboring an activating mutation in this gene. KRAS G12D is the most common activating mutation in PDAC, with KRAS mutation rates tightly orchestrating the progression of ductal PanINs to PDAC[14] (further discussion of the role of KRAS mutations in PDAC to follow). After KRAS is mutated, the next genomic events associated with PDAC progression are deletion/inactivating mutations of TP53[15] and p16/CDKN2A[16]. After these biologically catastrophic events (TP53 deletion sophomorically described as "pulling the breaks off a car" in undergraduate cancer biology classes), a cacophony of genomic chaos breaks loose in diseased pancreata (RNF43 deletion[17], GNAS[18] inactivation, SMAD4 loss[19]) to drive metabolic reprogramming, cellular dysplasia, genomic instability and dysregulation, and the downright biological havoc of tumor formation[20] (**Figure 1**). Thus, the "dogma" of stepwise PDAC progression follows the cadence of KRAS mutation, concomitant mutations of TP53 + CDKN2A, and finally, loss/mutation of SMAD4 driving the advancement of local and metastatic disease[21],[22].

Figure 1: From Maitra & Hruban 2008, as an homage to the early work of my mentor in establishing the genetic progression model of pancreatic adenocarcinoma. The progression from histologically normal epithelium to low-grade pancreatic intraepithelial neoplasia (PanIN), to high-grade PanIN, to invasive carcinoma (left to right) is associated with the accumulation of specific genetic alterations. On the basis of their temporal appearance in this progression model, the molecular abnormalities can be classified as early (KRAS2 mutation, telomere shortening), intermediate (p16/CDKN2A loss), or late (mutations of DPC4/SMAD4, TP53, BRCA2). Ref: Maitra, A., and R. H. Hruban. 2008. 'Pancreatic cancer', Annu Rev Pathol, 3: 157-88.
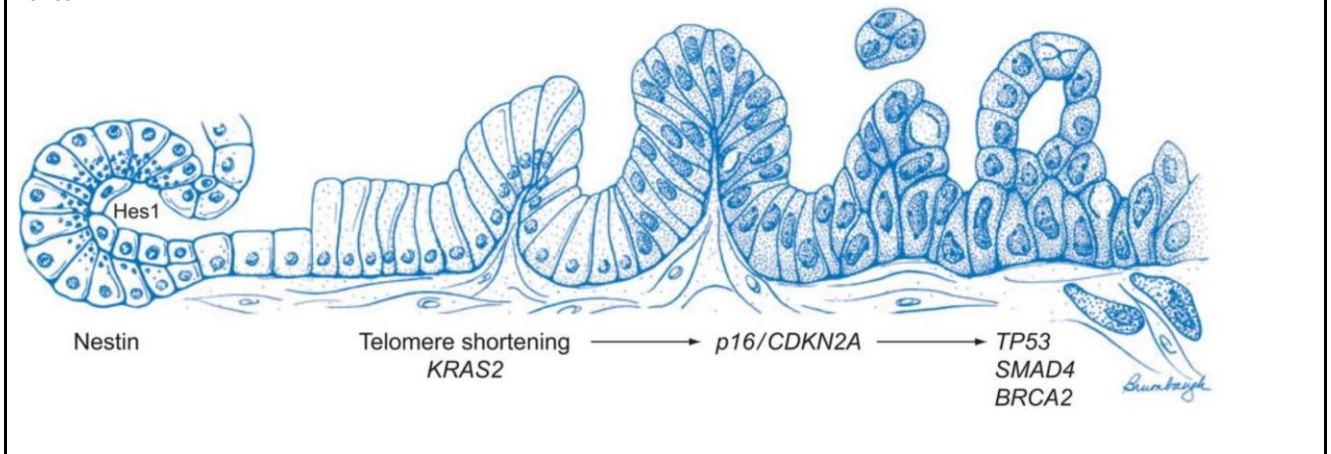
A word on the PDAC tumor microenvironment (TME).

I am not an immunologist, and have little vested interest in becoming one at this time. This bodes well for studying pancreatic cancer, as this tumor type is often described as "immune-cold"[23], with a hostile microenvironment comprised less of tired immune cells (as in other cancer types which are laden with a variety of T cells ripe for re-activation with immunotherapies[24]) and more of a dense, hypoxic[25], desmoplastic stroma built of fibroblasts and other pro-tumor cell types[26]. PDAC tumors, as they progress, actively exclude anti-tumor immune cells and recruit pro-tumor immune aggregates to the TME[27]. As such, immunotherapies, which are a very promising and efficacious therapeutic option in other malignancies, have all but failed PDAC patients[28],[29]. The most notable components of the PDAC stroma are fibroblasts, which are presumed to have their origins in pancreatic stellate cells that, via signaling from adjacently-developing tumor epithelium, differentiate into at least three fibroblast subtypes[30]. These cancer-associated fibroblast (CAF[s]) lineages have been shown to play a critical role in promoting the immune-evasiveness of tumor cells[31], and experimental depletion of CAFs has resulted in accelerated tumor progression and reduced survival in *in vivo* models[32], [33], as well as in the clinic[34]. The biology of the PDAC TME

3

is an increasingly complicated and robust research area[35], and it is widely-accepted that the TME exerts a reprogramming force so strong on PDAC lesions that it is at least partially responsible for dictating how tumors will metastasize, transform, and respond to therapy[36]. Because the PDAC TME is an exceedingly complicated research area,,for all of the projects to be discussed in this dissertation I have focused almost exclusively on the behavior and modeling of tumor epithelial cells.

Current state of genomic and transcriptional characterization of PDAC.

An extensive, decades-long effort to unravel the mutational and transcriptional features of PDAC has led to innumerable groundbreaking discoveries, ultimately establishing a growing landscape of mutations and signatures to better inform disease progression and therapeutic response. The importance of these discoveries are far broader than the scope of this dissertation, but a brief review of the state of the field is essential nonetheless. Characterization efforts of PDAC lesions have spanned from the development of rapid-autopsy programs at major cancer centers[37], to liquid biopsy platforms for early detection and disease monitoring of patients[38], to the initiation of clinical trials leveraging RNA-based PDAC subtypes[39]. The development and application of sequencing technologies have played a huge role in all of these efforts, and have fundamentally altered the working paradigm for how scientists and clinicians study and understand PDAC.

Initially, genomic and transcriptomic analysis were conducted separately, as the cost of sequencing used to be quite high and computational analysis extremely intensive. In 2015, Waddell et al.[40] performed the first whole-genome sequencing and copy-number variation (CNV) analysis of PDAC tumors. In 2017, the Cancer Genome Atlas Network published the first sequencing-based consensus study on 150 PDAC tumors, which represented the largest integrated genomics study in PDAC[41]. After a few years, scientists had developed the methods and technological capability to integrate genomic and transcriptomic data- thus ushering in a seminal 2019 study comprising 289 patient tissues, wherein whole genome and transcriptomic sequencing from both primary and metastatic PDAC lesions were characterized[42]. It truly was

not until relatively recently that the field of PDAC genomics had a foundational framework upon which clinically translational precision medicine strategies could be built.

Broadly, the seminal studies described above established that hypoxia is associated with worse prognosis in PDAC, cell cycle progression driven by acquired SNVs and contributes to metastatic disease, and that a number of currently inactionable genomic mutations arise following the progression of precursor lesions to tumors. Given the scope of this dissertation and the essentiality of this background information, the graphical abstracts of these seminal works are included in **Figure 2** to provide context for the genomic and transcriptional landscapes of PDAC.

Of critical importance for understanding PDAC biology, and concurrently discussed by both 2017 and 2019 characterization efforts, is that the mutational signatures and processes identified in primary PDAC lesions are conserved in metastases. The conservation of driver mutations in both primary and metastatic lesions has led some folks to posit that patients with both advanced and early disease may benefit from the same targeted therapies[43] (were they to exist), but this has not been proven true in either clinical or preclinical settings, as the genetic mutational landscape of PDAC remains largely inactionable. Furthermore, in the classical assumptions of cancer biology, during the "metastatic cascade" of cancer, cells in a primary tumor acquire *additional* mutations and increasing genomic instability to "prime" them for colonization of distant organ systems[44]. PDAC progression and metastasis represents a dissimilar oncogenic scenario from other solid tumor types[42], and is a contributing factor to why PDAC is inherently "harder" to treat than other solid tumors (at the present time). Pancreatic cancer cells from the primary lesion are instead epigenetically and transcriptionally remodeled[37],[45], or poised, for metastatic outgrowth, and identifying precisely which combination of epigenetic and transcriptional programs pushes primary tumor cells off their metastatic cliff remains an unresolved challenge to the field.

Figure 2: **A)** Graphical abstract from the TCGA characterization of PDAC, published 2017 under an open-access license. **B)** Graphical abstract from Connor et al., 2019, also published with open-access licensing. Refs. Cancer Genome Atlas Research Network. Network Cancer Genome Atlas Research. 2017. 'Integrated Genomic Characterization of Pancreatic Ductal Adenocarcinoma', Cancer Cell, 32: 185-203 e13. ; Connor, A. A., R. E. Denroche, G. H. Jang, M. Lemire, A. Zhang, M. Chan-Seng-Yue, G. Wilson, R. C. Grant, D. Merico, I. Lungu, J. M. S. Bartlett, D. Chadwick, S. B. Liang, J. Eagles, F. Mbabaali, J. K. Miller, P. Krzyzanowski, H. Armstrong, X. Luo, L. G. T. Jorgensen, J. M. Romero, P. Bavi, S. E. Fischer, S. Serra, S. Hafezi-Bakhtiari, D. Caglar, M. H. A. Roehrl, S. Cleary, M. A. Hollingsworth, G. M. Petersen, S. Thayer, C. H. L. Law, S. Nanji, T. Golan, A. L. Smith, A. Borgida, A. Dodd, D. Hedley, B. G. Wouters, G. M. O'Kane, J. M. Wilson, G. Zogopoulos, F. Notta, J. J. Knox, and S. Gallinger. 2019. 'Integration of Genomic and Transcriptional Features in Pancreatic Cancer Reveals Increased Cell Cycle Progression in Metastases', Cancer Cell, 35: 267-82 e7.

The transcriptional programs colloquially endowed to PDAC tumors has been a contentious research area[46], and as of 2011, at least 3 different, clinically-applied[47] RNA-based classification schemes for PDAC have been published. Referred to by the lead authors on each of these bodies of work, the classification methods are named Collisson[48], Moffitt[49], and Bailey[50]. While the subtypes of PDAC are very important and much work has been done to compare the subtype schemas, the patient outcomes between them, the superiority of one schema over another, et cetera, for all intents and purposes I have chosen to incorporate analyses and data obtained only by applications of Moffitt subtyping into this dissertation. This is for good reason, as Moffitt et al. break down PDAC tumors into 2 groups: Basal (chemoresistant with worse prognosis and a more aggressive phenotype) and Classical (better prognosis, more amenable responses to therapy). GATA6 expression is a prognostic biomarker for Classical tumors, while keratin 5 is used to identify Basal tumors. Both biomarkers are now used as stratification criteria

for patients on subtype-driven clinical trials[51]. The simplicity of this subtyping model and its bioinformatic ease-of-application have elevated the Moffitt Subtypes to my "classification of choice"- and this is *my* dissertation, after all. There will be more data and discussion of this forthcoming.

A brief note on epigenetics and histone biology.

DNA to RNA to protein is, of course, biology's central dogma. However, this mantra makes a glaring omission of the epigenetic processes and molecular scaffolds that cradle DNA and ultimately dictate which genes are transcribed and in what manner. In Chapter 2 of this dissertation, I present a series of studies focusing on an epigentically-modifying class of compounds, histone deacetylase inhibitors (HDAC inhibitors, HDACis). The biological context of HDACis might well be lost on the reader, however, unless some background is provided here. Histones are made in the cytoplasm (during cellular replication) and transported to the nucleus by histone chaperone proteins[52]. DNA, after being replicated and neatly condensed into chromatin, is meticulously coiled around nuclear arginine- and lysine-rich histone core octamers to form nucleosomes[53].

"HDACs" is an abbreviation for histone deacetylases, which are functional counterparts to histone acetylases, otherwise referred to as HATs. Both are histone-modifying protein/enzyme complexes that, through a series of amino acid removals or additions at the N-terminal tails of histone amino acids, alter the accessibility of chromatin to regulate transcription. HATs neutralize the positive charge on histone lysine residues by transferring an acetyl group onto them. This neutralization causes a "molecular loosening" of DNA-histone binding, and allows DNA binding proteins to interact with "open" chromatin regions to promote transcription of exposed genes. HDACs have the opposite function- they reverse the addition of acetyl groups to histone lysine tails (removal), yielding chromatin that is tightly coiled. HDACs function as "chromatin stabilizer" proteins and repressors of transcription[54]. In cancer especially, the ratio of chromatin that is acetylated versus deacetylated (open and active versus tightly-wound and transcriptionally

inactive) is often shifted to favor the transcription of genes important for increased tumor cell growth, proliferation, nutrient uptake, etc.[55] This is an over-simplification, as the research domain of epigenetic regulation is vast and highly complicated. However, for the purposes of my work, these are the key points to focus on.

Given the seemingly deliberate shift in histone acetylation/deacetylation by tumor cells of various cancer types, the development of HDAC inhibitors as anti-cancer therapeutics became a hotly-researched field. HDAC inhibitors achieve a similar molecular effect as HATs, in that they prevent HDACs from removing acetyl groups on histones, keeping chromatin open and available for transcriptional machinery to access. HDAC inhibitors, as both natural and manufactured compounds, are classified into five groups depending on the type of histone structure that they act on, their cell type-specific functions, their dependence on zinc cofactors, where they bind (nucleus, cytoplasm, or both), and their evolutionary homology (benchmarked as their similarity to different yeast transcriptional complexes)[56]. HDACis in the context of cancer treatment typically help modulate an anti-tumor immune response, induce cancer cell cycle arrest, are antiproliferative, and result in cell death in many, but not all, tumor types[57].

In summary, much like a spool ravelling or unraveling its thread, HDACs, HATs, and HDACis work on nucleosomes to expose or sequester regions of DNA. Tumor cells leverage these epigenetic modifiers to transcribe regions of the genome that enhance their survival and promote cell proliferation. HDAC inhibitors were developed as a way to clinically intervene with a tumor cell's ability to unravel or tighten up regions of its DNA in the interest of its own growth and survival. However, because HDACis given as anticancer mono-therapies have been unsuccessful, there is a vested interest for clinicians and researchers alike in determining the mechanisms of how tumors regulate their epigenetic machinery in the first place, and do so again in response to epigenetically-modifying drugs to achieve an enduring, resistant phenotype.

Single cell sequencing for uncovering intratumoral heterogeneity of PDAC lesions.

To complicate matters further, the dawn of single-cell sequencing methods has alerted us to the notion that all of this tumor evolution, epigenetic shape-shifting, fibroblast activation, stromal construction, and malignant progression happen *heterogeneously*: if you look closely enough, no two tumor cells are "truly" the same (intratumoral heterogeneity), no two patient tumors are identical (intertumoral heterogeneity), and therefore no two "clones" or patient tumors can reasonably be expected to respond to therapy in the same manner[58]. Intratumoral heterogeneity, in terms of different genomic profiles, epigenetic modifications, and transcriptomic states coexisting in a single tumor, is a well-documented and widely accepted principle in tumor biology[59],[60],[61],[62]. However, the development and advancement of single-cell (sc) DNA, RNA, ATAC, and multi-omic protocols (with accompanying advancement in bioinformatic tools to make sense of this wealth of data) has helped to uncover an unprecedented level of detail in PDAC tumor biology. As an example of this insight, let's revisit the Moffitt transcriptional subtypes of PDAC. Through traditional bulk RNA sequencing approaches, RNA sequencing data from either a patient tumor or blood sample leads to the classification of a lesion as either Basal or Classical, and a patient's treatment is planned accordingly. In recent years, as a function of scRNAseq approaches, we now understand that individual tumors exhibit *subtype admixture*, where some regions have classical-like features, while other tumor areas in the same lesion are definitively more basal-like[63]. In this scenario, while the "overall tumor" might appear Classical-like via bulk RNA sequencing, there would be underlying regions of more aggressive Basal tumor cells that bulk RNAseq would "overlook". This patient might be placed on a treatment regimen appropriate for a Classical tumor subtype, and soon progress on therapy due to the proliferation of the more-aggressive Basal-like cells operating in the absence of resource competition from their now-deceased Classical cousins. There are myriad examples in the literature now of the incredible methods (both bioinformatic and bench-based) that have been developed in this new age of

single-cell science. In this dissertation, different single cell technologies will be applied to address fundamental questions of pancreatic cancer biology. It is my hope that the work presented here will not only showcase the power of multi-modal analytics, but also demonstrate the importance of applying *appropriate* tools to deconvolute cancer biology to impact our understanding of this wretched   malignancy.

Chapter 1: Occult polyclonality of preclinical pancreatic cancer models drives in vitro evolution.

Authors: Maria E. Monberg[1,2,3,*], Heather Geiger[4*], Jaewon J. Lee[1,3], Roshan Sharma[4], Alexander Semaan[1,3,] Vincent Bernard[1,3], Justin Wong[5], Fang Wang[6], Shaoheng Liang[6], Daniel B. Swartzlander[1,3], Bret M. Stephens[1,3], Matthew HG Katz[7], Ken Chen[6], Nicolas Robine[4†], Paola A. Guerrero[1,3], Anirban Maitra[1,3,†]

Affiliations:

1. Department of Translational Molecular Pathology, The University of Texas MD Anderson Cancer Center, Houston, TX, USA
2. University of Texas MD Anderson Cancer Center Graduate School of Biomedical Sciences, Houston, TX, USA
3. Sheikh Ahmed Center for Pancreatic Cancer Research, The University of Texas MD Anderson Cancer Center, Houston, TX, USA
4. New York Genome Center, New York, NY, USA
5. Department of Epidemiology, The University of Texas MD Anderson Cancer Center, Houston, Texas, USA
6. Department of Bioinformatics and Computational Biology, The University of Texas MD Anderson Cancer Center, Houston, TX, USA
7. Department of Surgical Oncology, The University of Texas MD Anderson Cancer Center, Houston, TX, USA

Chapter 1 Introduction

Pancreatic Ductal Adenocarcinoma (PDAC) is a highly lethal malignancy, projected to be the second-leading cause of cancer-related death in the United States by 2030[64,65]. With a dismal 5-year survival rate of 10%[66] and few clinically meaningful therapeutic advances in recent years, the need for clinical and research advances is urgent. Preclinical models of PDAC represent essential prerequisites for advancing cancer research and experimental therapeutics in this lethal disease. The most commonly used and widely published preclinical models of PDAC that have been, and continue to be, leveraged in research laboratories globally are adherent cell lines distributed by the American Type Culture Collection (ATCC). For example, a perusal of current Google Scholar metrics demonstrates ~35,000 publications for PANC-1 and ~20,000 publications for MiaPaCa2, two prototypal ATCC cell lines nearly ubiquitous in every PDAC cancer research laboratory's incubator. Included in many of these publications, and typically used as contemporaneous "control" cells in experiments, are two immortalized, non-transformed human pancreas-derived cell lines – so-called Human Pancreatic Ductal Epithelial (HPDE) and Human Pancreatic Nestin-expressing (HPNE) cells. While the reach of these preclinical models in furthering our knowledge of PDAC biology is extensive [2-67], several inherent assumptions have been made regarding the stability of the genomic and transcriptomic clonal architectures of these cells over time, including the fidelity to "normal" parameters for HPDE and HPNE during *ex vivo* passage.

The justifiably increased focus on rigor and reproducibility in scientific research studies has meant more stringent requirements for authentication of cell line resources, but the microsatellite assays typically used for confirmation of cell identity provide minimal insights into genomic and transcriptomic variabilities that might arise when the apparently identical line is propagated at different laboratories[68] or in disparate culture conditions, such as two-dimensional (2D) *versus* three-dimensional (3D) growth. A recent seminal publication by Ben-David et al[69] identified widespread genomic and transcriptomic variabilities in single cell clones isolated and expanded from the same parental cancer cells, which further translated into differences in drug

12

responsiveness *in vitro*, suggesting a staggering level of pre-existing intra-culture heterogeneity within cancer cell lines. Although PDAC cells from surgical resections were not included in this analysis, it underscores the need for an in-depth benchmarking study using commonly used cancer and non-transformed "control" cells, in order to fully glean the extent of intra- and inter-culture heterogeneity that exists in these preclinical model systems.

In addition to the use of adherent cell lines, efforts at better recapitulating the biology of *in vivo* disease have led to the burgeoning adoption of patient-derived organoid (PDO) models as an *ex vivo* platform in the PDAC field. Encouragingly, early passages of PDAC PDOs maintain genomic and transcriptomic features of the tumor of origin, and harbor a gene signature of response to commonly used cytotoxic agents, enabling therapeutic prediction [70-71]. Nonetheless, whether the clonal architecture of PDOs remains stable over more prolonged *ex vivo* propagation, considering both the time in culture and the lack of extrinsic cues from the tumor microenvironment *in vivo*, remains less studied.

Here we present an in-depth single cell genomic and transcriptomic assessment of clonal heterogeneity in a panel of established and globally utilized PDAC cell lines (Panc-1, MiaPaCa2, HPAF-II and BxPC-3), immortalized "control" cells (HPNE and HPDE), and in an independent PDO which is compared to its earlier passage prior to prolonged *ex vivo* propagation. We demonstrate that pancreatic cell lines - neoplastic and non-neoplastic - are composed of remarkable sub-clonal heterogeneity at single cell resolution, which is unlikely to be detectable by conventional "bulk" profiling, and has not been previously reported on, despite extensive "traditional phenotypic" characterization of these lines [11,72-73]. Unexpectedly, HPDE cells harbor substantial genomic alterations and a transcriptome that essentially resembles cancer cells, questioning their use as a "control" line in research studies. We further demonstrate marked transcriptomic differences (including expression-based subtype classification) in microsatellite authenticated MiaPaca2 cells obtained from three independent sources. Another notable finding of our study is the observation of marked transcriptomic and epigenetic divergence (incorporating the appearance of distinct therapeutically actionable pathways) when adherent (2D) parental

13

Panc1 cells are grown in 3D cultures. Finally, we describe the significant genomic and transcriptomic divergence of a later-passage PDO from an earlier passage, reiterating the importance of limiting the window for *ex vivo* therapeutic prediction and other biological experiments in this model type. Overall, our findings provide data-driven benchmarks for the limitations of the most commonly utilized preclinical models and platforms in PDAC research, with implications for the rigor and reproducibility of data generated in the *in vitro* setting.

Materials and Methods included in Chapter 1

Cell line selection and 2D culture

For non-neoplastic cell lines, HPDE and hTERT-HPNE were used, given their prevalence as "normal controls" in literature (over 800 citations for each line in PubMed). hTERT-HPNE (ATCC Cat. CRL-4023, passage no. 1) was plated in Complete Growth Medium, consisting of 75% DMEM without glucose (Sigma D-5030) with an additional 2mM L-glutamine and 1.5 g/L sodium bicarbonate, 25% Medium M3 Base (Incell Corp. M300F-500), 5% fetal bovine serum (ThermoFisher Scientific Cat. 10082147), 10 ng/mL human recombinant EGF, 5.5 mM D-glucose (1g/L) and 750 ng/mL puromycin. HPDE (Kerafast Cat. ECA001-FP, passage no. 4) cells were cultured using Keratinocyte Basal Medium with supplied supplements (Lonza, Clonetics KBM, Cat. CC-3111). For PDAC-derived cell lines, we wanted to ensure that lines selected were both widely-used in the field, and be representative of a range of characteristics in terms of differentiation and epithelial versus mesenchymal origin. MP2-A cell line was purchased from the American Type Culture Collection (ATCC Cat. CRL-1420). MP2-B was obtained from a collaborating lab and plated upon arrival (passage no. 2). MP2-C was thawed and plated from an in-house stock vial (passage no. 3). All MiaPaCa-2 cells were cultured using DMEM (ATCC Cat. 30-2002) supplemented with 10% fetal bovine serum for up to 2 expansions. BXPC3 (ATCC Cat. CRL-1687, passage no. 1) and HPAF-II (ATCC Cat. CRL-1997, passage no. 1) cell lines are commercially available, and cultured using RPMI 1640 (Gibco) supplemented with 2mM glutamine, 10% fetal bovine serum (ThermoFisher Scientific Cat. 10082147). Panc-1 cell line

(ATCC Cat. CRL-1469, passage no. 3) for 2D studies was cultured in DMEM with 2mM glutamine and 10% fetal bovine serum (ThermoFisher Scientific Cat. 10082147). Cell lines were harvested for single-cell dissociation and sequencing at 80-90% confluency. A volume of 3mL of media from each cell line was harvested and sent to the MD Anderson core facilities for mycoplasma testing. All cell lines were washed with PBS and incubated with 0.25% Trypsin for 3-5 minutes. For all lines except HPDE, trypsin was neutralized using each respective cell line's media; in HPDE, trypsin was neutralized using a Trypsin Inhibitor (Invitrogen Cat. 17075-029). Cell lines were centrifuged for 5 minutes at 1200rpm, resuspended in cold PBS + 0.04% BSA (Roche Ref. 03116956001), filtered using Flowmi 40uM pipette filter tips (Sigma BAH136800040), and counted to ensure debris-free single cell suspensions. A portion of cells were sent to the MD Anderson core facility for molecular fingerprinting, and all cell lines were counted using a Countess II automated cell counter. 2,000 cells were loaded per lane into the 10x Chromium Platform for scCNV sequencing, and 10,000 cells per lane were loaded for scRNA sequencing.

Panc-1 3D spheroid culture

For 3D spheroid growth, Panc1 cells from the same passage as the cultured 2D cells were thawed, washed with PBS, suspended in growth-factor reduced Matrigel (Corning #356231), and plated in 80uL spheres on 24-well Nunclon Delta surface plates (TMO140620). Spheroids were incubated for 10 minutes at 37℃ to allow the matrigel to harden, and 650uL of DMEM + 2mM glutamine and 10% fetal bovine serum were added. For spheroid dissociation in single-cells, media was removed, and spheroids were manually dissociated in 500uL of TryplE Express (Gibco Cat. 12604013). DMEM media was then added, and spheroids were centrifuged at 1500rpm for 5 minutes. To dilute the matrigel and obtain single-cells, cells were resuspended in 5mL PBS, filtered twice with 70uM cell strainers (Corning CLS 431751), resuspended once more in cold PBS + 0.04% BSA, filtered again using Flowmi 40uM pipette filter tips, counted, and loaded at 10,000 cells per lane into the 10x Chromium Platform for scRNA sequencing.

Sample acquisition for organoid generation

A patient was recruited at the University of Texas MD Anderson Cancer Center through informed written consent following institutional review board approval (Lab00-396 and PA15-0014). The study was conducted in accordance with Good Clinical Practices concerning medical research in humans per the Declaration of Helsinki. An EUS-FNA biopsy procedure was conducted and confirmation of pancreatic ductal adenocarcinoma present in biopsy-obtained tissue specimens was provided by a pathologist. The tissue specimens were subsequently delivered to the research laboratory setting, where they were processed for organoid generation.

Organoid generation

Dissociated cells were resuspended in PaTOM media[74] and centrifuged at 1500rpm for 5 minutes. Cell pellet was gently resuspended in Matrigel Growth Factor Reduced (Corning) and plated as a dome in a Nunclon Delta Surface 24-well plate (Thermo Fisher). Cells embedded in matrigel were incubated at 37C for 15 minutes and covered with PaTOM media supplemented with Y-27632 dihydrochloride (Tocris). Organoids were expanded and grown up to passage 4 (PDO early), at which point there were a sufficient number of cells in culture to be processed for single cell sequencing while also maintaining a stock in culture for further growth. After an additional 10 passages, PDO cells were harvested for single cell sequencing to be compared as "PDO late" in this study.

Library construction for whole exome sequencing (WES) of HPDE and HPNE cell lines

DNA was prepared as described previously[75], including fragmentation with a Covaris LE 220 ultrasonicators system (Covaris) and library construction with the SureSelect XT HT–targeted enrichment protocol (Version A1, July 2017). Libraries were subsequently hybridized to a whole-exome capture library (SureSelect AllExonV7; Agilent, C/N: 5991-9039) and sequenced on a NextSeq500 (Illumina) using 300-cycle kits, paired-end.

Whole exome sequencing and segmentation analysis

Bcl2Fastq (2.20.0, Illumina) was used to convert raw Illumina data (bcls) into fastqs. Fastqs were then trimmed with SureCallTrimmer (v4.0.1, AGeNT v2.0, Agilent), aligned to hg19 with BWA (Burrows-Wheeler Aligner, 0.7.15-r1140, Li 2020, and barcodes were collapsed with LocatIt (v4.0.1, AGeNT v2.0, Agilent) to family size of 1. Resulting bam files were then processed by GATK (v4.1.2.0) according to best practices[76], including base quality recalibration (BQSR). Segmentation analysis was performed as described by GATK best practices[76]. Briefly, we use the PBMC data, sequenced with the same platform and library to create a CNV panel of normals (PoN) to establish a baseline. We then collected read counts for HPDE/HPNE on padded (100bp) targeted regions, and then standardized and denoised using the PoN. Read counts were then standardized and denoised before making segmentation calls.

Single-cell RNA and CNV library construction and sequencing

All cell lines were processed using 10x Genomics platforms: Single Cell 3' Reagent Kits v2 for scRNA and the Chromium Single Cell DNA Reagent Kit for scCNV. All libraries were assessed for quality on Agilent TapeStation 2200 and quantified using both Agilent TapeStation 2200 reagents and Qubit dsDNA HS Reagent kits (Invitrogen Cat. Q33231) before loading onto NextSeq500 (Illumina). Multiplexed scRNA libraries were sequenced using 150-cycle kits, paired-end, Read 1 26 cycles, Read 2 98 cycles, i7 index 8 cycles, i5 index 0 cycles. Multiplexed scCNV libraries were sequenced using 300-cycle kits, paired-end, Read 1 150 cycles, Read 2 150 cycles, i7 index 8 cycles, i5 index 0 cycles. Cell Ranger version 2.0 was used to convert Illumina base calls (bcls) to FASTQ files. FASTQ files for scCNV data and scRNA were aligned to the reference genome GrCh38 using files provided by 10x Genomics. Cell Ranger DNA Software v1.1 was used for subsequent downstream analysis of each cell line's aligned data.

Single-nuclei ATAC library construction and sequencing

17

Of the Panc1 monolayer and spheroid cultures, a subset of whole cells was isolated from the pools processed for scRNA + CNV sequencing. Using the nuclei isolation protocol and methods proscribed by 10x Genomics (Demonstrated Protocol CG000169, Rev D), we were able to load 5,000 nuclei per well for Panc1-3D and 7,000 nuclei per well for Panc1-2D for processing using the 10x Genomics Single Cell Atac Kit, v1. As with the previously described scRNA and scCNV libraries, all quantification and quality control was conducted on an Agilent 2200 TapeStation using D1000 High Sensitivity reagents, with additional quantification using Qubit dsDNA HS Reagent kits. A pooled library containing both Panc1-2D and Panc1-3D snATAC libraries was loaded on the NextSeq500 using 150-cycle kits, paired-end, dual-index mode, Read 1 50 cycles, Read 2 50 cycles, i5 index 16 cycles, i7 index 8 cycles. Cell Ranger version 3.1.0 and cellranger-atac version 1.2.0 were used to convert Illumina bcls to fastq files and align samples to reference genome GrCh38.

scCNV clonal analysis

Using bedtools to intersect coordinates, and book-ended 5.12Mb intervals along each chromosome of chr1-22 and chrX, chromosomal locations and copy number values as provided by 10x Genomics software in node_cnv_calls.bed were mapped to evenly sized intervals along each chromosome. Next, a weighted average based on the size of the overlap of each interval in node_cnv_calls.bed was used to obtain a mean copy number value per cell, per 5.12Mb interval. Finally, cells listed as noisy or with a haploid genome (mean ploidy < 1.5) were excluded from the visualization. A literature search was conducted to identify commonly amplified/deleted genes in PDAC, and the output of that search was combined with a Maitra Lab in-house panel of commonly mutated genes in pancreas cancers. Using Ensembl v84 for gene locations and bedtools to intersect coordinates, chromosomal locations and copy number values as provided by 10x Genomics software in node_cnv_calls.bed were mapped to gene-specific loci. Cells listed as noisy or with a haploid genome (mean ploidy < 1.5) were excluded, and then a random 1000 cells per cell line were chosen using the "sample" function in R.

scRNA Seurat analysis of cell lines

Seurat (v3.1)[77] merged analysis was used to profile the scRNA cell line data. For removal of mitochondrial genes in cell lines, we subsetted all cells with less than 20% mitochondrial gene expression. Log normalization, variable feature identification (FindVariableFeatures), z-scoring (ScaleData) were applied to the merged object of all cell lines, and principal component analysis (RunPCA, npcs = 30) and subsequent dimension reduction (UMAP) were applied. Seurat's FindMarkers command was used to identify cell lines that were representative of mesenchymal, epithelial, or neither phenotypes based on surface expression marker gene sets, as previously published by our laboratory[78].

For confirmation of AURKA and BRCA expression in HPDE and HPNE cell lines, scRNAseq data for these samples were combined into a single seurat object, scaled and normalized as previously described, and seurat's FindMarkers command was used to measure expression of each gene.

Gene Set Enrichment Analysis (GSEA) for MiaPaca2 clusters

To obtain significantly enriched pathways on a per-cluster basis from MP2 cell lines, marker genes were extracted using FindMarkers function in Seurat, on a per-sample basis (ex: FindMarkers, ident.1 = "MP2.A", ident.2 = c("MP2.C", "MP2.B"). Resulting genes were ranked by -log10(FDR) multiplied by fold-change directions, and the output file was formatted according to requirements for downstream input to GSEA. This yielded an output wherein upregulated genes had positive values and downregulated genes had negative values. Pre-ranked GSEA was thus performed using fgsea R package v1.12.0[79] specifying 10,000 permutations, and fgsea output was filtered based on FDR and adjusted p-values for each pathway.

Copy number inference of MiaPaca2 cell lines from scRNA-seq

Copy number alterations from scRNA-seq were inferred using inferCNV R package v1.0.4 (https://github.com/broadinstitute/inferCNV). Raw gene counts from filtered cells were used, and cutoff was set to 0.1. HPNE cells were used as reference.

Gene Set Enrichment Analysis (GSEA) for Panc1 sample-specific clusters

To obtain significantly enriched pathways for clusters specific to either Panc1-2D or Panc1-3D, marker genes were extracted on a per-cluster basis using FindMarkers function in Seurat from a merged Panc1-2D + Panc1-3D object (ex: panc3_c2.markers <- FindMarkers(object = panc1, ident.1 = 2, ident.2 = c(0,1,3,4,5,6))). Resulting genes were ranked by -log10(FDR) multiplied by fold-change directions. This yielded an output wherein upregulated genes had positive values and downregulated genes had negative values. Pre-ranked GSEA was thus performed using fgsea R package v1.12.0 specifying 10,000 permutations, and fgsea output was filtered based on FDR and adjusted p-values for each pathway, as previously described for MiaPaca2 GSEA analysis.

snATAC analysis of Panc1 for motif activity, coverage plotting, and integration with matched scRNA

Using Seurat v3 and its extension package Signac version 1.0.0 (https://github.com/timoast/signac), along with additional R packages for gene annotation (EnsDb.Hsapiens.v86) and the JASPAR 2020 Motif Database (JASPAR2020), 10x genomic output files (metadata, fragments file, fragments index, filtered peak matrices) to generate Seurat objects containing motif information, gene annotations, and genomic ranges. Quality control on nuclei was done by quantifying nucleosome signal, TSS enrichment, number of peaks in fragmentation regions, and nucleosome signal according to Signac software recommendations (TSS Enrichment > 2, nucleosome signal < f10, blacklist ratio < 0.05, percent reads in peaks > 15, peak region fragments between 1,000 and 20,000). Samples were normalized using term frequency-inverse document frequency (TF-IDF) normalization, top features were identified, and

dimensional reduction using singular value decomposition (SVD) on the TF-IDF matrix using peaks as features was done on both individual samples and a merged analysis object that had been created using fragmentation and peak data to identify common features to use as merging anchors. Motif activities were subsequently calculated using chromVar, as adapted for Signac. We then identified motifs that were enriched in each subcluster per sample, as well as differentially enriched between the two samples (merged analysis). To correlate regions of chromatin activity with scRNA data, per-sample snATAC-Seurat objects containing gene activity data were scaled, normalized, processed with latent semantic indexing (LSI), and UMAP dimensional reduction. We use all peaks that have at least 100 reads across all cells, and reduced dimensionality to 50, as recommended by Seurat guidelines. The processed snATAC dataset was then merged with the previously-described processing of scRNA data for Panc1 samples, with merging based on common anchors identified between the datasets, using scRNA data as a reference (FindTransferAnchors), to ensure commonalities and cluster structure between the datasets. Next, gene lists were curated using the GeneCards Human Gene Database- genes specifically activated by each enriched motif were queried and plotted using scRNA data (DotPlot).

Cladogram analysis of cell lines

We sought to quantitatively assess the transcriptional similarity among the cell lines and establish if the families of origin for the cell lines are preserved. We use graph based methods called diffusion maps to compute the distances between the cell lines. In particular, we first map the cells from high dimensional transcriptomic space to a low dimensional rescaled diffusion space[80], where phenotype distance between cells are more faithfully represented and compute distances between the cells in this new space.

Briefly, diffusion maps[81] is a family of techniques to reduce the dimensionality of any high-dimensional data and have gained a lot of application in the analysis of single-cell data[82],[83],[84]. Essentially, they transform data from high dimensional gene expression space to a space of

much lower dimensions, where usual Euclidean distance is reflective of the cellular phenotypic distance. Computing distances in diffusion space requires choosing the optimal number of diffusion coordinates. However, it has been proposed that rescaling the diffusion coordinates by their eigenvalues can circumvent this issue[80].

For this, we combined all the samples and the resulting data was then reduced in dimensionality first using PCA. Diffusion Maps was then computed on the resulting PCA for which we first constructed a k-nearest neighbor (k = 30) graph using Euclidean distance and converted the resulting distance matrix into an affinity matrix using an adaptive Gaussian kernel (Setty 2019, van Dijk 2018). The resulting affinity matrix was row normalized (each row sum to 1) to obtain a Markov matrix, whose eigenvectors represent the diffusion coordinates. These coordinates were rescaled using the associated eigenvalues as described in (Setty 2019). Finally, we computed the Euclidean distance between every pair of cells between any two samples in the rescaled diffusion space. Thus, we defined the phenotypic distance between the two samples as the average distance between all pairs of cells as computed above. The resulting distance between samples was represented as a cladogram using the dendrogram function on linkage function in the scipy.cluster.hierarchy package in Python with parameter method = "average". This was also represented as a heatmap using the clustermap function in seaborn package in Python.

Phenotype map of existing gene sets

We sought to understand the intra-sample heterogeneity of MiaPaCa2 samples by doing subtype analysis. We utilized gene sets from Moffitt et al. (cited in introduction) and used the expression of the genes to assign every cell to one of the subtypes. We constructed a simple assignment scheme to achieve this. We began by computing the average subtype expression for each single cell, i.e. average over the genes that define the subtype. We then reasoned that a single cell can be labeled as belonging to the subtype with the highest average expression.

scCNV processing for scRNA clonal expression correlates

CNV calls per segment, per cell (from "node_cnv_calls.bed") were intersected with mappable regions (as defined in "mappable_regions.bed") using bedtools (v2.29.2). Next, the copy number for each mappable region for each cell was defined as the integer copy number with the most total bases covering the region. Finally, only regions of at least 2Mb on autosomes (chr1-22) were retained for downstream analysis. Cells defined as noisy in the QC summary file ("per_cell_summary_metrics.csv") were removed prior to downstream analysis as well.

This data was converted to a cell x region matrix, with all integer values. Next, for each chromosome and chromosome arm, mean copy number was calculated by weighting based on the total length at each integer copy number, across all mappable regions. Ploidy was defined based on the median of these values across all whole chromosomes. Cells with ploidy more than one standard deviation from the mean across cells were removed.

Next, visual assessment of the chromosome arm mean copy number values per cell was used to determine which regions warranted further examination. Per sample, the chromosome arms that showed variation in a large percentage of cells were: MP2-B – chr7p, chr10p, chr10q, chr12q; MP2-C - chr5p, chr5q, chr10p, chr10q, chr14q; Panc1-2D – chr14q, chr15q. Next, all mappable regions in these chromosome arms were plotted for further visual assessment. In Panc1-2D, chr15q mappable regions starting at coordinates <40Mb or >80Mb, which showed a different profile from the other mappable regions, were also excluded. In MP2-B, only mappable regions from 93.5-126.3Mb on chr12q were considered, as the remaining regions had consistent copy number across cells. As all examined cell lines appeared to be triploid overall, deletion defined as mean copy number < 2.75, while amplification defined as mean copy number >= 3.75. Next, clones were defined as described in the main text. The end result of the scCNV workflow for each sample was a segment x clone matrix, where the segments were the mappable region coordinates and the values were integer copy number values.

scCNV-scRNA integration

23

The mappable region coordinates were intersected with the gene coordinates (from Ensembl v84, same as in the CellRanger reference) to produce a gene x clone matrix. This matrix was used as input to clonealign (v2.0), which was used to assign cells in the RNA to each clone. Default parameters (including min total nUMI per gene of 20 and min total nUMI per cell for all copy-variant genes of 100) were used to filter genes and cells before running clonealign. Next, clonealign was also run with default parameters, except for the minimum probability required to call a cell as assigned to each clone. This parameter was set to 90% for MP2-B and Panc1-2D. For MP2-C this was lowered to 50%, due to very low numbers of cells with high confidence clone calls found in this sample.

Seurat (v3.1) was used for dimension reduction (UMAP). For this analysis, all annotated genes expressed in at least 10 cells were included. Next, only cells assigned to a clone with confidence above the threshold were included for downstream analysis. Finally, standard analysis was performed including SCTransform for normalization and variable gene selection, followed by principal component calculation on the variable genes (RunPCA). The first 30 PCs were used for input into UMAP (RunUMAP) for the MiaPaca2 samples, while the first 50 were used for Panc1.

Seurat's FindMarkers command was used for differential expression between clones. For MP2-C, clones 1 and 3 were combined into one group to create a pairwise comparison versus clone2. This was because cells called as either of these clones showed very similar expression. All default parameters were used except for reducing the log-fold-change threshold to 0.10 from 0.25.

GSEA of clonealign-defined scRNA clones

Pre-ranked GSEA was thus performed via the GSEA software version GSEA_4.0.3. Molecular Signature Databases h.all.v7.1.symbols_1.gmt (hallmark pathways) and c6.all.v7.2.symbols.gmt (oncogenic signature gene sets) were both used to align gene lists extracted from clonealign-defined-scRNA clones in Seurat (see figures 2G, 2J, Supp. 6C, Supp.

24

6D), as described above using FindMarkers. A false discovery rate (FDR) cutoff of 25% was used to analyze the GSEA results for significant pathway enrichment per sample. Manual curation of genes lists from significantly-enriched per-clone pathways was conducted to identify individual genes relevant to pancreatic cancer biology (ie KRT13, LGALS1).

Dimensionality reduction and cell clustering of PDO Pair

Initial single-cell analysis was performed using Seurat v3.1.0 (1). Cells containing less than 200 genes were removed, and log-normalized expression of 2,000 variable genes were used to reduce the data into two-dimensional space. Cells from PDO1 early and PDO1 late samples were combined using FindIntegrationAnchors and IntegrateData functions. To retain the highest number of cells for subsequent analyses, no additional filters were initially applied. Cells with higher expression of mitochondrially encoded genes were filtered out *post hoc* based on the results of the clustering.

Cell state trajectory analysis of PDO Pair

Trajectory inference was performed using Monocle v2.13.0 (2). Analysis was done using raw counts obtained from Seurat objects with preserved cellular metadata. Top 1,000 variable genes were used to reduce the data and order the cells. Pseudotime heatmap was created using genes with dynamic expression changes obtained using differentialGeneTest function specifying fullModelFormulaStr = "~sm.ns(Pseudotime)" and q-value cutoff of 1×10^{-40}. Branched pseudotime heatmap was created using BEAM function and q-value cutoff of 1×10^{-5}. Genes were clustered based on pattern of expression changes and extracted from Monocle object for subsequent analysis.

Chapter 1 Results

Single cell analysis identifies clonal heterogeneity of pancreatic cancer and non-transformed cells.

We cultured six pancreatic cell lines, including three MiaPaca2 lines from independent sources and a pair of Panc1 lines subjected to differing growth conditions, for a total of nine samples analyzed with single-cell transcriptomic profiling (scRNAseq, 10x Genomics) and seven samples also analyzed with genomic copy number variant detection (scCNVseq, 10x Genomics). All samples were submitted for fingerprinting via MD Anderson Core Facilities prior to sequencing to confirm cell line identity. Visualization of the combined scRNA-seq data (77,068 cells) with UMAP[85] (**Figure 3A**) revealed substantial heterogeneity across the cell lines, including only partial overlap in apparently identical cells obtained from distinct sources or cultured under different conditions (*see later*). We first validated that cell lines of published epithelial or mesenchymal differentiation state maintained key marker identities [86] (**Figure 3B**). For example, we observed high expression of the epithelial transcripts *EPCAM* and *KRT8* in the previously described "epithelial" lines, HPAF-II and BxPC3, and conversely, the prototypal mesenchymal transcript *vimentin* (*VIM*) was essentially restricted to the previously described "mesenchymal" lines Panc1 and MiaPaca2. HPNE cells, which were originally derived from a *nestin* (*NES*) and *NOTCH2* expressing pancreatic progenitor cellular population [87], were confirmed to retain both markers **(Figure 3B)**. Notably, HPNE cells, along with Panc1 and MiaPaca2, also demonstrated extensive *CD44* expression, underscoring the enrichment of putative stem-like cells in culture. We observed that cell lines that had undergone differing culture conditions (Panc1 2D, Panc1 3D) or were from distinct laboratories of origin (MiaPaca2-A, B, and C) were still more transcriptionally similar to each other than to the other cell lines (**Figure 3A**).
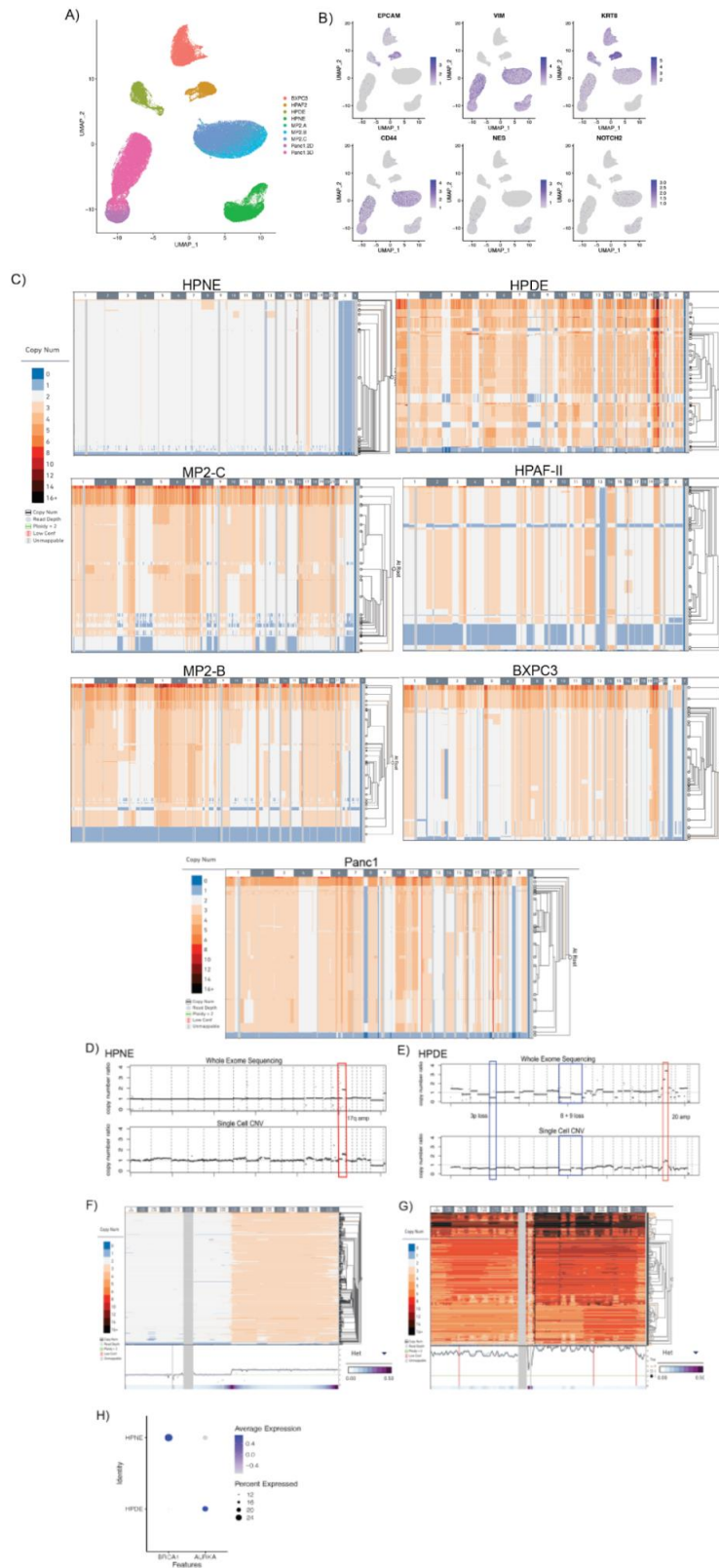
Figure 3: PDAC Cell Lines display heterogeneity at single-cell level

A) Uniform manifold approximation projection (UMAP) plot of single cells from PDAC cell lines used in this study.

B) UMAP Feature Plotting for known cell-type markers (EPCAM, MUC1 for epithelial; vimentin, and KRT8 for mesenchymal cellular origin).

C) Representative scCNV plots for cell lines. Columns indicate chromosomes (numbers labeled in gray and white), rows indicate individual cells organized into clonal clades. Phylogeny determined using 10x Genomics scCNV analysis software.

D) scCNV comparison to WES of HPNE cell line depicting amplified 17q as the only notable CNV event.

E) scCNV comparison to WES of HPDE cell line. CNV events representing losses of chromosomal arms 3p, 8p, and 9p and amplifications at chromosome 20.

F) scCNV high-resolution cell phylogeny of HPNE for all chromosome 17 locations showing ploidy = 3 for all cells at 17q arm, region inclusive of BRCA1 loci. Columns indicate chromosomal intervals measured in Mb, rows indicate individual cells. Chromosomal regions depicted (labeled along top x-axis) are representative of CNV segments outlined in red in Figure 1D.

G) scCNV high-resolution cell phylogeny of HPDE for all chromosome 20 locations showing ploidy >3 (as high as 13 in some cells at some locations) for all cells. Columns indicate chromosomal intervals measured in Mb, rows indicate individual cells. Chromosomal regions depicted (labeled along top x-axis) are representative of CNV segments outlined in red in Figure 1E. Corresponding scRNA data shows elevated expression of AURKA, located within amplified HPDE region as a potential target of amplification.

H) scRNAseq data of HPNE and HPDE cell lines shows elevated expression of BRCA1 in >20% of HPNE cells, increased AUKRA expression in >20% of HPDE cells.

27

To quantify transcriptional similarity, we computed phenotypic distance, defined as the distance between the samples in the diffusion space (*see Methods*). Upon projecting the distances onto a cladogram, we observed that all three culture variations of MiaPaCa2 cell lines fall into a common clade (MP2-A, MP2-B, MP2-C), while Panc1 cells, irrespective of growth as monolayer or in 3D, branch into their own clade (**Figure 4**). To ensure rigor and reproducibility in our work, and to assure the reliability of our analysis when yet simpler algorithms are applied, we confirmed our findings by running a Pearson correlation analysis (data not shown) [88]. In doing so, we report that the overarching structure of how cell line clades are organized remains highly similar to what was determined by diffusion mapping.
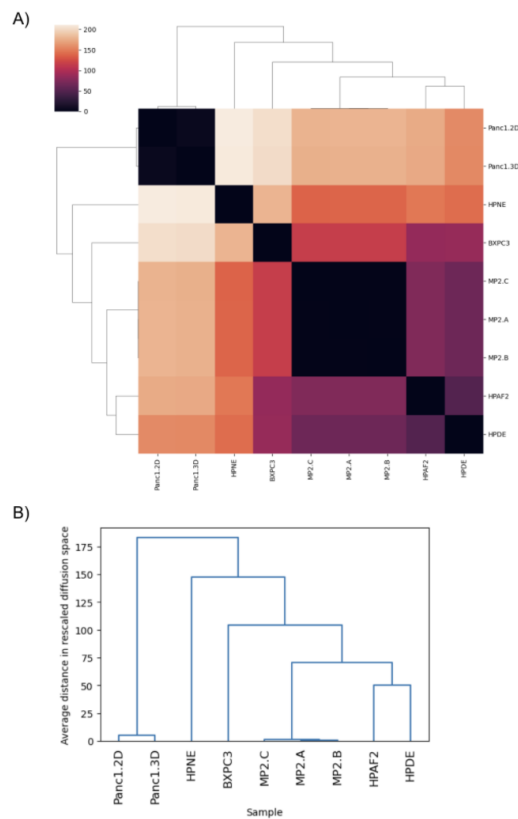
Figure 4: Phenotypic distances calculated in scRNAseq data measure biological relatedness.
A) Phenotype mapping and cladogram analyses of cell lines depicting evolutionary relatedness between them as a function of relative diffusion space (indicated by heatmap legend).

B) Phenotypic Cladogram of cell line scRNAseq data. The x-axis indicates the sample names and y-axis indicates the phenotypic distances.

C) Segmentation plotting derived from normalized copy number ratios of scCNV clones from each cell line. Columns indicate chromosomes, rows indicate ploidy ratio.
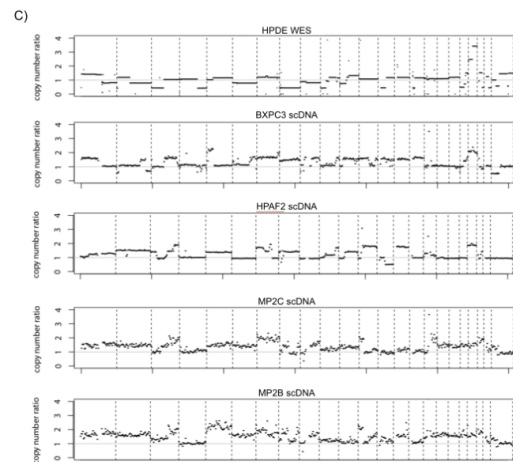
Next after the scRNA-seq data, we moved on to look at the scCNV analysis. The scCNV analysis demonstrated an overall striking degree of subclonal heterogeneity within each of the pancreatic cell lines, with various divergent genome-wide copy number alterations identified

28

within subsets of each parental entity (**Figure 3C**). We found 10x Cell Ranger DNA software had underestimated scCNV event calls, likely due to low sequencing coverage susceptible to this data type. To adjust for underestimation, we used our in-house bulk WES data for HPDE and HPNE as bioinformatic controls to re-estimate baseline CNV events, and then normalized cells across each sample to create a "pseudo-bulk" profile based on copy number ratios for each cell line (**Figure 4C**). In this "pseudo-bulk" summary, previously described hallmark genomic events characteristic of PDAC lesions [1-6] were readily observed, albeit in some cases only in a subset of genomic subclones for each line. Specifically, amplifications in regions of chromosomes 1,2,3,5,7,8,11,14, and 17, and losses at regions of chromosomes 3 (HPDE), 9 (BxPC3, MP2-B, MP2-C, HPDE), and 13 (HPAF-II) were distinguishable.

Finally, we mapped the clonal families of each cell line to genes known to be amplified, deleted, or mutated in PDAC (see *Methods*), and uncovered extensive heterogeneity in amplification and deletion profiles on a per-locus basis (**Figure 5**). We report that HPNE has a benign CNV profile at these loci, with little heterogeneity in copy number across clones of this culture (**Figure 5A**). Conversely, the BxPC3 cell line, which is historically used as a *KRAS* wild type PDAC cell line, harbors copy number >= 4 in nearly all clones at the *TERT* gene locus, wherein over 2/3 of cells have a copy number for TERT more than 1 above the mean ploidy (**Figure 5B**).
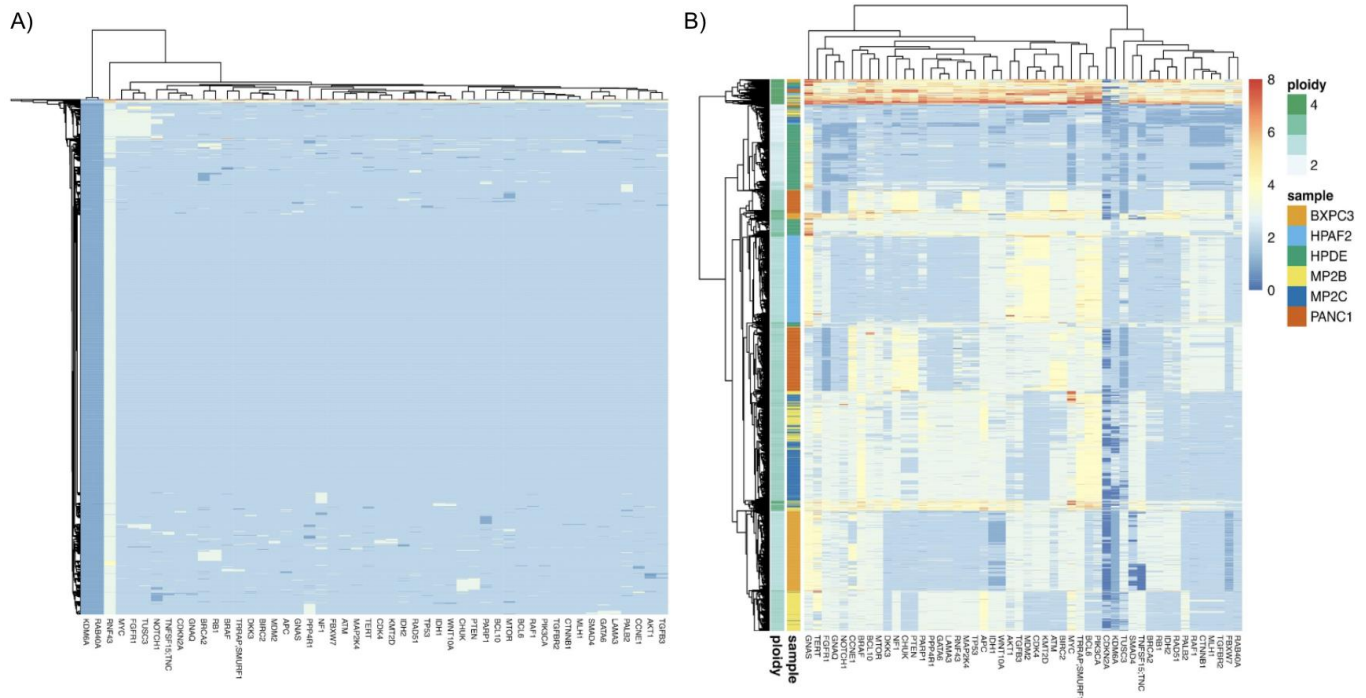
Figure 5: PDAC cell lines harbor differential CNV events at oncogenic loci.
Heatmap with copy number per cell (rows) per gene (columns) for a series of known oncogenes, for **(A)** HPNE cells and **(B)** all non-HPNE cell lines with scCNV profiled. Showing a random subset (1000) of cells per cell line.

BxPC3 TERT copy number was also confirmed via fluorescence in situ hybridization (FISH), as compared to copy number events at this locus in cell lines HPDE, HPNE and HPAF-II (**Figure 6**). Of interest, a number of BxPC3 clones harbored amplifications at the BRAF locus (**Figure 5B**). It is known that in contrast to melanoma, cases of *KRAS* wild type PDAC, including the BxPC3 cell line itself, acquire in-frame deletions of *BRAF* that result in constitutive activation of the kinase domain [89]. However, amplification of the mutated "driver" oncogenic locus (e.g. *KRAS, BRAF, EGFR*) is not unusual, as it can provide additional survival and growth cues.

Figure 6: Fluorescence in situ hybridization validation of notable scCNV-detected copy numbers.
A) FISH validation of amplifications of AURKA (green) and TERT (red) in HPNE, HPAF-II, BxPC3 and HPDE cell lines, corroborating reported scCNV findings of amplification events at these loci. Two-tailed P values determined using Mann Whitney tests for pairwise comparisons in Prism 9 (v9.0.0). For TERT: HPNE-HPDE pval < 0.0001, HPAF2-HPNE pval = 0.4076, BXPC3-HPNE pval < 0.0001. For AURKA: HPNE-HPDE pval < 0.0001, HPAF2-HPNE pval < 0.0001, BXPC3-HPNE pval < 0.0001. Scale bar = 5 microns.
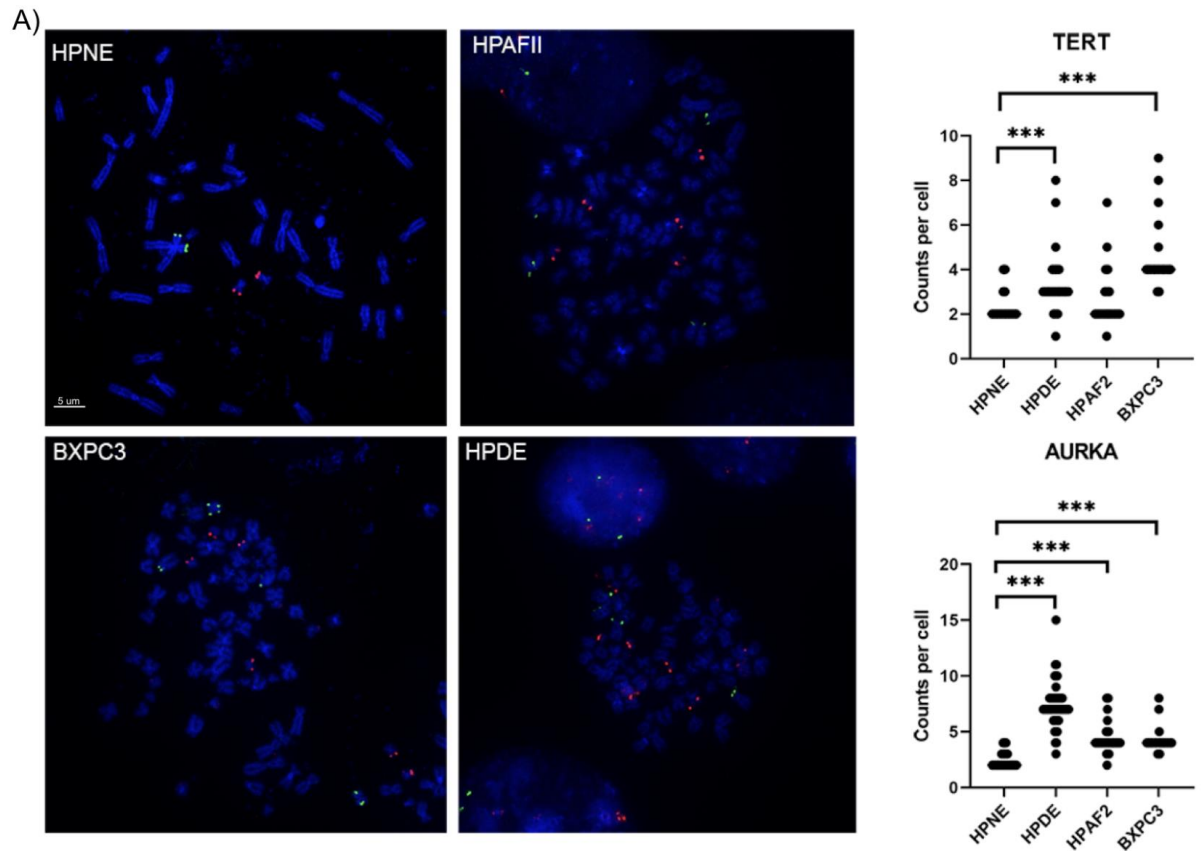
Single cell profiling reveals pitfalls of commonly utilized immortalized pancreatic controls.

The Human Pancreatic Duct Epithelial (HPDE) cell line is a widely used model system for human pancreatic carcinogenesis [13,90] typically as a non-transformed, immortalized "control". HPDE cells were derived from explanted human pancreatic ductal epithelium obtained from a pancreas resected for benign etiology, and immortalized using retrovirus-mediated expression of human papillomavirus 16 (HPV16) oncoproteins E6 and E7 [33]. The immortalizing effects of E6 and E7 are mediated primarily by targeting of the p53 and retinoblastoma (Rb) tumor suppressor genes [91]. Parental HPDE cells are wild type at the endogenous *KRAS* locus, non-transformed *in vitro*, and non-tumorigenic in mice, unless transformed through ectopic expression of mutant *KRAS*, in combination with other tumor promoting genomic events [92].

We thus hypothesized that the HPDE cell line would be transcriptomically distanced from the PDAC-derived lines, given its broad experimental application as a control line. However, our scRNAseq interrogation instead shows HPDE is most transcriptionally similar to HPAF-II, and on a distinct clade from the second commonly used "control" line, HPNE (**Figure 4B**). On scCNV profiling, we find that HPDE cells retain a subclonal architecture akin to a neoplastic genotype in some clones (**Figures 3C and 3E**). We also find evidence of distinct amplification and deletions at loci linked to key PDAC-progressor genes (**Figure 5B**). We conducted "conventional" bulk whole exome sequencing (WES) on HPDE cells curated in our laboratory from the same pool used to generate scCNV and scRNAseq datasets (see *Methods*). This confirmed that HPDE cells had undergone further bi-allelic losses of chromosomal arms 3p, 8p, and 9p, which are all "hot spots" housing known tumor suppressor genes in PDAC and other solid tumors (**Figure 3E, top**), and this finding was validated in the "pseudo-bulk" CNV profile generated from scCNV data (**Figure 3E, bottom**). Notably, all HPDE subclones harbor an amplification event (CN >10 in a minor fraction of subclones) at chromosome 20q (**Figure 3G**), bookending the *AURKA* gene locus within the most common region of overlap. Almost no heterogeneity was detected in the amplification event, reiterating that all HPDE single cells sequenced have undergone this amplification at some level (**Figure 3G,** bottom purple bar measuring near-0 Heterogeneity value). FISH confirmed AURKA amplification in HPDE (**Figure 6**), indicating that high AURKA copy numbers in scCNV clones were not a function of technical artifacts in this dataset. Examination of *AURKA* transcript expression, when HPDE scRNAseq data was normalized to HPNE scRNAseq data, showed a spectrum of expression levels in HPDE, at least 20% of cells (presumably representing the subclones with highest levels of genomic amplification) expressing 2-4 fold higher expression of *AURKA* transcripts compared to HPNE cells (**Figure 3H**). The encoded protein Aurora kinase A is commonly overexpressed in pancreatic cancers, and contributes to both chromosomal instability through destabilization of the mitotic spindle assembly and towards tumor progression via phosphorylation of substrate proteins [93,94]. One can speculate that the widespread genomic perturbations observed in HPDE are at least partially a

consequence of instability introduced by aberrant *AURKA* activity, in conjunction with the functional inactivation of p53 caused by HPV oncoprotein expression. To the best of our knowledge, this is the first description of *AURKA* amplification in HPDE, a purportedly "control" cell used in PDAC research, including in experimental therapeutics studies.

These findings in HPDE demarcate an important distinction from the second immortalized cell line commonly used as an experimental "control", Human Pancreatic Nestin-expressing (HPNE) cells [30]. In contrast to HPDE, HPNE cells are non-ductal in derivation (as demonstrated by lack of epithelial markers, and widespread expression of progenitor cell transcripts *NES*, *NOTCH2* and *CD44* on scRNA-seq (**Figure 3B**). In contrast to HPDE, HPNE cells were immortalized using retroviral transduction of the human telomerase reverse transcriptase (*hTERT*), which has been used in more recent times for derivatizing immortalized epithelial cells. Unlike HPDE cells, scCNV sequencing demonstrates that HPNE cells have not evolved a divergent subcellular taxonomy, but rather are extremely homogenous in their copy number profiles when viewed both broadly and at key oncogenic loci (**Figure 3C, Figure 5A**). This scCNV finding is consistent with WES analysis of HPNE (**Figure 3D*, top***), which shows a "flat" bulk segmentation profile, and is confirmed on the "pseudo-bulk" profile generated from scCNV data (**Figure 3D*, bottom***).

While we do not observe amplifications or deletions of most of the HPNE genome, there is a discernible amplification event at chromosome 17q. As with HPDE, we interrogated genes contained within the amplified 17q locus (**Figure 3F**), and *BRCA1*, among others, stood out as a candidate gene. When interrogating scRNAseq data, we report that at least 24% of HPNE cells in culture highly express BRCA1 transcripts relative to HPDE cells (**Figure 3H**) The encoded Brca1 protein is a component of the homologous recombination repair (HRR) machinery, and *BRCA1* is uncommonly mutated in PDAC (~1%), typically in the germline, and associated with HRR defective cancers [95-96]. While the direct mechanism by which 17q would have been amplified remains to be investigated, we speculate that in the case of HPNE, the relative

"genomic quiescence" reported here may be due, in part to the overexpression of *BRCA1* enabling DNA repair mechanisms.

Ultimately, while HPNE does not exhibit the subclonal heterogeneity observed with HPDE, its lack of a ductal transcriptional profile and enrichment in markers associated with progenitor populations of uncertain histogenesis need to be factored in the use of these cells as an appropriate control for PDAC cells. To that end, the need for developing improved preclinical patient-derived "control" models for PDAC research is apparent from our findings.

Custodial variability of MiaPaca2 cell lines drives transcriptomic heterogeneity.

An identical parental line, when maintained under comparable passaging conditions in different laboratories (MiaPaca2), reflects a degree of custodial variability that impacts the translational value of that cell line as a controlled model. Previous work challenged the long-maintained assumption in cancer biology research that cell lines are clonal, stable entities, and explored the existence of phenotypic variability between widely used HeLa [15] and MCF7 [16] cell lines via cross-laboratory multi-omic comparisons. In such studies, cultured cells were maintained in uniform conditions after being obtained from different laboratory settings. Subsequent analysis revealed extensive inter-laboratory heterogeneity with respect to phenotype, copy number variations, and even drug response experiments, elucidating the high degree of variability underlying presumed "same" cell lines. Now, in light of single-cell analytics, we sought to investigate the extent of deviation from assumptions of clonality, both within and between cultures, in PDAC cell lines.

The MiaPaca2 cell line was initially generated from a primary PDAC lesion of a 65-year-old male, where the tumor had involved the pancreatic body, tail, and demonstrated periaortic invasion [11]. We assayed 3 "strains" of the MiaPaca2 cell line: one ordered directly from the American Type Culture Collection (ATCC), located in Gaithersburg, MD (MP2-A), a vial originating from an academic laboratory in Boston (MP2-B) and one that had been grown in our laboratory at MD Anderson Cancer Center (MP2-C). Following fingerprinting of the MiaPaca2

34

cells, we confirmed using ddPCR that all three versions of the cell line carried the same activating

KRAS[G12C] mutation (**Figures 7A-C**), as previously published in characterization studies of this

cell line [11,97,98].

Figure 7: Hotspot KRAS mutations confirmed in PDAC cell lines. Droplet Digital PCR (ddPCR) results of KRAS probes for hotspot mutations G12C, G12D, and G12V applied to MP2 samples A-C and Panc1. **A-C)** Confirms same KRAS G12C mutation in all 3 cell lines. **D)** Panc1 ddPCR results indicating both KRAS G12D mutation.

A) MP2_A
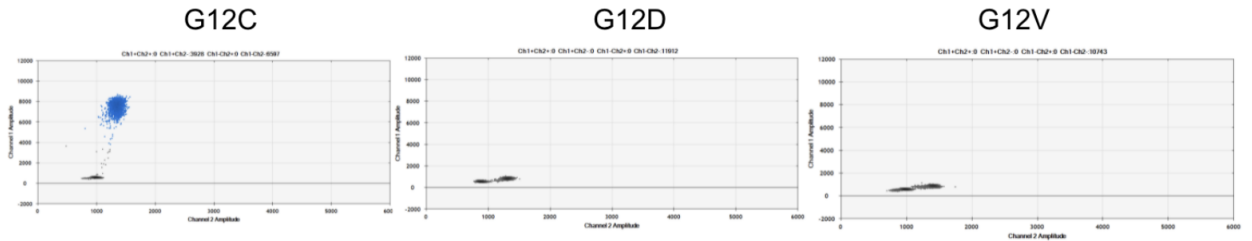
B) MP2_B
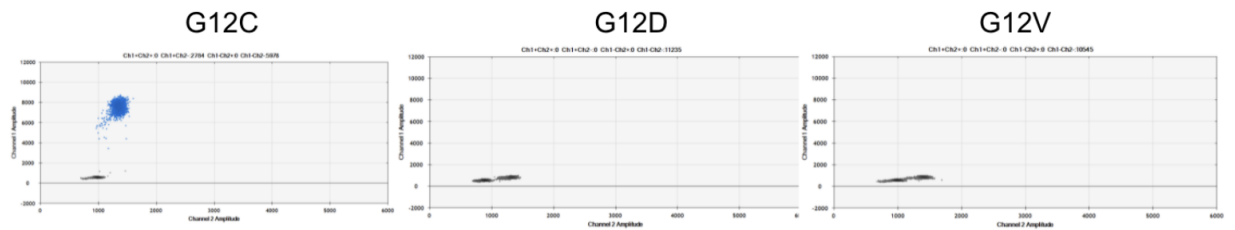
C) MP2_C
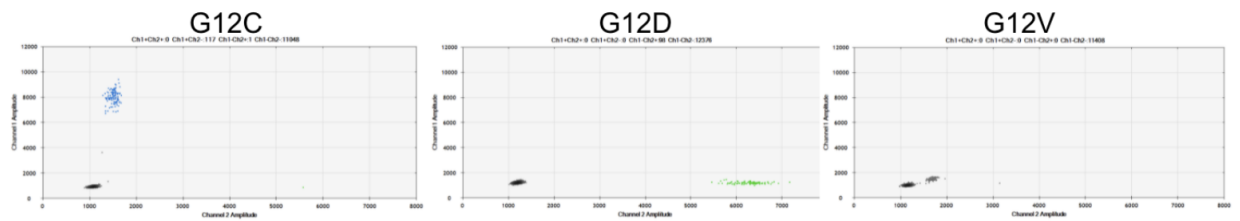
D) Panc1
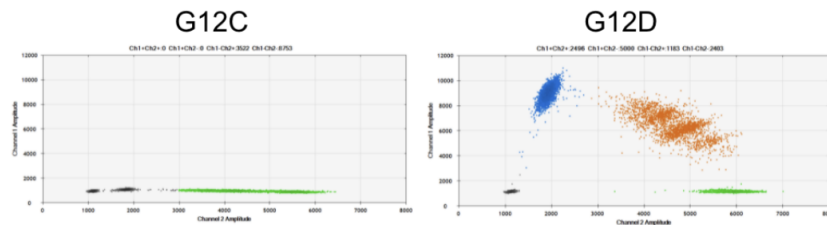
We report phenotypic divergence between these assumptively "identical" cultures that appears to be driven by changes at the RNA level. In our comparative scRNA-seq analysis of these samples, we find that the MiaPaca2 lines segregate mostly independently, with only a single small cluster where all three overlap (**Figures 8A, 8B**). MP2-A and MP2-B also share an additional region of overlap, but distinct from MP2-C.

Gene Set Enrichment Analysis (GSEA) was performed to identify general pathways that are differentially altered between the samples (**Figure 8C**). MP2-A is enriched in GSEA hallmark pathways related to p53, oxidative phosphorylation, and protein secretion. In contrast, MP2-B downregulated GSEA hallmark interferon gamma response, and MP2-C has no statistically significant enrichment in hallmark pathways based on scRNA-seq GSEA analysis (**Figure 8C**).
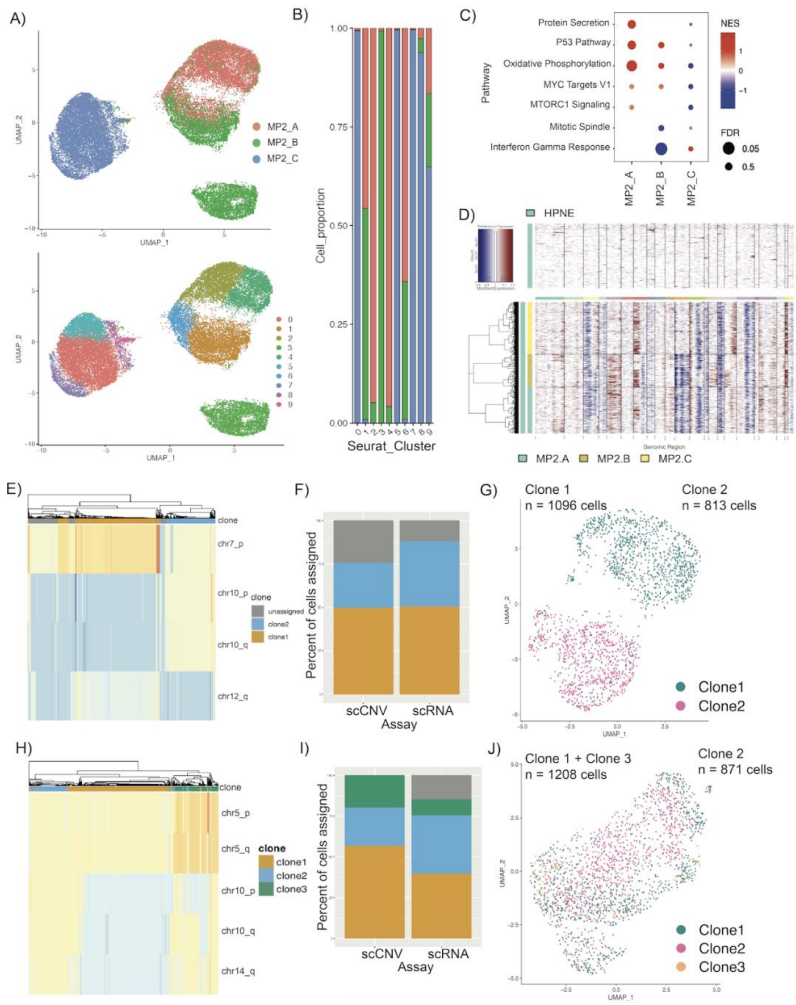
Figure 8: Characterization of custodial variability in MP2 cultures by scRNA and scCNV analysis.

A) UMAP overlaying MP2 samples and their distinct clusters.

B) Bar graph displaying distribution of cells per MP2 culture across clusters; MP2-A in red, MP2-B in green and MP2-C in blue.

C) Bubble plot showing enrichment of pathways in MP2 cultures compared to each other with normalized enrichment score (NES) on the x-axis. Size of the bubble represents false discovery rate (FDR); red indicates upregulation, blue indicates downregulation of the pathway.

D) inferCNV heatmaps derived from scRNAseq data of all three MP2 samples, using HPNE as an analytical reference.

E) Genomic clones 1 (orange) and 2 (blue) identified from scCNV data of MP2-B based on CNV events at chromosomes 7, 10, and 12.

F) Percentage of cells assigned to clones in scCNV and scRNA data. scCNV clones were mapped to corresponding scRNA data using CloneAlign.

G) UMAP data of MP2-B scRNA expression of single cells overlaid with CNV clones assignment for each cell; Clone 1 in green and Clone 2 in pink.

H-J) Same as (D-F) for MP2-C.

We find evidence for a highly similar ancestral clone between the MP2-B and MP2-C strains, including several examples of chromosomes ubiquitously amplified in one strain versus subclonally amplified in the other (chromosomes 3q, 5, 7p) (**Figure 3C**). We were also able to orthogonally validate this when we applied InferCNV [99] to scRNAseq MP2 data (**Figure 8D**). Further, these strains markedly differ in amplification and deletion events that correspond to chromosomal loci implicated in PDAC. For example, in MP2-C we find that nearly all cells have copy number >= 4 for oncogenes BLC6, PIK3CA, and BRAF. In contrast, MP2-B has lower copy

number for these genes in a large fraction of cells, despite similar overall ploidy levels (**Figure 5B**). These initial findings demonstrate the remarkable heterogeneity, when viewed at the single cell level, across cell lines assumed to be derived from the identical parental origin.

Evolution of divergent genomic subclones in MiaPaca2 strains has transcriptomic implications.

While profiling at single-cell resolution makes evident the transcriptional and genomic heterogeneity of PDAC cell lines, integrating subclonal lineages and relationships between these independent datasets is crucial towards uncovering the impact of genomic alterations on transcriptomic diversity. Previous work in which DNA and RNA were assayed in the same cells has shown that many genes display copy-number gene-dosage effects on transcriptional expression [100,101,102]. Building on this finding, Campbell et al. developed the clonealign algorithm [103], which established a framework for how genomic-transcriptome associations may be mapped in single-cell datasets derived from the same parental culture, but generated using individual assays. Using paired scRNA and scCNV from MiaPaca2 cells as a proof-of-concept for this method, we applied segmentation and copy number profiling from the scCNV data to clusters identified in scRNA transcriptomic profiles using clonealign (see *Methods*). An important caveat of this method is that clonealign's inherent design filtered out a large number of cells sequenced by scCNVseq. Thus, the findings discussed here are based on a subset of the more comprehensive subclonal families and profiles previously described. Using clonealign filtering criteria to scCNV-derived MP2-B cells (**Figure 8E**), two distinct subclones were defined. One with 4 copies of chromosome arm 7p and 2 copies of chr10 (p and q), versus one with 3 copies for all of these chromosome arms. Of note, the clone with 3 copies of 7p (instead of 4 copies) also had lower copy number for a subset of 12q (2 vs. 3). Applying the same clonealign filtering criteria to scCNV-derived cells from MP2-C (**Figure 8H**), three distinct subclones were defined: 1. With lower copy number (2 vs. 3) in chromosome 10 (p and q arms) and 14q. 2. With copy number = 3 in all of chr5, chr10, and chr14q. 3. With higher copy number (4 vs. 3) in chr5, and lower copy number (2 vs. 3 copies) in 10p, but higher in 10q and 14q (3 vs. 2 copies).

38

After the major subclonal populations were established from scCNV profiles, we used clonealign to identify subclones in the scRNA data that could be reliably mapped back to scCNV profiles (see *Methods*). Notably, we find that for MP2-B, the two unique genomic profiles we see in the scCNV data (**Figure 8E**) correspond almost perfectly to transcriptional subpopulations as visualized in our UMAP analysis (**Figures 8F, 8G**). Next, we used GSEA analysis to search for differences in expression signatures within each of the two delineated subclones. Subclone 1 of MP2-B (1096 cells) is characterized by four hallmark pathways, while MP2-B subclone 2 (813 cells) is defined by six, completely distinct gene sets (**Table 1**).

Table 1. Summary of GSEA results on gene lists derived from scCNV clones, which were analyzed with clonealign and subsequently mapped so scRNAseq data. CNV_events describe the major amplification or deletion events that were common to groups of cells per sample, and therefore used to define clonal families by clonealign. Cell_count depicts the number of cells harboring a set of CNV events. Hallmark_enriched and Oncogenic_enriched list gene set pathways that were enriched in scRNAseq clusters corresponding to scCNV-defined clones.

CNV_clone	CNV_events	cell_count	Hallmark_enriched	Oncogenic_enriched
MP2_B_C1	chr7_p.amp, chr10_p.del, chr10_q.del, chr12_q_subseg.neu	1096	MYC, Glycolysis, Oxidative Phosphorylation, E2F	LEF1, P53, Cyclin D1
MP2_B_C2	chr7_p.neu,chr10_p.neu,chr10_q.neu,chr12_q_subseg.del	813	TNFA, UV Response, Apical Junction, KRAS, MTORC1, Unfolded Protein Response	MTOR, EIF4E, RAF, NEF2L2
MP2_C_C1 + MP2_C_C3	chr5.amp, chr10_p.del, chr10_q.neu, chr14_q.neu; chr5.neu,chr10_p.del,chr10_q.del,chr14_q.del	1208	Angiogenesis, P53	CRX, CAHOY Astroglial, ESC_V6.5, VEGF
MP2_C_C2	chr5.neu, chr10.neu,chr14.neu	871	N/A	N/A
MP2_C_C3	chr5.neu,chr10_p.del,chr10_q.del,chr14_q.del		combined with clone 1 as described in Main Text	N/A
Panc1_3D_C1	chr14_q.neu, chr15_q.del	904	TNFA, Estrogen Response Late + Early, Fatty Acid Met., Cholesterol Homeostasis, Coagulation, IFGamma Response, Inflammatory Response, IFAlpha Response	EGFR_UP.V1, PRC1_BMI_UP.V1, ERBB2_UP.V1, BCAT.100_UP.V1, PRC2_SUZ12_UP.V1, MEK_UP.V1, ESC_V6.5_UP_LATE, MEL18_DN.V1, CSR_EARLY_UP.V1, AKT_UP_MTOR_DN.V1, JNK_DN.V1, KRAS.DF.V1, ATF2_S_UP.V1_DN
Panc1_3D_C2	chr14_q.del, chr15_q.neu	223	N/A	EIF4E
Panc1_2D_C1	chr14_q.neu, chr15_q.del	3251	G2M, E2F Targets, Estrogen Response Late, Bile Acid Metabolism, Apoptosis, Cholesterol Homeostasis	N/A
Panc1_2D_C2	chr14_q.del, chr15_q.neu	404	N/A	N/A

Given the difference in enrichment of cancer-related hallmark pathways that we found between the two MP2-B subclones, we then re-ran GSEA versus MSigDB's Oncogenic signatures. We found that subclone 1 is enriched for oncogenic pathways LEF1 upregulation, P53, and Cyclin D1, whereas subclone 2 is enriched for MTOR upregulation, EIF4E, RAF, and NEF2L2 (**Table 1**).

Interesting significantly upregulated genes in subclone 1 from these oncogenic pathways include KRT13 and LGALS1 (in the LEF1 upregulation pathway; padj=4.39e-49 and 1.35e-21 respectively). Although KRT13 is not ubiquitous in clone 1, the difference in percent of cells that express the gene is striking (32% in clone 1 vs. 3% in clone 2). This gene has previously been shown to predict worse overall survival in pancreatic cancer [104]. LGALS1 overexpression has also been negatively associated with survival in PDAC patients [105], and knockdown of LGALS1 in vitro reduced cell migration and invasion capabilities in pancreatic cancer associated cells [106]. Clone 2 shows significant upregulation of NEAT1 (in the MTOR pathway, padj=1.20e-9). This gene has also been shown to promote PDAC growth and metastasis and predict poor prognosis [107]. As both subclones were found at relatively high frequency (**Figure 8I**), it would suggest that neither has a clear fitness advantage over the other. Therefore it is not entirely unexpected that we see different genes that promote cancer growth in each subclone.

For MP2-C, we also see some degree of correspondence between the genomic profiles (**Figure 8H**) and the transcriptional subpopulations (**Figures 8I, 8J**), but the correlation is less striking than the one-to-one correspondence observed in MP2-B. In MP2-C, a very different pattern of enrichment is observed in both hallmark and oncogenic pathway sets. MP2-C subclones 1 and 3 were merged (due to very similar distribution across RNA transcriptomic clusters) for a total of 1208 cells, the population of which is significantly enriched for two hallmark pathways and five oncogenic pathways (**Table 1**). Surprisingly, MP2-C subclone 2 (871 cells) is not significantly enriched for any hallmark or oncogenic gene sets (**Table 1**). Importantly, there were also zero overlapping gene sets between MP2-B and MP-C, across any subclonal comparison.

In summary, we confirm previous reports that progeny of the apparently identical parental cell line experience substantial genomic and transcriptomic divergence on prolonged *ex vivo* passaging, that such divergence is observed both within, and across, cultures of the parental cell line, and at least in some instances, the transcriptomic divergence can be ascribed to distinct subclonal genomic alterations.

Modeling of tissue-based transcriptional PDAC subtypes using scRNA-seq data in established cell lines.

Recently developed transcriptome-based subtyping of PDAC have demonstrated both predictive and prognostic significance in early studies. The dichotomous Moffitt classification schema of "basal-like" and "classical" subtypes was initially established using bulk RNA sequencing strategies applied to human tumor samples[49]. PDAC transcriptional subtypes are known to associate with specific microenvironmental niches, and primary tumors have been shown to undergo subtype switching in response to microenvironmental cues[108]. However, it is not well established whether cell lines can reliably classified into Moffitt subtypes as freshly dissociated tumor tissue or PDO models, nor whether there would be an observable degree of subtype admixture when single-cell methods are applied to subclonal derivatives of parental cell lines. To investigate this, we sought to group the MiaPaca2 transcriptomic subclones into the dichotomous PDAC subtypes of the Moffit classification schema.

We observed that MP2-A and MP2-C have all (9,768 and 10,886 cells respectively) represented by the Moffitt "basal-like" subtype, while MP2-B has subtype admixture, with 3,456 cells sorting as the "basal-like" subtype and 3,556 cells sorting as "classical" (**Table 2**).

Table 2. Distribution of PDAC scRNA cells across Collisson + Moffit PDAC subtypes. Cell Count / Percentage of total.

Cell Line	Moffitt- Basal	Moffitt- Classical	Collisson- Classical	Collisson- Exocrine	Collisson- Quasimesenchymal
MP2-A	9768 / 100%	0 / 0%	0 / 0%	0 / 0%	5420 / 55.49%
MP2-B	3456 / 49.29%	3556 / 50.71%	2408 / 34.34%	1896 / 27.04%	2708 / 38.62%
MP2-C	10886 / 100%	0 / 0%	3276 / 30.09%	3724 / 34.21%	3886 / 35.70%
BXPC3	5606 / 54.88%	4609 / 45.12%	3532 / 34.58%	2175 / 21.29%	4508 / 44.13%
HPAF-II	2367 / 51.27%	2250 / 48.73%	1777 / 38.49%	961 / 20.81%	1879 / 40.70%
HPDE	2879 / 55.41%	2317 / 44.59%	1594 / 30.68%	1479 / 2.46%	2123 / 40.86%
HPNE	6318 / 49.80%	6370 / 50.20%	518 / 4.08%	5221 / 41.15%	6949 / 54.77%
Panc1-3D	7440 / 51.03%	7139 / 48.97%	4883 / 33.49%	3537 / 24.26%	6159 / 42.25%
Panc1-2D	2891 / 53.76%	2487 / 46.24%	1671 / 31.07%	1331 / 24.75%	2376 / 44.18%

Upon further investigation, we found that these samples were being "forced" into one subtype or the other on the basis of a few genes being present or absent, as opposed to having a robust expression of the majority of genes specified by "basal-like" or "classical" subtypes. For example, MP2-A cells were sorted as "basal-like" based on the expression of *AREG* and *KRT15* (**Figure 9A**), while MP2-C cells were sorted to "basal-like" based only on the expression of *AREG*, *GPR87*, *KRT15*, and *LEMD1* (**Figure 9C**). Similarly, the MP2-B sample, for which we detected genes relevant for both "basal-like" and "classical" subtyping, we found that "classical-like" cells were classified as such based on only *LYZ*, while "basal-like" cells were classified as such due to expression of *AREG*, *GPR87*, *KRT15*, and *KRT7* (**Figure 9B**).

Figure 9: Expression of few genes dictates transcriptional subtyping of cell lines. Moffitt Classification, per gene, per cell across basal and classical subtypes in **A)** MP2-A, **B)** MP2-B, and **C)** MP-C displaying how a sparse expression of subtype genes across thousands of cells in each sample forces an artificial classification.
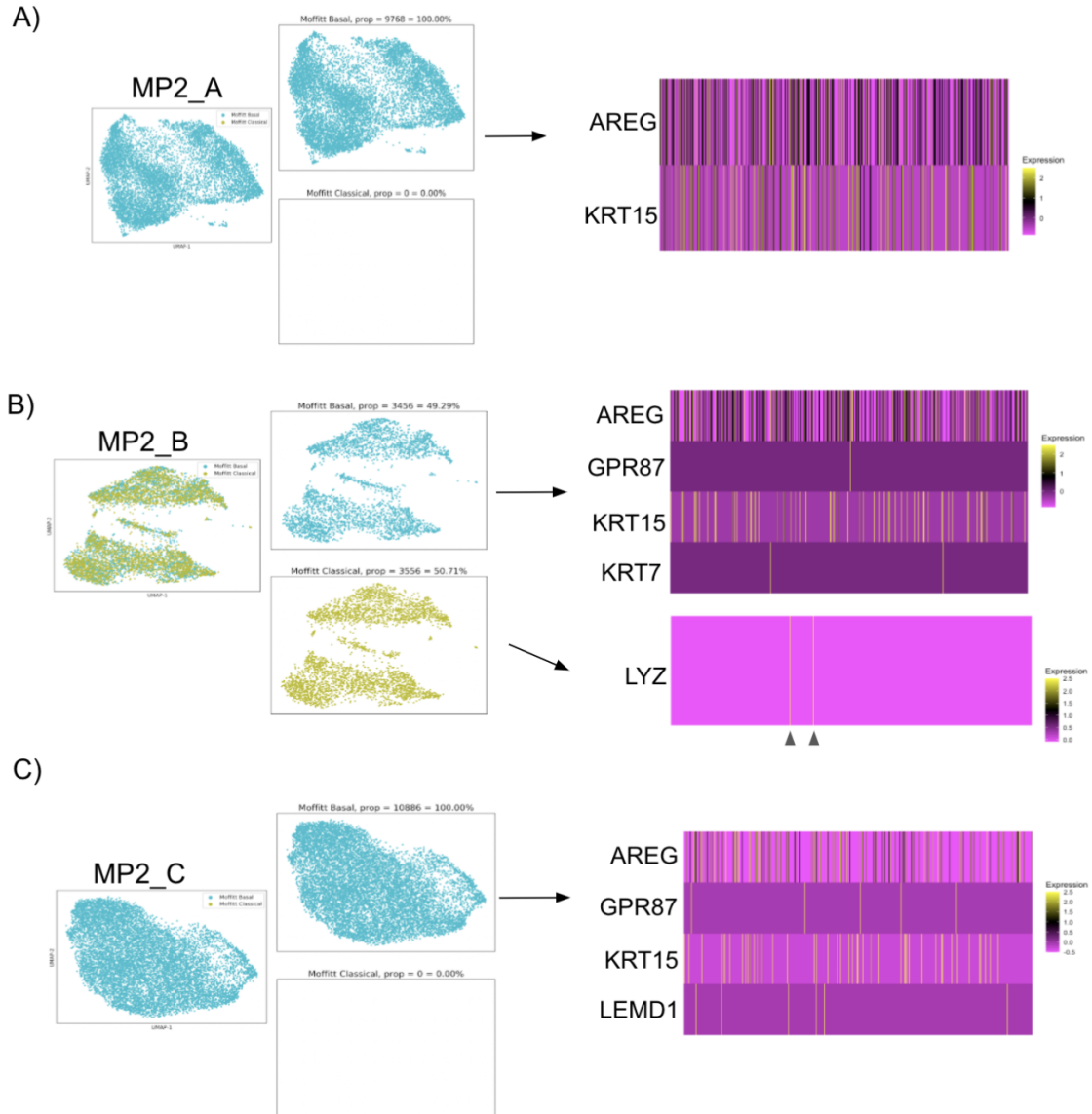
Given the thousands of cells present and the depth of sequencing on these samples, it is unlikely that this scant gene representation is due to dropout rates or data sparsity, which could result in skewed scRNA data. Rather, our data indicates that PDAC cell lines are sub-optimal models for application of tissue-based classification systems like Moffitt, largely because they might lack expression of substantial numbers of transcripts required for meaningful classification. This finding may impact how prevalent PDAC classification schemes are applied to monolayer

44

culture models and any subtype-based therapeutic outcome predictions derived from these that are then extrapolated to patients.

Epigenetic alterations define transcriptional divergence observed in monolayer and 3D models.

Ex vivo 3D models of tumor growth are being increasingly adopted, as a number of comparative studies between 3D spheroids and 2D monolayer cultures have shown that 3D culture more faithfully recapitulates *in vivo* biology [109,110,111]. Additional work has also shown that 2D monolayers might lack critical features associated with *in vivo* tumor progression, such as hypoxia [112-113]. Within the context of single-cell analytics, there is scant data to address the extent of transcriptional adaptations that occur in the process of modifying "conventional" monolayer culture to a 3D spheroid model. We find here that upon growth in 3D, Panc1 cells exhibit demonstrable transcriptomic divergence, as well as increased transcriptional diversity, compared to matched 2D culture grown from the same parental vial, upon scRNA-seq analysis. While Panc1-2D and Panc1-3D cultures are overall more similar to each other compared to other cell lines at the transcriptome level (**Figure 3 and Figure 4B**), they do not overlap when visualized using UMAP (**Figure 10A,** *left*). To look further into pathway level differences between the 2D and 3D models, we computed differentially expressed genes and processed them with GSEA (**Figure 10B;** also see *Methods*). This differential expression was done by subcluster within each of the monolayer and spheroid, so that one can see heterogeneity both within and between each of these. Panc1 spheroids show upregulation of epithelial mesenchymal transition in the largest subcluster relative to the monolayer. Meanwhile, we also see strong differences in pathways within spheroid subclusters, with significant upregulation of the p53 pathway and downregulation of G2M checkpoint and E2F target pathways in one subcluster relative to the other two. This kind of heterogeneity was not seen within the 2D model, with no significant difference in pathways found between the two subclusters.
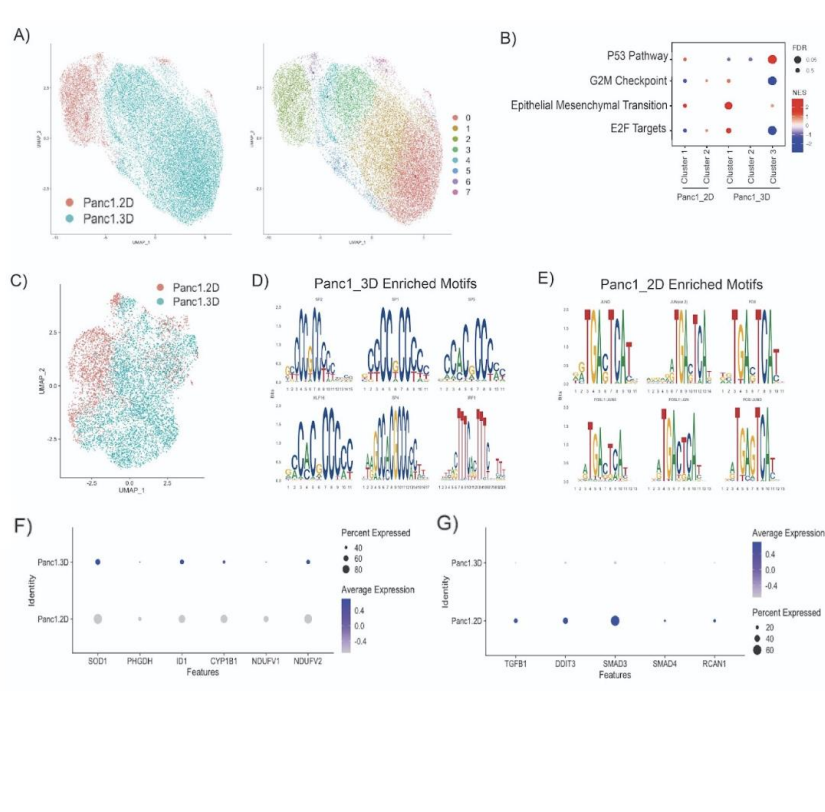
Figure 10: Spheroid growth model promotes transcriptional heterogeneity and epigenetic remodeling.
A) UMAP overlaying scRNA of Panc1 samples and their unique clusters.

B) Pathway enrichment profiles defined by GSEA analysis for Panc1-2D and Panc1-3D spheroid cell clusters. Size of dot represents FDR, red indicates upregulation, blue indicates downregulation of the pathway.

C) UMAP representing snATAC-seq data of merged Panc1 samples.

D), E) Analysis of merged Panc1 snATAC data shows enrichment in Sp/Klf motifs in spheroid data, and enrichment of Fos/Jun motifs in 2D monolayer culture.

F) Comparison of expression of genes associated with Sp/Klf transcription factors in scRNA of Panc1 2D and Panc1 3D.

G) Comparison of expression of genes associated with Fos/Jun transcription factors in scRNA of Panc1 2D and Panc1 3D.

As with MiaPaca2 samples, we sought to understand the basis of transcriptomic differences observed on scRNA-seq data, but using a slightly different analytic approach. As described earlier, spheroids were grown from the same parental population of Panc1 cells as the monolayer culture. scCNVseq was conducted on this parental population, and subsequent scRNAseq + snATACseq was conducted after culturing the cells in their respective conditions. We then mapped this parental scCNV profile to paired scRNAseq data after growth under monolayer or spheroid conditions, to understand subsequent transcriptomic reprogramming given identical parental genomic material.

Applying the same clonealign filtering criteria we used in our approach for MP2 cells, we defined two mutually exclusive subclones based on lower copy number (2 vs. 3) in either 15q (subclone 1) or 14q (subclone 2) for Panc1 (**Figures 11A, 11B**). When we mapped these clonealign-defined unique genomic subclones to specific transcriptional programs across the two datasets, subclone 1 was comprised of 3,251 cells and subclone 2 of 404 cells in Panc1 2D

46

scRNA-seq data (**Figure 11C**), while in the Panc1-3D scRNA dataset, subclone 1 was represented by 904 cells, and subclone 2 by 223 cells (**Figure 11D**). To confirm that these clonealign calls were not an artifact and that the monolayer and spheroid truly share similar scCNV profiles, we ran InferCNV [44] on the scRNA data for each growth condition (**Figure 11E**). This confirmed the clonealign results, with the majority of (but not all) cells in each condition showing lower copy number in chr15 compared to chr14 and a small subset of cells showing the reverse.
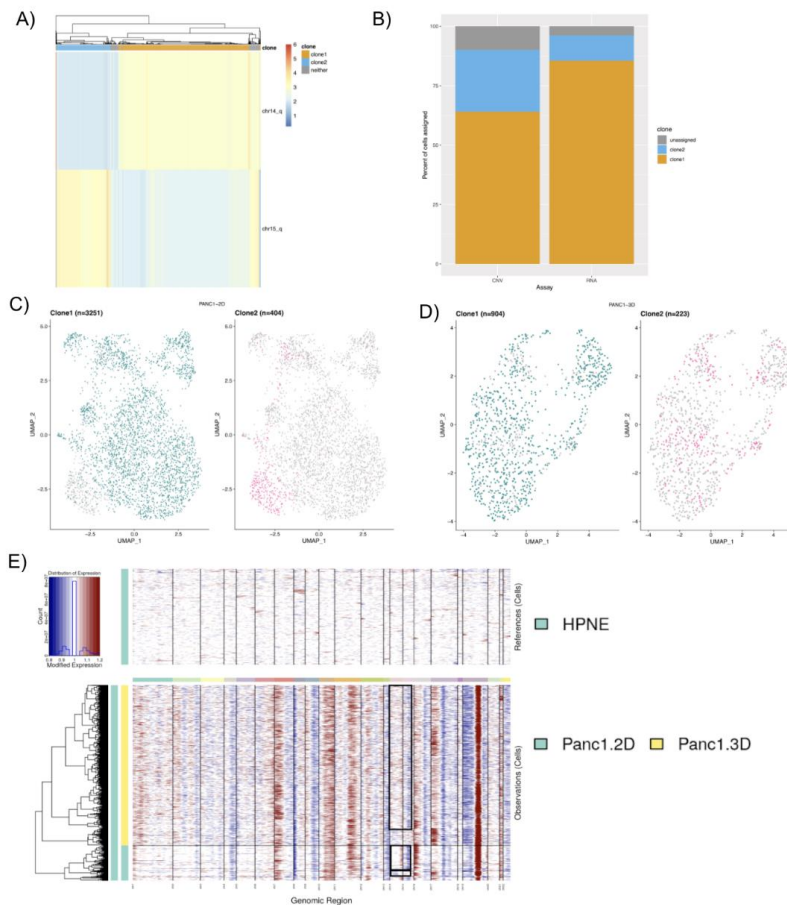
Figure 11: Genome-transcriptome mapping from parental Panc1 scCNVseq yields differential expression profiles between monolayer and spheroids.

A) Clonealign results using the same genomic scCNV background. Clones demarcated by CNV events at chromosomes 14q and 15q. Cells per clonal group are along the x-axis, y-axis indicates CNV events used for subsetting clones.

B) Clonealign scCNV clone correspondence to Panc1 2D scRNA data.

C) UMAP of scCNV-derived clones mapped to corresponding scRNA-derived cells for Panc1 2D and **D)** Panc1 3D.

E) inferCNV derived from scRNAseq of Panc1 2D and Panc1 3D, HPNE as reference. Black box depicts differential chr15 deletion, corroborating clonealign findings for scCNV-based clone designations.

There was little to no overlap in the enriched hallmark pathways (sharing only late estrogen response and cholesterol homeostasis pathways) or oncogenic gene sets (no common pathways) for either of the two subclones between the two growth conditions, with only subclone 1 in Panc1 3D even demonstrating a substantial number of discernible gene sets (**Table 2**). In

other words, despite the common parental scCNV profiles, the transcriptomic divergence between the two growth conditions appears to be driven almost entirely by non-genomic events, such as epigenetic alterations.

Given the observed decoupling between Panc1 scCNV and scRNA datasets when comparing spheroids to 2D monolayer, we thus hypothesized that epigenetic modifications may be responsible for remodeling in the spheroid setting. To address this, we performed snATAC-seq and applied the Seurat analysis extension package Signac [114] across a population of 9,785 nuclei analyzed from Panc1 monolayer and 7,453 nuclei analyzed from Panc1 spheroids isolated from the same population, processed in parallel, as the cells used for scRNAseq. As a first measure of epigenetic heterogeneity after conducting a quality control analysis on the sequenced nuclei (**Figures 12A, 12B**), we find the nuclei in at least two different chromatin states within each growth condition (**Figures 12C, 12F**). Further motif enrichment analysis within each population shows unique subcluster motif profiles (**Figures 12D, 12E, 12G, 12H**).
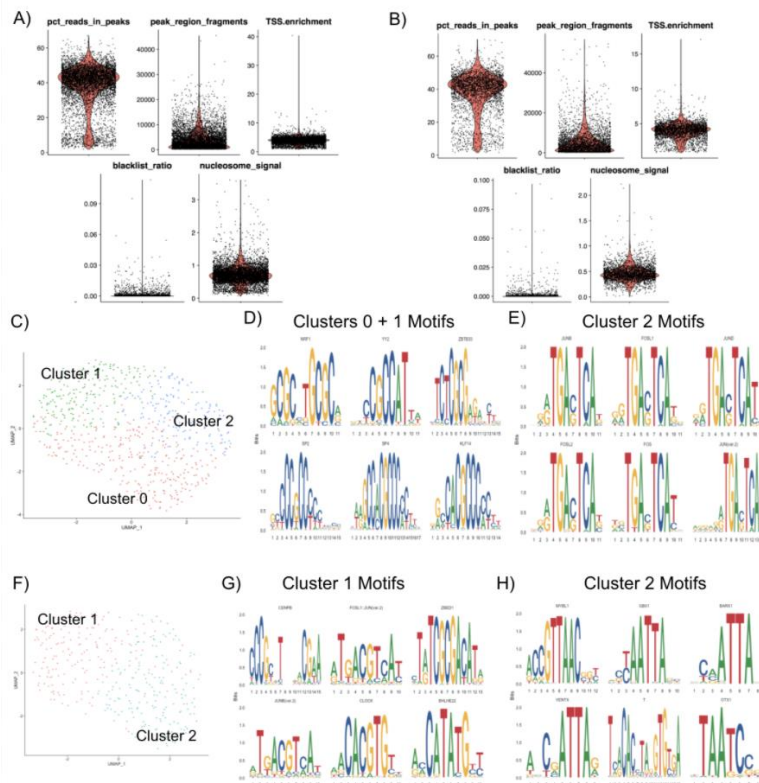
Figure 12: Chromatin modifications have transcriptional consequences in spheroid model.

A) Individual analysis of Panc1 spheroid nuclei shows 3 predominating states of chromatin architecture (clusters 0-2) that correspond to unique enrichment patterns.

B) Clusters 0 and 1 of Panc1 spheroid nuclei are enriched for SP motifs, NRF1, YY2, ZBTB33, and KLF14.

C) Cluster 2 of Panc1 spheroid nuclei is enriched for FOS/Jun motifs.

D) Individual analysis of Panc1 2D (monolayer) nuclei shows 2 predominating states of chromatin architecture (clusters 1, 2) that correspond to unique enrichment patterns.

E) Cluster 1 of Panc1 monolayer nuclei is enriched for Fos/Jun motifs, ZBED1, CENPB, CLOCK, and BHLHE22.

F) Cluster 2 of Panc1 monolayer nuclei is enriched for MYBL1, GBX1, BARX1, VENTX, T, and OTX1. Quality-control metrics for single nuclei sequenced and analyzed for **(G)** Panc1 spheroids and **(H)** Panc1 monolayer samples.

48

We bioinformatically merged Panc1-2D with Panc1-3D nuclei to obtain a differential motif enrichment profile between the samples (**Figure 10C**). Notably, we observed enrichment of Sp/Klf-associated motifs in the spheroid model (**Figure 10D**), and Fos/Jun motifs enriched in the 2D snATAC-seq data (**Figure 10E**). We then confirmed the overexpression of putative target candidate genes in scRANseq data affiliated with the enriched motifs that we had identified in corresponding snATAC-seq datasets (**Figures 10F, 10G**). In doing so, we find that the regulatory consequences of Sp/Klf motif enrichment are in genes associated with modulation of reactive oxygen species and metabolism such as SOD1 [115], ID1 [116], and NDUFV2 [117]. The low expression, or, in some cases, downregulation, of these genes in the monolayer culture suggest that in the process of epigenetic reprogramming, Panc1 spheroids also undergo a metabolic reprogramming by upregulating oxidative phosphorylation or glycolysis. Conversely, the enrichment of Fos/Jun motifs results in the transcriptional upregulation of classic effectors in this signaling pathway, such as SMAD3, SMAD4, TGFB1, and DDIT3[118]. These starkly different expression and chromatin profiles between these models could have implications in the results of studies concerning metabolism in PDAC.

In summary, our results suggest that the striking differences observed in scRNA-seq profiles between spheroid and monolayer growth systems are due to a divergence in the underlying epigenetic landscape, and the resulting differences in transcription factor activity and downstream pathways may have significant implications for the way these models are used interchangeably for *in vitro* experimentation.

Long-term maintenance of organoids leads to transcriptomic change.

PDOs have emerged as a promising preclinical model for therapeutic prediction and functional studies across multiple cancer types, including in PDAC[18,19,119,120,121]. Much like established cell lines, PDOs are maintained and expanded via *ex vivo* passaging in specially

formulated "organoid" media. Early passages of PDOs retain the clonal genomic alterations observed in the parental tumor, as well as the transcriptomic signature(s) predictive of response to cytotoxic agents. However, whether the transcriptome of PDOs evolves over time in culture is less well studied. Therefore, we generated scRNA-seq profiles on a PDAC PDO at two timepoints, "early" and "late", separated by 10 passages.

We found that in the later passage of the PDO, two transcriptionally distinct clusters (**Figure 13A**) had emerged, which respectively formed two separate cell fates on trajectory inference (**Figure 13B**). Transcripts upregulated in cell fate 1 showed enrichment of epithelial-mesenchymal transition, cell growth, reactive oxygen species (ROS) biosynthesis, and axon development, while transcripts in cell fate 2 were enriched for telomere maintenance, DNA replication, cell cycle, and hypoxia pathways (**Figure 13C**). To test whether there were genomic alterations accompanying the transcriptomic divergence, we inferred copy number aberrations from the scRNA-seq data using the inferCNV package [44], which revealed a chromosome 16p gain in the later passage PDO, and an additional chromosome 19q loss specifically in cell fate 2 (**Figure 13D**).

Bearing in mind the emerging translational relevance of transcriptional subtyping of PDOs, we paneled for genes relevant to the Moffitt subtyping schema to understand subtype-specific shifts that may occur during *ex vivo* passaging. The earlier passage PDO has demonstrable expression of "basal-like" transcripts (**Figure 13E, *bottom***), but these did not overlap with the "basal-like" transcripts expressed by the later passage PDO (**Figure 13E, *top***). More striking was the differential expression of transcripts that define the "classical" subtype, which are expressed almost exclusively by the later passage PDO (**Figure 13F, *top***).
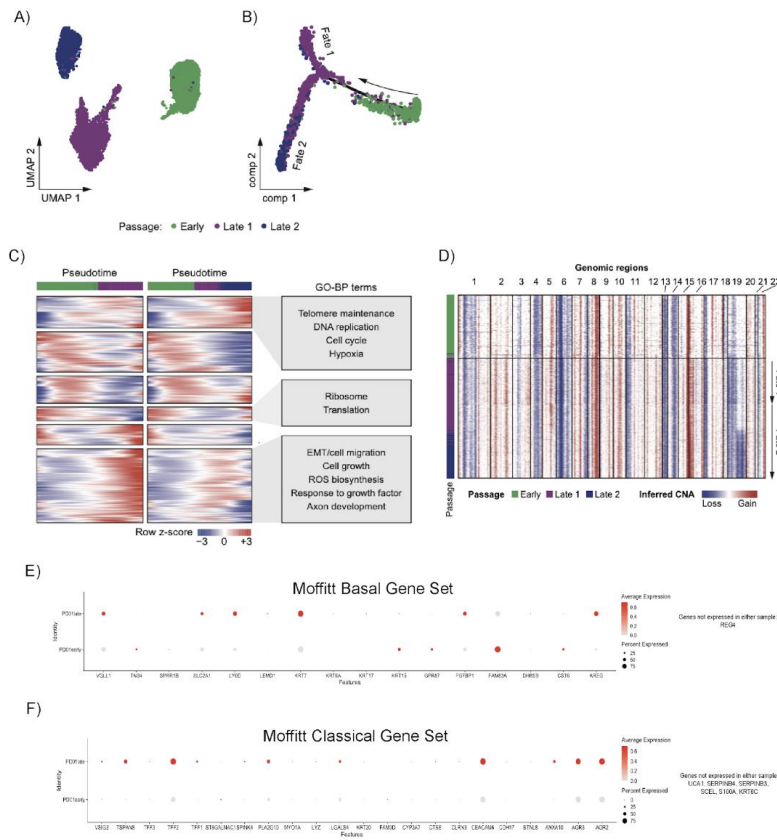
Figure 13: Patient-derived organoids evolve with time.
A) UMAP plot of cells from a different PDO at early (green) and late (purple, navy) passages.

B) Pseudotime analysis performed using Monocle of single cells from early (green) and late (purple, navy) passage organoids.

C) Branched heatmap (left) showing dynamic gene expression along the pseudotime trajectory for each cell fate in B. Pseudotime progresses from left to right. Enriched Gene Ontology biological process terms for each gene cluster are listed on the right.

D) Heatmap showing inferred copy number alterations of early and late passage organoids. Cells (rows) are ordered by pseudotime. Red represents copy number gains and blue represents copy number losses.

E) Comparison of expression of Moffitt Basal subtype genes in scRNA of early (bottom) vs. late (top) PDO1.

F) Comparison of expression of Moffitt Classical subtype genes in scRNA of early (bottom) vs. late (top) PDO1.

We confirmed that this mix of classical and basal genes in PD01late is not due solely to admixture within any given cell, and show that some cells classify as basal and others as classical, resulting in a true subtype admixture that suggests gradual transcriptional reprogramming in the PDO over time (**Figure 14**). We thus observe a subtype admixture over time, which is consistent with findings by Raghavan et al. [20], demonstrating that later passages of PDOs in culture undergo transcriptional reprogramming towards a "classical" phenotype, and reiterating the inherent plasticity of cellular subtypes. Of note, a recent assessment for "basal-like" and "classical" cells in PDAC tissues by subtype-specific protein markers has uncovered bi-phenotypic "hybrid" cells [122], while Ting and colleagues have shown evidence of subtype "drift" in PDAC tissues with various therapies [123], both lines of evidence supporting the plasticity of subtype states. As PDOs become increasingly adopted in translational research, the impact of

transcriptomic reprogramming in later passages should be accounted for in the context of any predictive modeling studies.

A)
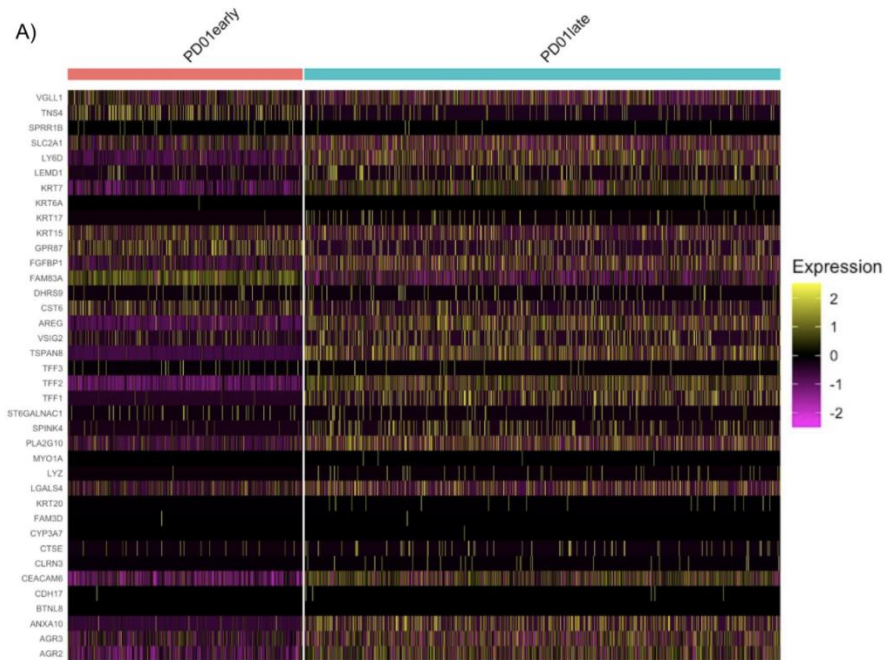
Figure 14: PDO evolves towards molecular subtype admixture over time.

A) Heatmap annotated per cell in Early versus Late PDO culture (columns) and genes (rows) associated with Moffitt Classical and Basal molecular subtypes. PDO1 early expresses genes almost exclusively associated with the Basal Subtype, while many cells within PDO1 late express genes that are either classical or basal in nature.

Chapter 1 Discussion

As a globally utilized backbone of cancer research, established PDAC cell lines have played an indispensable role in enhancing our understanding of disease biology, and therefore, ensuring the accurate characterization of these tools is a prerequisite for ensuring downstream success in translational studies. Using in depth single cell analytics, we demonstrate striking subclonal heterogeneity in the most commonly used PDAC cell lines. While established PDAC models are assumptively oligoclonal and reflect human tumors on a global level based on published data [11,19], the level of subclonal heterogeneity observed on single cell analysis here is unexpected, leading us to propose the phrase "occult polyclonality" as the overarching genomic *sine qua non* of PDAC cell lines. Our data are comparable to the recent findings of Navin, Michor and colleagues, who identified between seven to 22 subclones on scCNV analysis of triple negative breast cancer tumors and cell lines [124].

Notably, these investigators also reported that cancer cells retain a "reservoir" of subclonal diversity, such that isolated single cell clones re-diversify their genomes within a relatively short time frame, at a calculated pace of one CNV event every four cell divisions. In line with this observation, we report that three independent strains of the same PDAC parental cell line (MiaPaCa2) demonstrably deviate from one another on single cell analysis, both in terms of underlying transcriptional profiles and the outgrowth of unique genomic subclones. As another concordant finding between the two studies, we confirm that "major" subclonal genomic events have a significant impact on transcriptomic divergence and clustering, not only within the altered chromosomal loci, but also more broadly in terms of enriched gene sets and pathways. The report by Navin, Michor and colleagues in breast cancer, and our own data in PDAC, harbors the potential to have a profound impact on the rigor and reproducibility of research, both within and across laboratories. For example, it calls into question the assumptions behind isogenic perturbation experiments in cultured cell lines, or the use of archived cell line specific profiling data for drawing inferences that are temporally disparate from the data generation point.

We further show that culturing a PDAC cell line typically grown in adherent monolayers as a spheroid model alters the underlying chromatin architecture and induces a more diverse transcriptional repertoire. In particular, we demonstrate acquisition of transcription factor programs in 3D culture that could confound the interrogation of therapeutic dependencies when compared to the identical cell line grown in a 2D condition. While we do not posit that one culture condition is necessarily more reflective of *in vivo* biology than the other, it is noteworthy that certain dependencies (such as metabolic dependencies) initially identified in monolayer conditions have not subsequently been validated within an *in vivo* context.

As model sophistication increases to more widespread adoption of the PDO format, we also report that, perhaps not unexpectedly, the molecular identities of PDOs tend to evolve over time, recapitulating what is observed with cell lines. In particular, our demonstration of selection against a basal phenotype in a PDO during *ex vivo* culture contributes to the growing body of evidence that therapeutic prediction studies germane to the parental tumor are best limited to

early passages of derivative PDOs. While later passages of PDOs can continue to serve as a *bona fide* preclinical model for PDAC research, they might need periodic re-interrogation with single cell analytics (or a reliable surrogate assay) to measure divergence over time.

Finally, we report here that the commonly used contemporaneous "controls" for PDAC cell lines, especially HPDE cells, are not actually as "normal" as current literature would lead one to believe. Previously undescribed in the literature, we identify considerable subclonal heterogeneity using single cell analysis (with an "occult polyclonality" that mirrors PDAC cell lines), and "major" chromosomal copy number events in HPDE and HPNE that translate to transcriptional upregulation of *AURKA* and *BRCA1*, respectively. Future studies may warrant a thorough investigation of whether omission of these chromosomal events in the context of comparative functional assays led to skewed results. Better yet, the systematic development, characterization, and dissemination of more reliable *in vitro* cell line "normal" controls for PDAC studies may be a requisite for maintaining the rigor of preclinical findings in the field.

Chapter 2: AP1 transcription factor enrichment facilitates resistance to histone deacetylase inhibitors in pancreatic cancers.

Chapter 2 Introduction

Pancreatic ductal adenocarcinoma (PDAC) is the third leading cause of cancer-related death in the United States, with a 5-year survival rate hovering near 5%[1]. Current chemotherapeutic regimens extend survival by merely a few months, while immunotherapy with immune checkpoint inhibitors (e.g. anti-PD1) have essentially led to no meaningful responses in this malignancy. DNA sequencing studies have shown that less than a quarter of PDAC cases harbor actionable DNA mutations[65], although the advent of KRAS inhibitors [125,126,127] has the potential to change the actionable genomic landscape of this malignancy. Moreover, studies using "warm autopsy" tissues in terminal PDAC have demonstrated significant transcriptomic and epigenomic heterogeneity[128,129,130,131], underscoring the need to expand beyond DNA mutations for interrogating potential treatment vulnerabilities. PDAC lesions are known to employ a near-unlimited biological armamentarium to persist and develop therapeutic resistance, included but not limited to repurposing DNA repair pathways, developing new mutations in oncogenic KRAS, upregulating autophagy, and altering their metabolism[132]. Single cell profiling studies in PDAC samples have reiterated the existence of profound transcriptomic subclonal diversity in metastatic PDAC, which likely underlies the divergent therapeutic responses observed in any given patient, and eventual treatment failure[133,134,135]. Thus, elucidating pharmacological vulnerabilities within distinct clonal subpopulations of individual tumors, and how therapeutic agents reprogram subpopulations towards a resistant phenotype, represents a unique opportunity to develop effective precision medicine strategies[13].

In alignment with this goal, a number of clinical trials are now being designed to include biopsies of solid tumors pre- and post-administration of anticancer therapies (Mirati KRYSTAL and Matrix trials, for example), wherein post-treatment biopsies are collected seven days after cycle 1 administration of KRAS G12C inhibitors. Complementary to these approaches are paired preclinical studies utilizing patient-derived organoids to "match" responses on therapy[136]. These

approaches, new as they are, have yet to be applied to modeling responses to epigenetically-targeted agents.

The epigenome of PDAC is of great interest, as recent work has shown that epigenetic reprogramming in the primary tumor can 1) prime neoplastic cells for metastatic dissemination and 2) cause subtype differentiation between the so-called "basal" and "classical" phenotypes in PDAC[49],[137],[138],[139]. One of the most commonly used epigenetic therapies in the clinic is the class of agents known as histone deacetylase inhibitors (HDACi), including vorinostat (SAHA)[140]. Normal cells are relatively more resistant to HDACi-induced cell death as compared to tumor cells [141]. As such, in both solid tumors and leukemias, HDACi are undergoing clinical trials as monotherapy, or more commonly, in conjunction with other epigenetic agents (such as BET bromodomain inhibitors[142], chemotherapeutics, and radiotherapies[143]. One enticing opportunity for HDACi is the potential for combination with immunotherapy, due to preclinical data suggesting that chromatin "marks" can regulate expression of genes involved in immune suppression (e.g., PD-L1). For example, preclinical studies in melanoma models revealed that treatment with class I HDACis upregulated expression of PD-L1 in melanoma samples, leading to enhanced and durable gene expression that could be effectively leveraged with PD-1 blockade treatment to achieve a meaningful clinical response[144]. Unfortunately, in PDAC, the landscape of HDACi has been disappointing, although the mechanistic underpinnings for why these agents have failed are unknown.

AP1 transcription factors (TFs) are widely studied and well known to play critical roles in the development of human cancers, including PDAC[145],[146],[147]. In addition to playing a role in PDAC inhibition in the context of oncogenic mutant-KRAS, the JUN/AP1 family further promotes tumorigenesis by directing cross-talk between epithelial cells and the PDAC tumor microenvironment (TME), with higher AP1 enrichment underlying a more aggressive, poorly-differentiated tumor phenotype[148]. AP1 transcription factors Junb and Fosl1 are also known to

initiate PDAC in the context of KRAS G12D mutations[149]. Previous studies have also suggested that AP1 family members may be enriched following treatment with HDACi[150],[151]. However, it is unknown whether elevated AP1 in pre-treated PDAC lesions may be augmented by treatment with SAHA, representing an innate HDACi-resistance mechanism in PDAC and thus providing one possible explanation for the clinical failures of SAHA monotherapy.

As explained previously, baseline biopsies alone are insufficient to mediate the course of therapy for PDAC patients, as adaptive genetic mutations can occur as early as 1 cycle into a therapeutic regimen, rendering the treatment plan ineffective[152]. Using PDOs to model the acute adaptive mechanisms of response to epigenetic therapy, here we provide a "therapeutically informed" rationale for understanding adaptive resistance. We hypothesized that SAHA-induced epigenetic remodeling of PDAC lesions may be pivotal to treatment failure and tumor progression, and employed patient-derived organoid models (PDOs), paired single-cell RNA sequencing (scRNAseq) + single-nuclei ATAC sequencing (snATACseq), drug validation assays, and multiplexed immunofluorescence (OPAL) in clinical specimens to address this. Ultimately, our data show a consistent pattern of AP1 motif enrichment following SAHA monotherapy. By combining SAHA with potent AP1 inhibitor, T-5224, we report higher PDO cell death with combination therapy than either SAHA or T-5224 monotherapies achieved. Collectively, these data indicate a mechanistic synergy between HDACi and AP1 inhibition that could warrant potent *in vivo* potential.

Materials and Methods included in Chapter 2

Sample acquisition for organoid generation

A patient was recruited at the University of Texas MD Anderson Cancer Center through informed written consent following institutional review board approval (Lab00-396 and PA15-0014). The study was conducted in accordance with Good Clinical Practices concerning medical research in humans per the Declaration of Helsinki. An EUS-FNA biopsy procedure was conducted and

confirmation of pancreatic ductal adenocarcinoma present in biopsy-obtained tissue specimens was provided by a pathologist. The tissue specimens were subsequently delivered to the research laboratory setting, where they were processed for organoid generation.

Organoid generation

Briefly, upon arrival of tissue to the laboratory (within 2 hours of procedure), samples were minced with sterile surgical scalpels to 0.5–1 mm fragments in approximately 1 mL of media (RPMI supplemented with 1% BSA, Thermo Fisher). After centrifugation for 3 minutes at 125 ×g, cells were resuspended in DMEM with 2 mg/mL Dispase (Gibco), 1 mg/mL Collagenase II (Gibco), and 1% penicillin-streptomycin (Corning) and incubated in an orbital shaker for 45 minutes at 37°C. Dispase + Collagenase activity was quenched with 5% FBS, 1% penicillin-streptomycin in DMEM (Wash Media) followed by centrifugation for 5 minutes at 125 ×g. Cells were resuspended in 4 mL TrypIE (Gibco) and incubated in an orbital shaker for 8 minutes at 37°C. TrypIE was quenched with Wash Media, cells were centrifuged again for 5 minutes at 125 ×g, and dissociated cells were counted and resuspended in 350-700uL (depending on cell pellet size) of Geltrex™ LDEV-Free, hESC-Qualified, Reduced Growth Factor Basement Membrane Matrix (Gibco) and plated as domes on a Nunclon Delta Surface 12-well plate (Thermo Fisher). Matrigel was allowed to solidify for up to 45 minutes at 37°C, at which point approx. 1mL of PaTOM media[68] supplemented with Y-27632 dihydrochloride (Tocris) was added to each well of the 12-well plate, to ensure full submergence of organoid domes. Organoids were grown for a minimum of 7 days after seeding before being passaged for the first time.

Characterization of PDO responses to vorinostat and T5224 as single agents

To identify the vorinostat IC50 for each PDO, PDOs were harvested after 7-10 passages (depending on the individual growth rates of each sample for sufficient cell number). For dissociation, PaTOM media was removed and matrigel domes were dissolved using 1mL of Dispase in PBS solution (2mg Dispase/mL PBS added to each well of 12-well plate) at 37°C for

15 minutes with mechanical disruption. PDO cells were collected in a 15mL conical tube, washed with 5mL Wash Media (see above), centrifuged for 3 minutes at 125 ×g, and resuspended in 4mL TrypIE at 37°C until PDOs were fully dissociated into single cells. TrypIE was quenched using Wash Media, and cells were resuspended in PaTOM + 10% matrigel solution for counting and plating at a density of 2,000 cells/well in Ultra Low Attachment clear 96-well round-bottom plates (Corning). PaTOM + 10% matrigel solution was then added to each well for a final volume of 50uL. Following plating, plates were centrifuged at 850 rpm for 5 minutes, and incubated at 37°C. After 2 days, either vorinostat (10mM in DMSO stock, SelleckChem) or T5224 (Cayman Chemical, Item No. 22904) was diluted and administered to PDOs in a dose range of 100pM - 100uM (5 replicates per dose) for a total volume for 100uL per well for each experimental condition. After 5 days, cell viability was measured using CCK8 assay (Dojindo) on a Cytation 5 (BioTek) instrument using Gen5 software. Luminescence values of vorinostat-treated cells were then normalized to media and untreated controls and analyzed for IC50 values using Prism 9 software.

Characterization of PDO responses to vorinostat + T5224 as combination therapies

To identify potential additive impacts of AP1 inhibition with vorinostat in each PDO, PDOs were harvested, dissociated, and plated in 96-well plates as described above. After 2 days, vorinostat (10mM in DMSO stock, SelleckChem) was diluted to a 1uM dose, used as the "base solution" into which and T5224 was diluted for dose combinations of 1uM SAHA + T5224 (100pM - 100uM). Drugs were then administered to PDOs at 5 replicates per dose mixture (1uM SAHA + 100 pM T5224 per 5 replicates, 1uM SAHA + 1nM T5224 per 5 replicates, 1uM SAHA + 10nM T5224 per 5 replicates, and so on) for a total volume for 100uL per well for each experimental condition. After 5 days, cell viability was measured using CCK8 assay (Dojindo) on a Cytation 5 (BioTek) instrument using Gen5 software. Luminescence values of vorinostat-treated cells were then normalized to media and untreated controls and analyzed for IC50 values using Prism 9 software.

Vorinostat treatment to characterize acute PDO response, sequencing library preparation

After 7-10 passages (depending on the PDO line and individual growth rates) of growing as domes submerged in PaTOM, PDOs were dissociated using Dispase and TryplE (described previously), counted, and plated at a density of approximately 500,000 cells/200uL matrigel domes. PDOs were allowed to grow in drug-free media for 5 days, and were then treated with 1uM vorinostat for 24 hours. After 24 hours, ½ of PDO single cell suspensions were harvested for scRNAseq library preparation (3prime, 10x Genomics, target 5,000 cells per sample), and the remaining cells were used for nuclei isolation for snATACseq library preparation according to 10x specifications (10x Genomics nuclei isolation protocol CG000212 Rev D, target 2,000-5,000 nuclei per sample).

Single-cell RNA sequencing and data pre-processing

All sample libraries constructed with 10x Genomics 3prime v3 Chemistry were assessed for quality on Agilent TapeStation 2200 and quantified using both Agilent TapeStation 2200 reagents and Qubit dsDNA HS Reagent kits (Invitrogen Cat. Q33231) before loading onto NextSeq500 (Illumina). Samples were sequenced in paired batches, such that each PDO's treated and untreated datasets were generated simultaneously to avoid introducing batch effects in downstream pairwise scRNAseq analyses. Multiplexed scRNA libraries were sequenced using 150-cycle kits, paired-end, Read 1 26 cycles, Read 2 98 cycles, i7 index 8 cycles, i5 index 0 cycles. Cell Ranger version 2.0 was used to convert Illumina base calls (bcls) to FASTQ files. FASTQ files scRNA were aligned to the reference genome hg19 using files provided by 10x Genomics.

scRNA Seurat analysis of cell lines

Seurat (v3.1)[153] merged analysis was used to profile the scRNAseq data of PDO pairs. Treated and untreated pairs were merged into single Seurat objects (Seurat merge). For removal of

mitochondrial genes in cell lines, we subsetted all cells with less than 20% mitochondrial gene expression. Log normalization, variable feature identification (FindVariableFeatures), z-scoring (ScaleData) were applied to the merged object of all cell lines, and principal component analysis (RunPCA, npcs = 30) and subsequent dimension reduction (UMAP) were applied.

Single-nuclei ATAC sequencing and data pre-processing

Isolated nuclei suspensions were processed using 10x Genomics Single Cell Atac Kit, v1. As with the previously described scRNA libraries, all quantification and quality control was conducted on an Agilent 2200 TapeStation using D1000 High Sensitivity reagents, with additional quantification using Qubit dsDNA HS Reagent kits. A pooled library containing sample-specific treated and untreated PDO sample snATAC libraries was loaded on the NextSeq500 using 150-cycle kits (3 PDO pairs in one sequencing run, 2 PDO pairs in another). Sequencing was done using paired-end, dual-index mode, Read 1 50 cycles, Read 2 50 cycles, i5 index 16 cycles, i7 index 8 cycles. Cell Ranger version 3.1.0 and cellranger-atac version 1.2.0 were used to convert Illumina bcls to fastq files and align samples to reference genome GrCh38 to be compatible for downstream analysis requirements with the Seurat Signac toolkit.

Downstream pairwise analysis of snATACseq data to detect differentially enriched motifs in treatment groups

Using Seurat v3 and its extension package Signac version 1.5.0 (https://github.com/timoast/signac)[114], along with additional R packages for gene annotation (EnsDb.Hsapiens.v86) and the JASPAR 2021 Motif Database (JASPAR2021), 10x genomic output files (metadata, fragments file, fragments index, filtered peak matrices) to generate Seurat objects containing motif information, gene annotations, and genomic ranges. Quality control on nuclei was done by quantifying nucleosome signal, TSS enrichment, number of peaks in fragmentation regions, and nucleosome signal according to Signac software recommendations (TSS Enrichment > 2, nucleosome signal < 10, blacklist ratio < 0.05, percent reads in peaks >

15, peak region fragments between 1,000 and 20,000). PDO sample pairs were normalized using term frequency-inverse document frequency (TF-IDF) normalization, top features were identified, and dimensional reduction using singular value decomposition (SVD) on the TF-IDF matrix using peaks as features was done on both individual samples and a merged analysis object that had been created using fragmentation and peak data to identify common features to use as merging anchors. Motif activities were subsequently calculated using chromVar, as adapted for Signac. We then identified motifs that were enriched in each subcluster per sample, as well as differentially enriched between the two samples of each PDO pair (merged analysis). To correlate regions of chromatin activity with matched scRNA data, per-sample snATAC-Seurat objects containing gene activity data were scaled, normalized, processed with latent semantic indexing (LSI), and UMAP dimensional reduction. We use all peaks that have at least 100 reads across all cells, and reduced dimensionality to 50, as recommended by Seurat guidelines. The processed snATAC dataset was then merged with the previously-described processing of scRNA data for each PDO sample, with merging based on common anchors identified between the datasets, using scRNA data as a reference (FindTransferAnchors), to ensure commonalities and cluster structure between the datasets. Next, gene lists were curated using the GeneCards Human Gene Database- genes specifically activated by each enriched motif were queried and plotted using scRNA data (DotPlot).

Validation of AP1 proteins in HDACi-treated PDOs and Cholangiocarcinoma tissues
Tissue sections of clinical biopsy specimens from Johns Hopkins University were obtained from the lab of Dr. M. Baretti via a Materials Transfer Agreement with the Maitra Lab, approved by MD Anderson Cancer center. For deparaffinization of tissue slides in preparation for multiplexed immunofluorescence staining, slides were warmed at 65C for 90 minutes then rinsed with xylenes (3x10 minutes) followed by rehydration in alcohol dilutions (100%, 95%, 70%, 10 minutes each), rinsing with DI water, and fixation in 10% neutral-buffered formalin (NBF) for 20 minutes. Slides were then microwaved for 15 minutes at 90C (BioGenex EZ-Retriever i6000 system), and

63

stained with The Manual Opal 7-Color IHC Kit (Akoya Biosciences, Cat. NEL811001KT) following

manufacturer protocols and specifications. Antibody dilutions, catalog information, and

incubation times, and Opal color pair are listed below in **Table 3**.

Table 3: Antibody specifications for Opal 7-color IHC kit, used for tissue-based validation of AP1 activation.

Antibody	Order Added	Company	Catalog No.	AR	Dilution	Incubation	Opal
EpCAM	3	abcam	AB71916	9	1/200	O/N	780
aSMA	1	cell signaling	19245S	6	1/1000	1hr	520
JunB/AP-1	2	Novus	NBP1-89544	6	1/200	1 hr	690

After application of all antibodies to tissue specimens, slides were scanned using a Vectra

Polaris Automated Quantitative Pathology Imaging System (PerkinElmer) through the MD

Anderson Cancer Center North Campus Research Histology Core Laboratory with the following

spectral scanning exposure times: DAPI 3.74ms, OPAL-520 40ms, OPAL-690 13.35ms, and

OPAL-780 60ms. Phenochart Whole Slide Viewer Software (Akoya Biosciences) was used for

visualization of fluorescent images, and figure generation. Cell segmentation spectral intensity

quantification was done using VisioPharm software, also through the MD Anderson Cancer

Center North Campus Research Histology Core Laboratory. VisioPharm Software applies a

deep learning algorithm, via the custom development of analysis in-software apps, to segment

tumor cells based on EpCAM staining intensity per image pixel, and subsequently quantify

JunB expression in neural-network-determined tumor regions. Thus, "JunB intensity" as

depicted in Figure 3 and Supplemental Figure 5 represents the JunB median intensity value

after thousands of computational iterations across each pixel on a slide image, measuring JunB

expression in EpCAM-positive tumor-segmented regions of interest across pre- and post-

treatment biopsy samples. Ratio paired t-tests of pre-treatment versus post-treatment JunB

intensities were conducted using Prism 9 software to generate two-tailed p values.

Chapter 2 Results

PDAC organoids demonstrate variable responses to SAHA monotherapy.

Given the inherent heterogeneity of PDAC lesions and the translational applicability of the PDO model to understanding therapeutic responses of this disease[154],[155], we hypothesized that each PDO in this study may have a unique range of sensitivity to vorinostat as a monotherapy. PDOs were generated from pathologically-confirmed PDAC tissue, obtained fresh from lesions that had either been surgically resected or undergone endoscopic ultrasound-guided fine-needle aspiration (see Methods). We first characterized the responses PDOs across a range of doses, and report a relative IC50 of 1uM across all samples (**Fig 15A**). Next, we evaluated scRNAseq data of all PDOs (**Figure 15B**) to investigate whether there were any transcriptional or pathway similarities between the PDOs that may suggest an obvious "innate" resistance mechanism to HDACi, but found no clear patterns of common gene up- or downregulation when querying MSigDB Cancer Hallmark Pathways (**Figure 15C**) or scRNAseq cluster overlap in batch-corrected data between samples (**Figure 16**). This suggests intra-PDO heterogeneity (IPH) is likely a greater determinant of response to SAHA than inter-PDO heterogeneity in the monotherapy context.
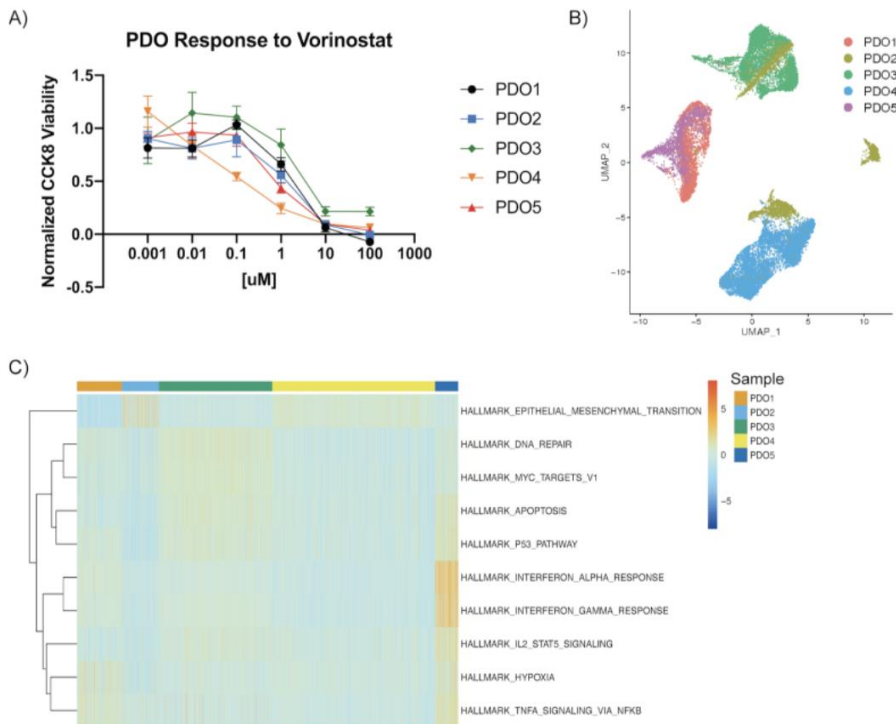
Figure 15: PDAC PDOs are not uniformly sensitive to vorinostat monotherapy.

A) Responses of 5 PDOs to range of vorinostat doses. Y axis = CCK8-measured viability normalized to untreated control cells. X axis = uM of vorinostat administered. Error bars shown for 5 replicates per dose. PDOs plated at density of 1.5k cells per well, and exposed to vorinostat for 5 days. Approximate IC50 = 1uM for all PDOs.

B) Normalized UMAP of scMC-integrated scRNAseq data generated from baseline control PDO samples to profile potential transcriptional commonalities that may predict responses to vorinostat treatment.

C) Heatmap of top 10 differentially enriched Hallmark GSEA pathways in baseline control PDO samples. Data is derived from scRNAseq data using ssGSEA escape package and MSigDB Hallmark Cancer Pathways.
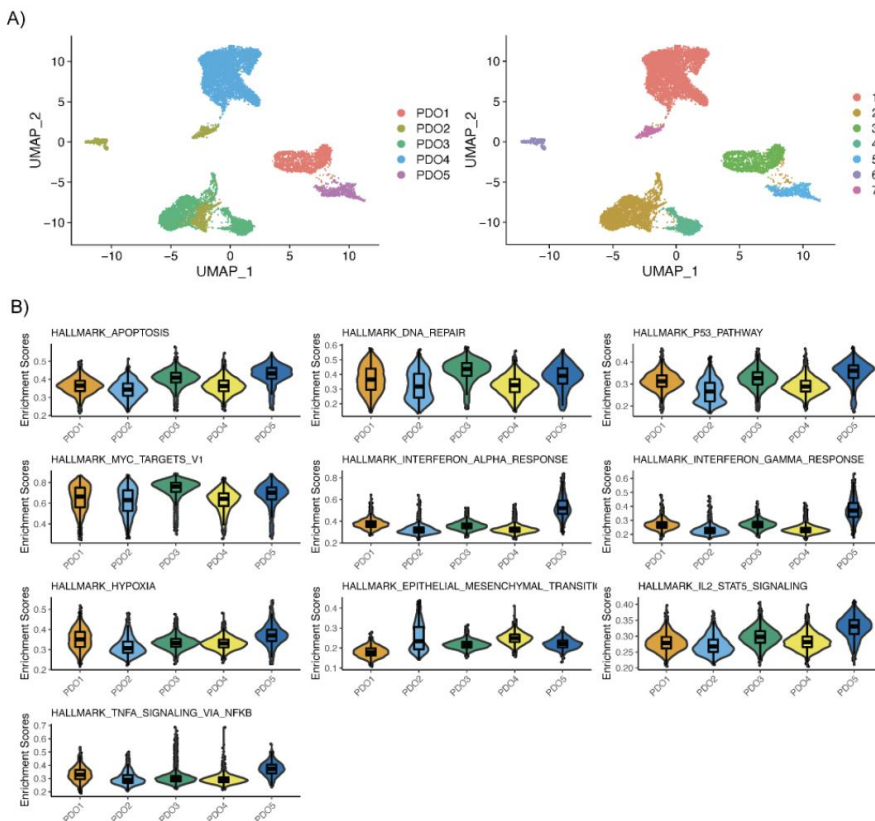
Figure 16: PDAC PDOs are differentially enriched for Hallmark Cancer Pathways.

A) Normalized UMAP of scMC-integrated scRNAseq data generated from baseline control PDOs. Plotted by PDO ID (left) and single-cell clusters (right).

B) Violin plots of comparative enrichment values across Top 10 defining Hallmark GSEA pathways between baseline control PDO scRNAseq samples.

66

AP1 family member motifs and genes are enriched in vorinostat-treated PDAC PDOs.

We next sought to characterize early vorinostat-induced chromatin modifications and their impact on response to HDAC inhibition in PDOs. Briefly, PDAC PDOs were plated and treated with 1uM of vorinostat for a 24-hour period, after which they were harvested for parallel scRNAseq + snATACseq library construction (10x Genomics) and sequencing (Illumina, see Methods). After quality controls of snATACseq libraries, 2 PDO snATACseq datasets had to be excluded from our analysis. However, after analyzing a minimum of 2,000 nuclei per sample with Seurat[32] extension package Signac[33] from the remaining 3 pre- and post-treatment nuclei (PDO2 shown in **Figure 17A**, PDOs 1, 3, and 4 in **Figure 18**), we discovered a clear pattern of AP1 motif enrichment (pval<0.005 for 6 AP1-associated motifs per sample comparison) in post-treatment nuclei compared (**Figure 17B**) to untreated controls (**Figure 17B, Figure 18**). Further, we find an increased number of peaks at loci of genes in the AP1 family[24],[156],[157], such as FOS and JUN (**Figure 17C**). We then validated snATACseq-based AP1 enrichment in our paired scRNAseq data of all 5 PDOs (16,171 control cells, 11,970 vorinostat-treated cells), analyzed with Seurat and scMC[158] algorithms to ameliorate any potential batch effects that might influence our results (**Figure 17D**). We used R package escape[159] with ssGSEA[160] and found broad AP1 pathway enrichment in SAHA-treated samples when analysis across 6 MSigDB AP1-based pathways in 4 of 5 PDO pairs (**Figure 19**, see Methods), in addition to clear expression level changes of individual genes associated with AP1 in all 5 PDO pairs (**Figure 17E**). While briefly described in the introduction of this chapter and by Wu et al. (2021, referenced above), the AP1 family of transcription factors was first discovered in the 1980s with the identification of *v-Fos* and *v-Jun* and their associations with oncogenic viruses, and follow up studies revealed the myriad roles of these transcriptional complexes in cell proliferation, growth, oncogenesis, cell differentiation, and apoptosis[161]. Capable of literally bending DNA as Fos, Jun, and company form complicated heterodimers with each other, the "transcriptional potential" of AP1 family transcription factors is broad and far-reaching, but their unique binding properties make AP1-family-regulated-transcription a highly specific and well-coordinated process[162]. AP1 transcription factors are not

67

ubiquitously expressed- they are present in only select cell types (are highly tissue-specific), and the level of activation of specific family-member components fluctuates depending on extracellular stimuli. While fleshing out all the known mechanisms of AP1 activation and recruitment of transcriptional machinery in different tissues and disease states is not the goal of this dissertation chapter, appreciating the critical role these transcription factors play in cellular growth, differentiation, and tumor progression is critical for conveying the relevance of the discovery of a potential HDACi-attenuated AP1 activation mechanism in pancreatic cancers. Further, pancreatic tumor cells deliberately activating AP1 as a way to skirt death via HDAC inhibitors presents a fascinating role for this developmentally-critical transcriptional family.
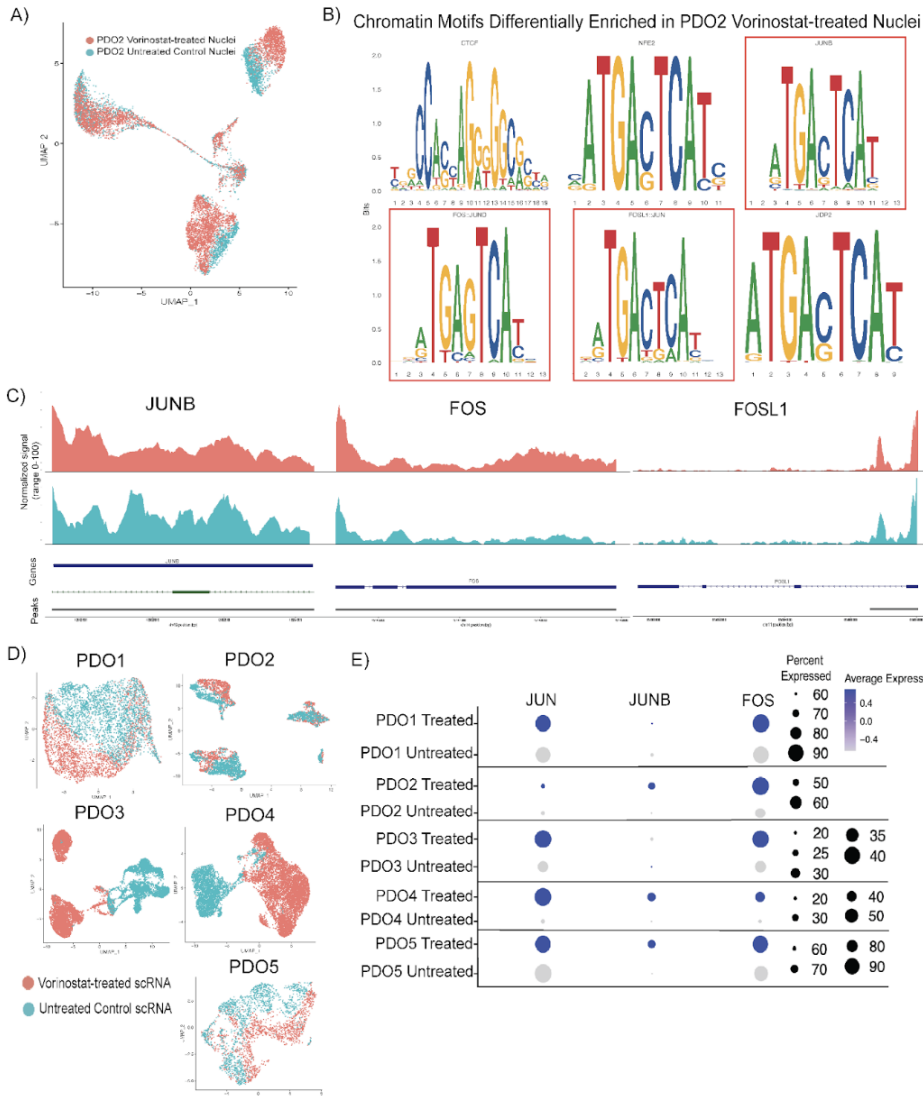
Figure 17: AP1 is enriched in vorinostat-treated PDAC PDOs.

A) UMAP of snATACseq of nuclei harvested from PDO2 comparing vorinostat-treated cells (orange) with untreated controls (teal).

B) Top 6 chromatin motifs (as determined by ChromVAR) differentially enriched in vorinostat-treated over untreaterd nuclei. 3/6 top motifs are AP1-associated (red boxes).

C) Chromatin tracks comparing peak enrichment in treated (orange) versus untreated (teal) nuclei at chromosome locations corresponding to AP1-associated transcription factors.

D) UMAPs of scRNAseq data depicting pairwise comparisons of each PDO sample. Vorinostat-treated cells in orange, untreated control cells in teal.

E) Dot Plots confirming scRNA-based expression of genes associated with AP1 motifs enriched in snATACseq datasets. All pairwise sample comparisons reveal increased expression of AP1-associated genes (JUN, JUNB, FOS) in at least 20% of vorinostat-treated cells.

69

A) PDO1 snATACseq UMAP

B) Chromatin Motifs differentially enriched in PDO1 Treated Nuclei

C) PDO1 snATACseq FOSB + JUN tracks

FOSB

JUN

D) PDO3 snATACseq UMAP

E) Chromatin Motifs differentially enriched in PDO3 Treated Nuclei

F) PDO3 snATACseq, AP1 family tracks

FOSB

JUNB

JUN

G) PDO4 snATACseq UMAP

H) Chromatin Motifs differentially enriched in PDO4 Treated Nuclei

I) PDO4 snATACseq FOSB + JUN tracks

FOSB

JUN

Figure 18: AP1 chromatin motif enrichment pattern conserved across 3 PDOs.

A) UMAP of snATACseq of nuclei harvested from PDO1 comparing vorinostat-treated cells (orange) with untreated controls (teal).

B) Top 6 chromatin motifs (as determined by ChromVAR) differentially enriched in vorinostat-treated over untreated nuclei of PDO1.

C) Chromatin tracks comparing peak enrichment in treated (orange) versus untreated (teal) nuclei at chromosome locations corresponding to AP1-associated transcription factors in PDO1.

D) UMAP of snATACseq of nuclei harvested from PDO3 comparing vorinostat-treated cells (orange) with untreated controls (teal).

E) Top 6 chromatin motifs (as determined by ChromVAR) differentially enriched in vorinostat-treated over untreated nuclei of PDO3.

F) Chromatin tracks comparing peak enrichment in treated (orange) versus untreated (teal) nuclei at chromosome locations corresponding to AP1-associated transcription factors in PDO3.

G) UMAP of snATACseq of nuclei harvested from PDO4 comparing vorinostat-treated cells (orange) with untreated controls (teal).

H) Top 6 chromatin motifs (as determined by ChromVAR) differentially enriched in vorinostat-treated over untreated nuclei of PDO4.

I) Chromatin tracks comparing peak enrichment in treated (orange) versus untreated (teal) nuclei at chromosome locations corresponding to AP1-associated transcription factors in PDO4.
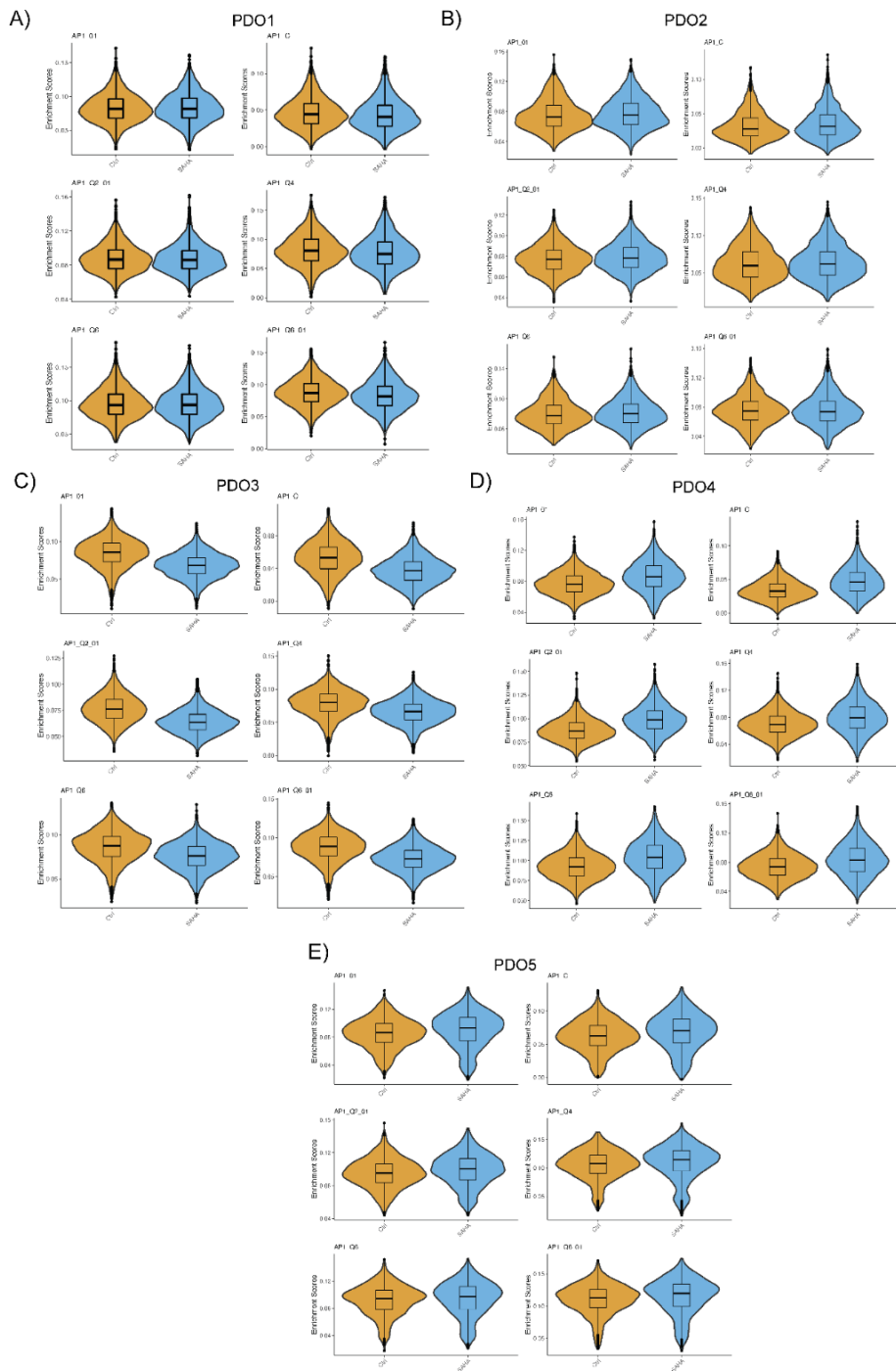
Figure 19: GSEA of MSigDb AP1 pathways confirms broad AP1 activation in ⅘ PDOs.

A-E) Violin plots of pathway enrichment scores in vorinostat-treated (blue) versus untreated control (yellow) scRNAseq data of 5 PDOs.

71

Combination with AP-1 inhibition enhances sensitivity to HDACi in PDAC.

Because the pattern of AP1-motif enrichment at either the chromatin, RNA, or both datasets was apparent across this cohort of PDOs, we that inhibiting the AP1 pathway was the most obvious mechanistic target to prevent PDAC cells from developing SAHA resistance. Using a high-throughput drug screen format (see Methods) and potent AP1 inhibitor T-5224[163],[164], we treated each PDO with a range of doses of T-5224 monotherapy, SAHA monotherapy, and a combination regimen of 1uM SAHA + varying T-5224 doses (see Methods). We report that while T-5224 at any dose did not impact PDO viability (**Figure 20A**, blue), combination of 1uM SAHA + T5224 did lower PDO viability at all T5224 doses administered (**Figure 20A**, red), achieving lower cell viability than 1uM SAHA alone (**Figure 20A**, black line). The combination result evidentiates a true HDACi + AP1i synergy that may be successfully leveraged in the *in vivo* or clinical settings to bolster the anti-cancer potency of vorinostat. Given these results, we wondered whether pretreatment expression of AP1 genes might have predictive value in determining a patient's response to SAHA monotherapy. Upon correlation analysis of scRNAseq-derived average expression of Fos and Jun in untreated PDO cells with PDO viability at 1uM SAHA (**Figure 20B**), we find no correlation whatsoever (FOS R^2 = 0.4977, JUN R^2 = 0.0604).

To confirm that AP1 transcription factors were being upregulated in a clinical setting following HDACi administration, we applied multiplexed immunofluorescence (mIF, AKOYA Biosciences OPAL kit, see Methods) to biopsies obtained pre- and post- administration of HDACi entinostat + pembrolizumab of cholangiocarcinoma samples. Unlike vorinostat, which is a pan-HDACi, entinostat only inhibits HDACs of Class I[165], therefore has a more limited repertoire of functional capability, and may not have as profound a chromatin remodeling impact on tumor cells as pan-HDACi compounds.

Consistent with our goal to profile the acute responses and epigenetic remodeling induced by HDACi in GI tumors, all "post" biopsies were collected following administration of Cycle 1 of therapy to patients. Indeed, we find that in 7/11 patients' post-treatment biopsies, AP1-family member JunB was widely upregulated in tumor epithelial cells (EPCAM) at the protein

level, and not in fibroblasts (αSMA) comprising the adjacent tumor microenvironment (Ratio paired t-test of pre- vs post-treatment JunB intensity values, two-tailed pval = 0.0116, **Figures 20C-E**). Clinically, all 11 patients in this Phase I trial progressed on therapy, suggesting that there may be a range of potential resistance mechanisms at play in cholangiocarcinomas including but not limited to AP1 activation.

The caveats of these mIF validation results, of course, are the small sample size, and most obviously the fact that these cholangiocarcinoma patients were given an immunomodulatory drug in addition to an HDAC inhibitor. It is absolutely reasonable to assume that, given the role immunotherapies play in reshaping the TME as well as primary tumor cells, patients in this cohort may have had better responses to the combinatorial regimen, and AP1 upregulation in primary tumor cells as a resistance mechanism to HDACi may have been ablated by pembrolizumab while the tumor cells opted for a different, currently unknown mechanism of resistance. Regardless, 7/11 patients with increased JunB in post-treatment biopsies still represents >60% of a cohort, and provides support for a model wherein HDACi induces an enrichment of AP1 motifs in tumor epithelial cells, and likely other gastrointestinal malignancies, which can then be attenuated to achieve tumor cell death.
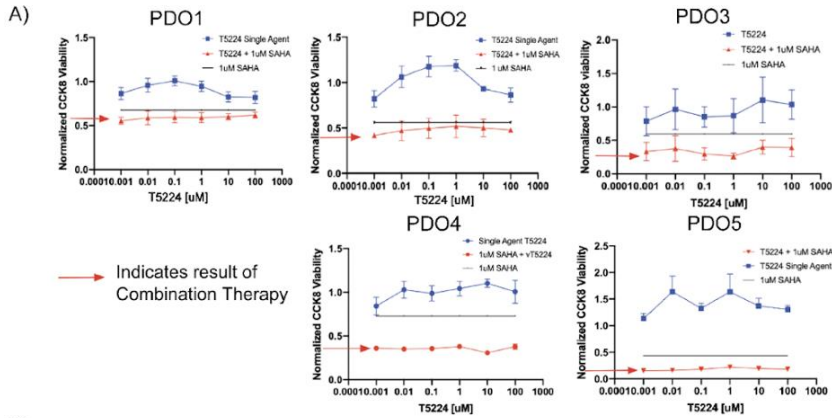
Figure 20: Characterization of AP1 attenuation in PDAC PDOs and clinical cholangiocarcinoma samples.

A) Responses of 5 PDOs to single agent AP1 inhibitor T5224 (blue), 1uM vorinostat (black line), and combination 1uM Vorinostat + variable T5224 doses (red line). Y axis = CCK8-measured viability normalized to untreated control cells. X axis = uM of vorinostat administered. Error bars shown for 5 replicates per dose. PDOs plated at density of 1.5k cells per well, and exposed to vorinostat for 5 days.
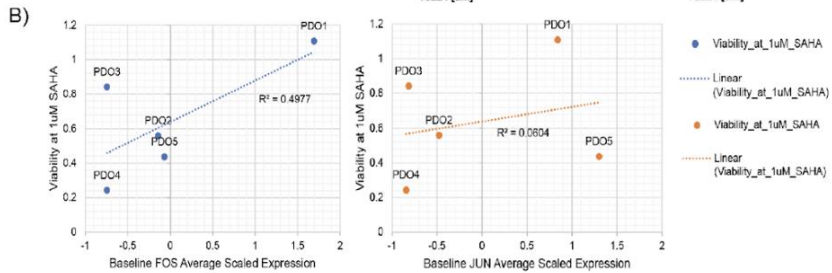
B) Linear regression of average baseline FOS and JUN expression in PDAC PDOs shows no significant correlation with PDO response to vorinostat.
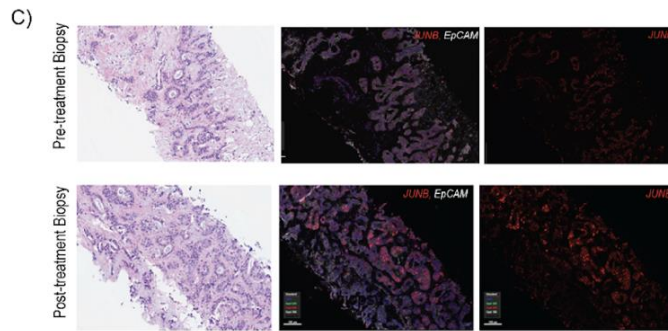
C) Multiplexed immunofluorescence of pre- and post-entinostat+pembrolizumab biopsies of cholangiocarcinoma tumor tissue. Post-treatment biopsy shows a global increase of JUN expression in EPCAM tumor cells, corroborating PDO scRNAseq findings that HDACi activates AP1 to promote tumor cell survival. Bars represent quantified median JunB intensities across EPCAM-positive tumor areas at each timepoint.
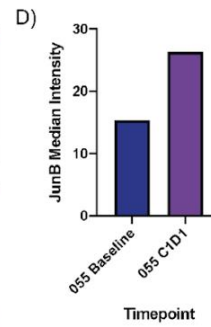
D) Quantification of total JunB staining intensity across all pixels using AI-based Visiopharm Software shows increased JunB in EpCAM-positive tumor cells in exemplary post-treatment biopsy sample compared to baseline.
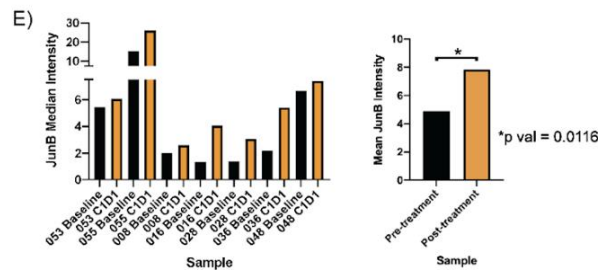
E) Quantification of total JunB staining intensity across all pixels using AI-based Visiopharm Software shows increased JunB in EpCAM-positive tumor cells in 7 patient biopsy pairs. Ratio t-test two-tailed p value = 0.0116.

Chapter 2 Discussion

Determining mechanisms of adaptive resistance to anticancer therapies represents a critical effort to improve clinical outcomes for pancreatic cancer patients. Here we provide evidence to suggest that PDAC, and potentially other GI malignancies, selectively activate AP1 transcription factors as a response to HDAC inhibition. In addition to initiating pancreatic cancer in the context of oncogenic mutant-KRAS, the JUN/AP1 family further promotes tumorigenesis by directing cross-talk between epithelial cells and the PDAC tumor microenvironment (TME), with higher AP1 enrichment underlying a more aggressive, poorly-differentiated tumor phenotype. However, it was unknown whether AP1 motif enrichment or baseline expression of AP1-family constituent genes in pre-treated pancreaticobiliary lesions may be augmented by treatment with SAHA, representing an innate HDACi-resistance mechanism in PDAC and thus providing one possible explanation for the clinical failures of SAHA monotherapy.

We show here that tumor cell remodeling brought on by AP1 activation, at the very least, staves off tumor cell death, decreases HDACi potency, and results in the survival of a more resistant cell population and tumor persistence. By inhibiting AP1 in combination with HDACi agents, increased tumor cell death can be achieved. While we do demonstrate inter-sample heterogeneity that impacts measurable PDO responses, the trend of AP1 activation is conserved across 5 different patient models in vitro by multimodal sequencing and profiling approaches, and further confirmed in clinical patient samples (7/11 patients). The caveats of our mIF validation results, of course, are the small sample size, and most obviously the fact that these cholangiocarcinoma patients were given an immunomodulatory drug in addition to an HDAC inhibitor. Further, entinostat may not have as profound a chromatin remodeling impact on tumor cells as pan-HDACi compounds, and may have even less of an AP1-activating effect in a GI tumor type with a markedly different TME composition. It is absolutely reasonable to assume that, given the role immunotherapies play in reshaping the TME as well as primary tumor cells, patients in this cohort may have had better responses to the administered combinatorial

regimen. AP1 upregulation in primary tumor cells as a resistance mechanism to HDACi may have been ablated by nivolumab while the tumor cells in the 4/11 patient samples that did not show elevated JunB in post-treatment biopsies opted for a different, currently unknown mechanism of resistance. Regardless, 7/11 patients with increased JunB in post-treatment biopsies still represents >60% of a cohort, and provides support for a model wherein HDACi induces an enrichment of AP1 motifs in tumor epithelial cells, and likely other gastrointestinal malignancies, which can then be attenuated to achieve tumor cell death.

Ultimately, this biological paradigm would benefit from further in vivo study and validation, as well as characterizing the degree of AP1 activation across other HDAC inhibitors not tested in the studies presented here. This study also provides a rationale to support characterization of the acute, early responses of tumor cells to therapeutic administration. We show that PDAC epithelial cells that persist after therapeutic administration are indeed more aggressive, and could thus comprise the predominating resistant cell populations in even a small subset of patients who eventually fail on therapy.

Chapter 3: Mechanisms of innate and adaptive resistance to direct KRAS small molecule inhibitors in pancreatic cancer, a preliminary investigation.

Chapter 3 Introduction

More than 90% of PDACs harbor KRAS mutations, and oncogenic Ras signaling is implicated in both tumor initiation and maintenance. Until recently, Ras was considered the "undruggable" oncogenic driver in PDAC, as developing effective targeted therapeutic strategies had proven challenging, as designing compounds or strategies optimized to targeting a small membrane-bound GTPase is apparently a very serious biochemical undertaking. Because of this, scientists in recent decades (yes, decades) have employed an abundance of strategies to target Ras pathway-adjacents (MEK, ERK, SOS, mTOR, RTK, etc[166]) across a wide breadth of cancers. In other words, we've truly tried *everything* we could think of when it comes to targeting Ras and understanding its biology. As if the technical challenges weren't great enough, the toxicities associated with drug combinations targeting downstream effectors like PI3K and MAP kinase have also posed a challenge to therapeutic administration. The discovery of direct allele-specific KRAS inhibitors (including the approval of the first inhibitor against KRAS G12C in lung cancer[167]) has the potential to transform the landscape of RAS-targeted therapeutics. However, resistance of tumor cells through adaptive genomic and non-genomic mechanisms, as well as altered metabolism and heterotypic cellular interactions within the tumor microenvironment (TME) will likely prevent monotherapies from producing durable responses[168],[169]. With many promising new KRAS-targeting therapies on the horizon, we are on the cusp of a potential paradigm shift in treatment for PDAC patients, and there is an urgent need to understand how to effectively implement Ras inhibition to maximally benefit patients.

The KRAS G12C mutation (G12C*) is present in approximately 1.6% of all PDACs, representing a rare but important mutational cohort of this disease. Mirati Therapeutics has developed a KRAS G12C* inhibitor (Adagrasib) and has begun clinical trial recruitment at MD Anderson for the first PDAC-centric trial of Adagrasib in KRAS G12C mutant-cases (MATRIX trials). Through the MDACC-Mirati alliance and the BTC initiative, the Maitra Lab, during the last part of my doctoral training, has been receiving pre- and post-treatment biopsies for generating

patient-derived organoid (PDOs) to "phenocopy" the disease course of patients in the clinic, and to interrogate resistance mechanisms in tumor cells exposed to Ras inhibition. As very preliminary work on these projects, I have begun to conduct PDO-based assays across a panel of KRAS G12C* inhibitors (MRTX849, AMG510, BI-3911 and BI-0800) to understand differential evolution in preclinical specimens, as each of these inhibitors targets mutant Ras in slightly different ways (more on this later).

In addition to being able to study the impacts of inhibiting the KRAS G1C mutation, preclinical modeling of response and resistance to inhibitors targeting mutant KRAS G12D (G12D*) in PDAC PDOs is also a key part of these study goals. The KRAS G12D* is present in nearly 41% of PDAC. Thus, the availability of the first two KRAS G12D inhibitors (MRTX1133 and BI-3052310) opens up yet another realm of possibilities for targeting mutant KRAS in PDAC due to the significant frequency of this alteration in patient populations. As such, I have begun to assess the efficacy of both KRAS G12D inhibitors in a panel of PDOs bearing KRAS G12D*.

Mutationally-specific Ras inhibitors provide boundless opportunities for many exciting experiments, but it is worth describing other important, mutationally-agnostic Ras-targeting agents that have been developed in recent years and are now also at the disposal of the Maitra Lab as a function of collaborations with MD Anderson's TRACTION platform. In 2019, Boehringer-Ingelheim announced the development of "pan-KRAS" inhibitors (BI-1701963 as an example), some of which are now undergoing study in clinical trials[170]. Very generally speaking, this class of RAS inhibitors tends to function as protein-protein inhibitors targeting the molecular interaction between SOS1 (Son of sevenless homolog 1) with KRAS, locking KRAS into the GDP-bound (off) state[171]. Often referred to in the literature as the "pacemaker" of KRAS, SOS1 binding GDP-KRAS catalyzes KRAS's cycling into its GTP-bound (on) state. SOS1 inhibition does appear to lead to antiproliferative effects in some cancer types[172], and are anticipated by the research community to yield adaptive resistance mechanisms in tumors[173], [174] similar to what has been observed and reported for the mutation-specific KRAS inhibitors. This mechanism is not to

be confused with an *even newer* class of "pan-RAS" inhibitors, which are rumored to work by binding KRAS G12D* in the GDP-bound state. These compounds are off-label, and I am scared of lawyers. For this reason, I will not be disclosing the name of the pan-RAS, GDP-binding inhibitory compound we've been given, I am utterly ignorant of its structure and direct binding sites to the Off-RAS protein, and am writing these words now to protect myself from legal prosecution and prevent accidentally spilling any industry secrets. This is a non-disclaimer disclaimer. Regardless, the applicability, efficacy, and adaptivity of these inhibitors with pancreatic malignancies remains unknown. Ultimately, the performance of these "more agnostic" agents against the mutationally-specific inhibitors described here will be explored by Maitra Lab members after I've departed from the group, using the experimental frameworks for evaluation that I've established.

An important note on the biological context of the samples discussed in this chapter: at the time of presentation to the clinic for trial recruitment and sample acquisition for PDO generation, the far majority of MD Anderson PDAC patients have advanced disease. Many have already been given and failed standard-of-care (SOC) regimens like Gemzar + Abraxane or FOLFIRINOX. Therefore, the "pre-treatment" biopsy samples the Maitra Lab receives refers only to pre-G12Ci/G12Di, and not "treatment naive". What we are able to evaluate as "adaptive response" following the administration of KRAS inhibitors, then, is in the context of a tumor that is *already resistant* to standard of care. What we are interested in exploring, given these clinical histories, is what additional genomic aberrations, transcriptional adaptations, or metabolic disruptions might be *further introduced* by a RAS inhibitor, and determining whether viable treatment options may be predicated upon profiling drivers of tumor evolution.

Materials and Methods included in Chapter 3

Organoid generation

Briefly, upon arrival of tissue to the laboratory (within 2 hours of procedure), samples were minced with sterile surgical scalpels to 0.5–1 mm fragments in approximately 1 mL of media

(RPMI supplemented with 1% BSA, Thermo Fisher). After centrifugation for 3 minutes at 125 ×g, cells were resuspended in DMEM with 2 mg/mL Dispase (Gibco), 1 mg/mL Collagenase II (Gibco), and 1% penicillin-streptomycin (Corning) and incubated in an orbital shaker for 45 minutes at 37°C. Dispase + Collagenase activity was quenched with 5% FBS, 1% penicillin-streptomycin in DMEM (Wash Media) followed by centrifugation for 5 minutes at 125 ×g. Cells were resuspended in 4 mL TryplE (Gibco) and incubated in an orbital shaker for 8 minutes at 37°C. TryplE was quenched with Wash Media, cells were centrifuged again for 5 minutes at 125 ×g, and dissociated cells were counted and resuspended in 350-700uL (depending on cell pellet size) of Geltrex™ LDEV-Free, hESC-Qualified, Reduced Growth Factor Basement Membrane Matrix (Gibco) and plated as domes on a Nunclon Delta Surface 12-well plate (Thermo Fisher). Matrigel was allowed to solidify for up to 45 minutes at 37°C, at which point approx. 1mL of PaTOM media[175] supplemented with Y-27632 dihydrochloride (Tocris) was added to each well of the 12-well plate, to ensure full submergence of organoid domes. Organoids were grown for a minimum of 7 days after seeding before being passaged for the first time.

Characterization of PDO responses to KRAS inhibitors

To identify IC50 values across samples for each inhibitor employed in this study, PDO cells were harvested after 2-4 passages (depending on growth rates for sufficient cell number). The same method was followed for each KRAS G12D* PDO (AM67, MS05, and Panc1 cells grown as 3D spheroids) used to study responses to G12D* small molecule inhibitors. For PDO matrigel dissociation, PaTOM media was removed and matrigel domes were dissolved using 1mL of Dispase in PBS solution (2mg Dispase/mL PBS added to each well of 12-well plate) at 37°C for 15 minutes with mechanical disruption. PDO cells were collected in a 15mL conical tube, washed with 5mL Wash Media (see above), centrifuged for 3 minutes at 125 ×g, and resuspended in 4mL TryplE at 37°C until PDOs were fully dissociated into single cells. TryplE was quenched using Wash Media, and cells were resuspended in PaTOM + 10% matrigel solution for counting and plating at a density of 2,000 cells/well in Ultra Low Attachment clear 96-well round-bottom

plates (Corning). PaTOM + 10% matrigel solution was then added to each well for a final volume of 50uL. Following plating, plates were centrifuged at 850 rpm for 5 minutes, and incubated at 37°C. After 2 days, vorinostat (10mM in DMSO stock, SelleckChem) was diluted and administered to PDOs in a dose range of 100pM - 100uM (5 replicates per dose) for a total volume for 100uL per well for each experimental condition. After 5 days, cell viability was measured using CCK8 assay (Dojindo) on a Cytation 5 (BioTek) instrument using Gen5 software. Luminescence values of G12Ci-treated cells were then normalized to media and untreated controls and analyzed for IC50 values using Prism 9 software.

Chapter 3 Background and Significance

The overarching goal of this proposal is to elucidate the molecular mechanisms of resistance against recently developed allele-specific KRAS inhibitors in PDAC. As part of a strategic alliance between MDACC and two companies developing direct KRAS inhibitors - Mirati Therapeutics and BI, we will have access to three KRAS G12C inhibitors (adagrasib [clinical], BI-3911 and BI-0800 [preclinical]), to the first ever KRAS G12D inhibitors (MRTX1133, and BI-3052310), and to a preclinical investigative pan-RAS inhibitor, BI-6674 for preclinical studies (**Table 4**). Ras normally functions as a molecular switch that cycles between an active, guanosine-5'-triphosphate (GTP)-bound state and an inactive, guanosine 5′-diphosphate (GDP)-bound form[122] (**Figure 21**). Oncogenic mutations in KRAS typically increase the steady-state levels of Ras in the GTP-bound state capable of driving pro-tumorigenic signaling through downstream effector pathways. Genetic ablation of KRAS expression leads to cell cycle arrest and death in cell line models and potent tumor regressions in animal models of PDAC[176],[177],[178]. Drug combinations that inhibit Ras downstream signaling can have potent anti-tumor effects but efficacy has been limited by toxicity in patients. Recent advances in medicinal chemistry have enabled development of direct small molecule inhibitors of KRAS, including most notably covalent inhibitors of the KRAS G12C and G12D oncoproteins that impair oncogenic signaling and cause tumor regressions in preclinical models[179].

Table 4: Investigational covalent KRAS inhibitors employed for study in PDAC PDOs.

Compound	KRAS allele	Company	Targeted KRAS on/off state
AMG510	G12C	Amgen	OFF
MRTX849	G12C	Mirati Therapeutics	OFF
BI-0800	G12C	Boehringer Ingelheim	ON
BI-3911	G12C	Boehringer Ingelheim	OFF
BI-3052310	G12D	Boehringer Ingelheim	OFF
MRTX1133	G12D	Mirati Therapeutics	OFF

Figure 21: Current small molecule approaches to inhibiting mutant KRAS G12C oncogenic signaling.

A) Schematic of covalent KRAS inhibition molecular strategies, adapted from Cox and Der, Science 2021, with addition of investigational compounds BI-0800 and BI-3911.
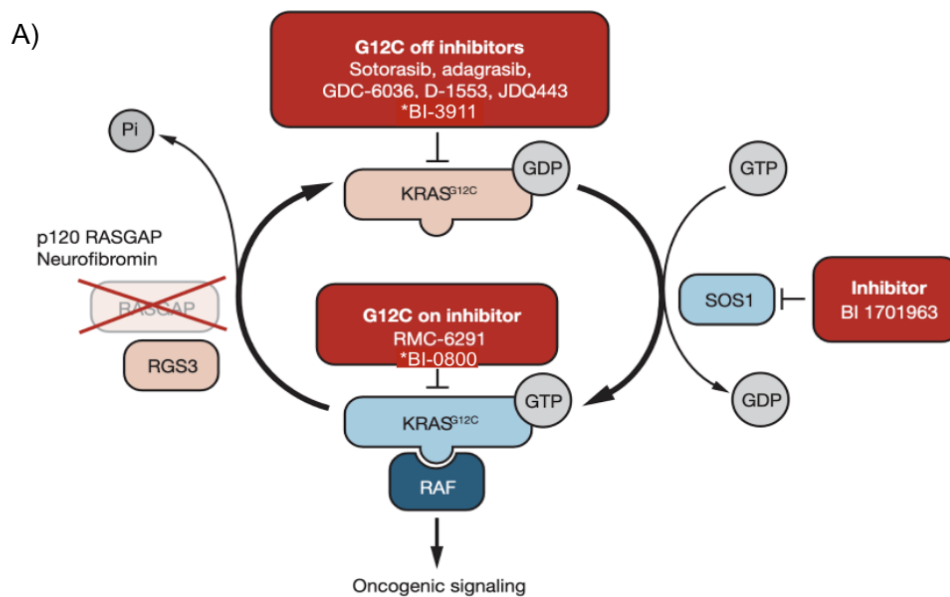
To study the impact of these inhibitors in the translational preclinical setting, I have employed PDOs and sought to "repurpose" experimental and sequencing methodologies developed and described in Chapter 2. In those experiments, I demonstrated that single cell RNA sequencing (scRNAseq) profiles from PDAC PDOs can be derivatized using appropriate bioinformatics pipelines to "match" with vulnerability signatures to specific pharmacological agents, including clinically feasible combinatorial regimens. As an example of preliminary data to demonstrate technical feasibility for proposed approaches, as described in Chapter 2, scRNAseq and snATACseq of vorinostat-treated PDOs finds a limited repertoire of actionable transcription factors (TFs) that is enriched within the resistant subclone, the inhibition of which could overcome the observed resistance to epigenetic therapies in PDAC. Given the success of this method in identifying complex mechanisms of resistance to therapeutic agents, it is my intention to use this platform to elucidate the mechanisms of resistance to KRAS-based therapies in PDOs, and in post-treatment biopsies from the 1st G12C trial (Mirati) ever conducted in pancreatic cancers. Additionally, I will be extending these approaches to a panel of KRAS G12D* PDOs to elucidate endogenous, underlying mechanisms of resistance to this even-newer class of small molecule inhibitors for pancreatic cancers. PDOs of both mutational backgrounds will eventually also be studied using pan-Ras inhibitors, as a point of comparison between upstream pathway inhibition of RAS versus targeting specific aspects of the mutant Ras protein complexes.

Chapter 3 Results

Preclinical assessment in G12C* PDOs shows differential small molecule sensitivity to KRAS inhibition.

Early clinical trials of two different KRASG12C inhibitors, sotorasib (AMG510) and adagrasib (MRTX849), have shown promising efficacy in non-small cell lung cancer (NSCLC) and colorectal cancer (CRC)[180],[181],[182],[183],[184]. While KRAS G12C mutations are rare in PDAC, multiple PDAC patients have now been treated with either sotorasib or adagrasib, with several patients demonstrating significant clinical benefit from these agents. Most notably, the KRYSTAL-1 study

of adagrasib monotherapy in KRAS G12C* tumors included ten PDAC patients who received the recommended phase II dose of the drug as second or third-line therapy (after standard chemotherapy). All ten (100%) of these patients received clinical benefit from the therapy, with five patients exhibiting partial responses (PR). Progression-free survival (PFS) for this small cohort of patients treated with adagrasib was 6.3 months – a remarkable observation. These data suggest that direct KRAS inhibition can confer substantial clinical benefit to PDAC patients, even in advanced, previously treated disease where patients have no other effective options. My own preliminary data, however, shows that G12C* PDOs do indeed harbor differential sensitivity to KRAS-on (BI-0800) versus KRAS-off (MRTX849, AMG510, BI-3911), with the singular KRAS-on compound in this assay being significantly more potent than the KRAS-off competitors (**Figure 22A**).
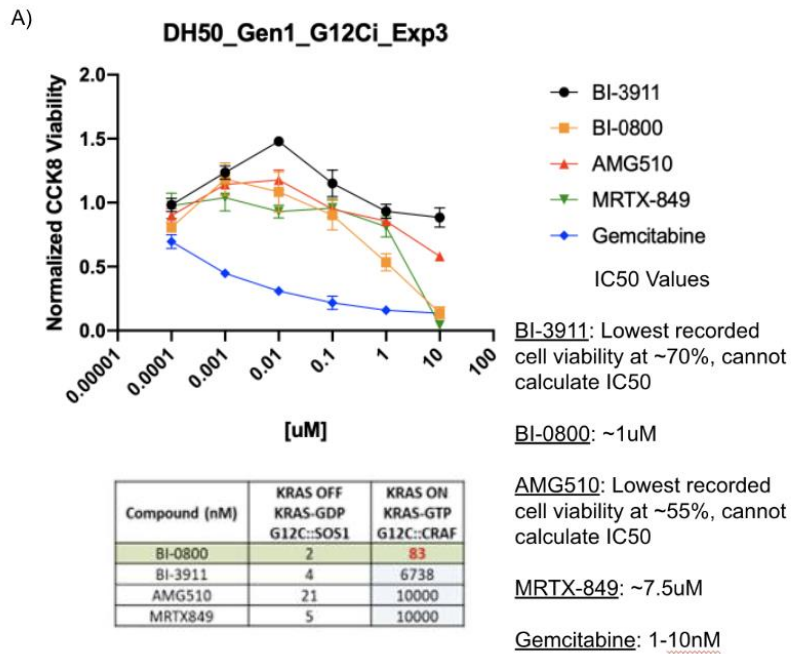
Figure 22: Preliminary data characterizing differential responses to KRAS G12C inhibition in G12C* PDAC PDO sample.

A) Preliminary characterization of response to KRAS G12C inhibitors in G12C* PDO shows increased sensitivity to KRAS-off BI-0800, while exhibiting a resistance phenotype to all other KRAS inhibitors in this panel.

B) scRNAseq profiling of rare KRAS G12C* organoid.

IC50 Values

BI-3911: Lowest recorded cell viability at ~70%, cannot calculate IC50

BI-0800: ~1uM

AMG510: Lowest recorded cell viability at ~55%, cannot calculate IC50

MRTX-849: ~7.5uM

Gemcitabine: 1-10nM

Compound (nM)	KRAS OFF KRAS-GDP G12C::SOS1	KRAS ON KRAS-GTP G12C::CRAF
BI-0800	2	83
BI-3911	4	6738
AMG510	21	10000
MRTX849	5	10000
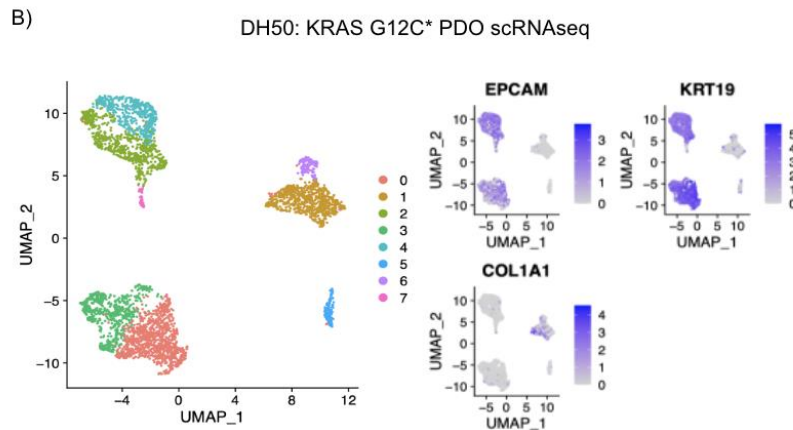
Thus, as future work following the completion of my doctoral studies, I will validate these reported findings in PDOs from patients enrolled in a multi-center clinical trial of KRAS G12C inhibitor adagrasib (MATRIX trial led by Dr. Pant at MDACC), and will deeply interrogate human biospecimens from this trial to understand response and resistance, ultimately enabling rational design of future KRAS inhibitor strategies.

PDAC PDOs develop resistance to KRAS inhibition after long term treatment with small molecule inhibitors.

In this part of my work, I hope to identify and validate KRAS G12Ci resistance mechanisms discovered in longitudinal PDO studies as a preclinical correlate to clinical evolution of therapeutic resistance. Patients enrolled in the MATRIX trial (PI Pant) will undergo longitudinal follow up with liquid biopsies and tumor biopsies at the time of eventual progression on therapy. As published by Awad[150] and others[185], treatment with KRAS inhibitors may allow for the proliferation of "baseline present" low-frequency sub-clonal populations which may provide mechanisms of secondary resistance likely evident in post-treatment biopsies. Convoluting the potential evolved resistance mechanisms to RAS inhibition in PDAC are recent studies showing that while KRAS signaling plays a critical role in shaping the PDAC tumor microenvironment (TME)[181], remodeling of the TME enables PDAC to bypass its dependency on oncogenic KRAS and develop secondary survival pathways[186]. Eventually, understanding how KRAS inhibition impacts both PDAC lesions and the surrounding TME will be a top priority for developing therapeutic strategies in the clinic. In the PDO context, 1 PDO sample does indeed have autologous fibroblasts in co-culture with epithelial cells, allowing us to study (albeit in a very limited fashion) the potential differential impacts of KRAS inhibitory molecules in both PDAC tumor epithelial cells and cancer-associated fibroblasts (CAFs). MRTX849 and BI-0800 were the most potent G12C inhibitors against this PDO sample (**Figure 22**), and were therefore selected for long term study. As a "first step" in studying the evolution of resistance, a series of long term PDO cultures were established: G12C* PDO DH50 was grown under three culture conditions: 1) untreated control, 2) treatment at IC50 of MRTX849, and 3) treatment at IC50 of BI-0800 (**Figure 23A**). Dosing of KRAS inhibitors was doubled every 2 passages, until a dose was reached where PDO cell growth was unrestrained by the administration of increasingly high doses of KRAS inhibitor (**Figure 23B**).

Figure 23: A) Schematic of G12Ci longterm PDO culture experiments for the identification of evolved resistance mechanisms. **B)** Brightfield images (10x) of long term PDO-DH50 cultures after dose escalation reached 8uM.

A)

B)

Untreated Control	BI-0800 8uM	MRTX849 8uM

Untreated Control PDOs are visibly smaller and less dense compared to treated cultures

Fibroblasts are healthier and more numerous in BI-0800 cultures
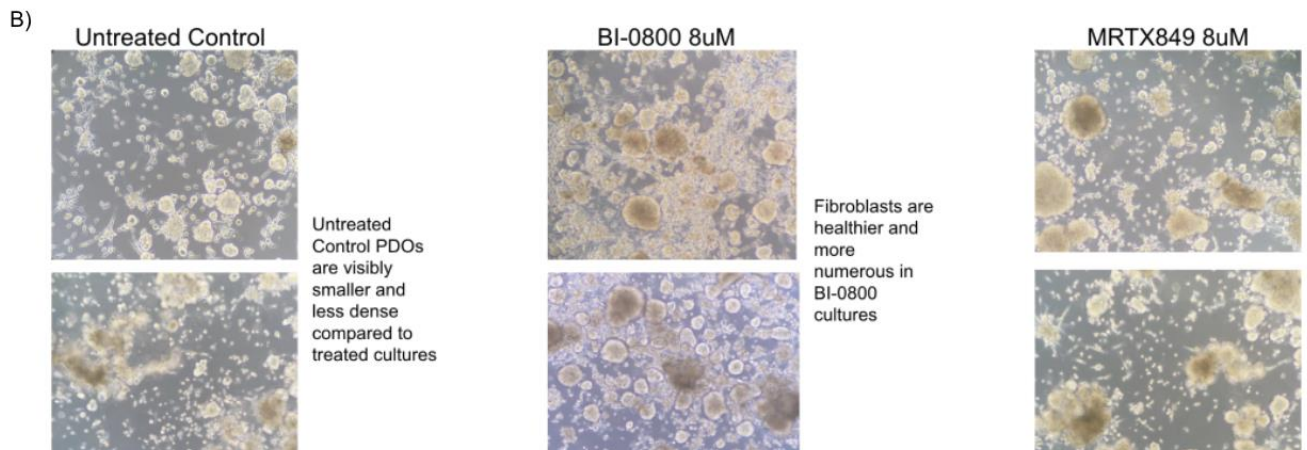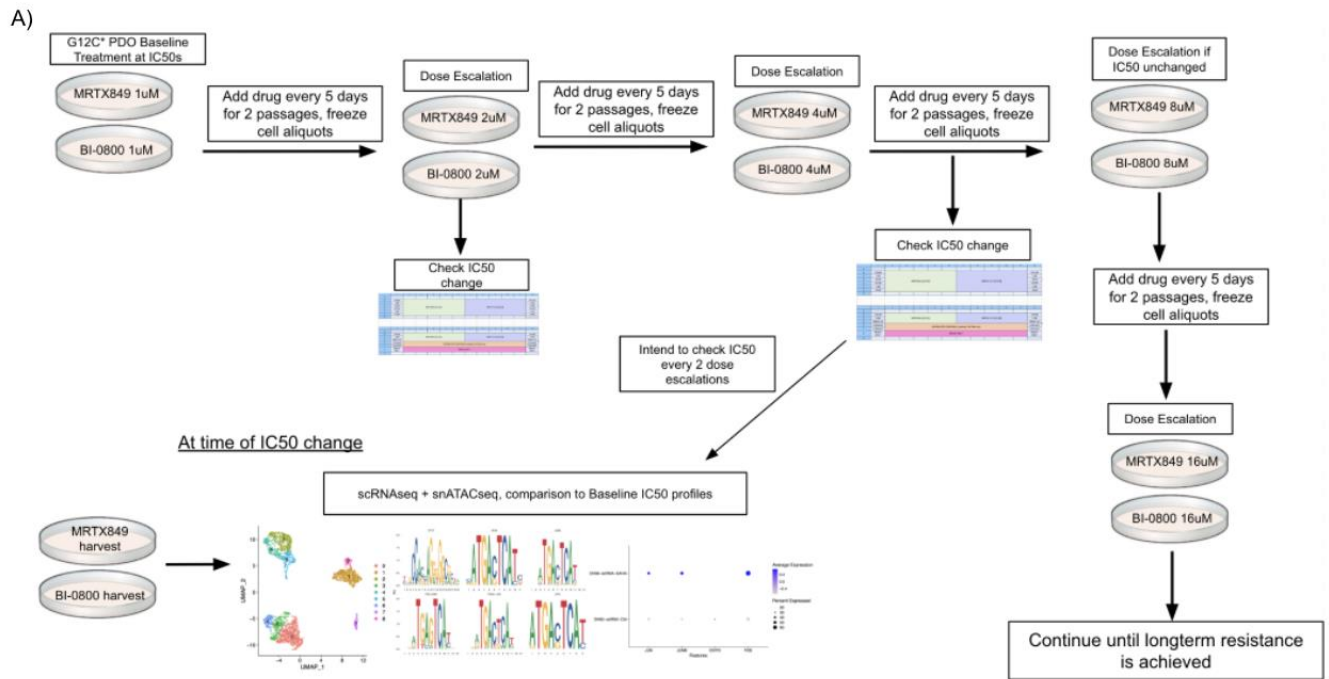
Upon rechallenging the long term- treated PDOs with the range of G12Ci doses from which initial, acute sensitivity was determined, we report that the IC50s for both MRTX849 and BI-0800 have indeed shifted right-ward in sample DH50, when compared to the long term untreated controls. This indicates that drug resistance has been achieved in this specimen for both inhibitors, when factors endogenous to in silico drift are accounted for (**Figures 24A, 24C**). However, upon comparison of baseline response values to long term culture responses to acute exposure for either inhibitor, we report that the long term cultures exhibit much lower viability

measurements at all doses of each drug (**Figures 24B, 24D**). This finding suggests that PDO

DH50 may, over time and as a function of "drift" in silico, be becoming a "more docile" and "more

sensitive" PDO in general, but not as a function of exposure to KRAS inhibition. This shift in PDO

character would be consistent with previous reports by us and others (see Chapter 1) suggesting

that organoids tend to become less aggressive over passage time.

In this same experiment, we also tested whether DH50 treated long term with BI-0800 (a

G12C-on mechanism of KRAS inhibition) might have become sensitive to MRTX849 (a G12C-

off mechanism of KRAS inhibition), and vice-versa. We report that DH50 treated long term with

BI-0800 is no more sensitive to treatment with acute MRTX849 than it is to being rechallenged

with acute BI-0800 (**Figure 24E,** no statistically significant differences between green and gray

bars at any dosage). Conversely, DH50 treated long term with MRTX849 appears more resistant

to acute treatment with BI-0800 than it is to acute rechallenging with MRTX849 (**Figure 24F,** blue

bars slightly taller than gray bars measuring viability).
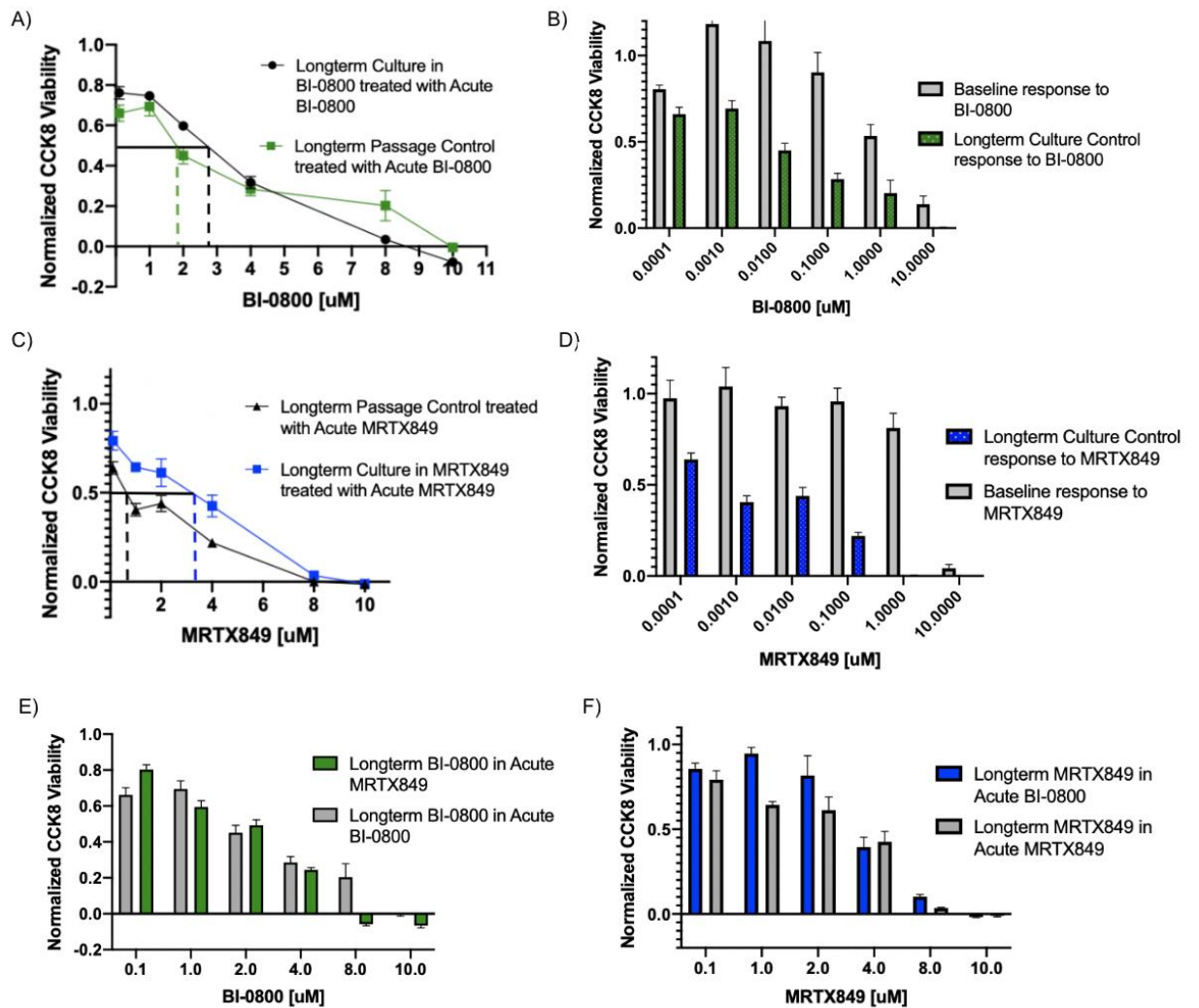
Figure 24: Characterization of longterm PDO treatment with KRAS G12C small molecule inhibitors.

A) Comparison of CCK8-determined viability of DH50 in longterm culture up to 8uM of BI-0800 challenged with acute BI-0800 treatment (green) compared to untreated culture controls challenged with acute BI-0800 treatment (black). IC50 shifts to ~3uM in longterm dosed cultures, indicating a developing resistant phenotype against BI-0800.

B) Comparison of CCK8-determined viability of DH50 longterm untreated control (green speckled) versus DH50 baseline (grey) responses to acute treatment with BI-0800.

C) Comparison of CCK8-determined viability of DH50 in longterm culture up to 8uM of MRTX849 challenged with acute MRTX849 treatment (blue) compared to untreated culture controls challenged with acute MRTX849 treatment (black). IC50 shifts to ~3.5uM in longterm dosed cultures, indicating a developing resistant phenotype against MRTX849.

D) Comparison of CCK8-determined viability of DH50 longterm untreated culture control (blue speckled) versus DH50 baseline (grey) responses to acute treatment with MRTX849.

E) Comparison of CCK8-determined viability of DH50 in longterm culture up to 8uM of BI-0800 challenged with acute MRTX849 treatment (green) versus DH50 in longterm culture up to 8uM of BI-0800 challenged with acute BI-0800 treatment (grey). Results show no statistically significant differences in response or sensitivities to a KRAS-OFF inhibitor induced following resistance to KRAS-ON inhibitor.

F) Comparison of CCK8-determined viability of DH50 in longterm culture up to 8uM of MRTX849 challenged with acute BI-0800 treatment (blue) versus DH50 in longterm culture up to 8uM of MRTX849 challenged with acute MRTX849 treatment (grey). Results show no statistically significant differences in response or sensitivities to a KRAS-ON inhibitor induced following resistance to KRAS-OFF inhibitor.

Mutation-specific inhibition is more effective than pan-RAS inhibition in acute G12C* context.

Also as a result of collaborations with MD Anderson's TRACTION platform, the Maitra Lab has acquired therapeutic agents under development with Boehringer-Ingelheim, the purported pan-RAS inhibitors mentioned above, and I've been eager to evaluate the effects of pan-RAS versus mutation-specific inhibition in patient-derived samples. As such, I've used MiaPaca-2 cell lines to evaluate the efficacy of pan-RAS-Off versus G12*-On inhibition, compared to 2 G12C* PDX lines acquired through an MTA with the NCI, so-called specimens 65R and 76R. I have found that, especially at low doses, BI-0800 (which covalently binds the GTP-bound mutant G12C Kras protein) outperforms the pan-RAS inhibitor compound (**Figures 25A, C, E**). Both agents, however, are much better at killing G12C* pancreatic cancer cells than the commonly-administered Gemcitabine, as well as the Mirati Therapeutics G12C-Off inhibitor, MRTX849 (**Figures 25B, D, F**). Of note, both NCI-PDX samples are slower-growing than MP2 cells, with PDX-76R being the slowest-growing of all. NCI-PDX-65R is also the most sensitive specimen to all therapies, with viability ranges achieved by Gemcitabine alone to be far below 50% at even very low doses of drug administration (**Figure 25D**). In all cases, Normalized CCK8 viability = (raw treated counts - raw media background value) / (raw untreated counts - raw media background value).
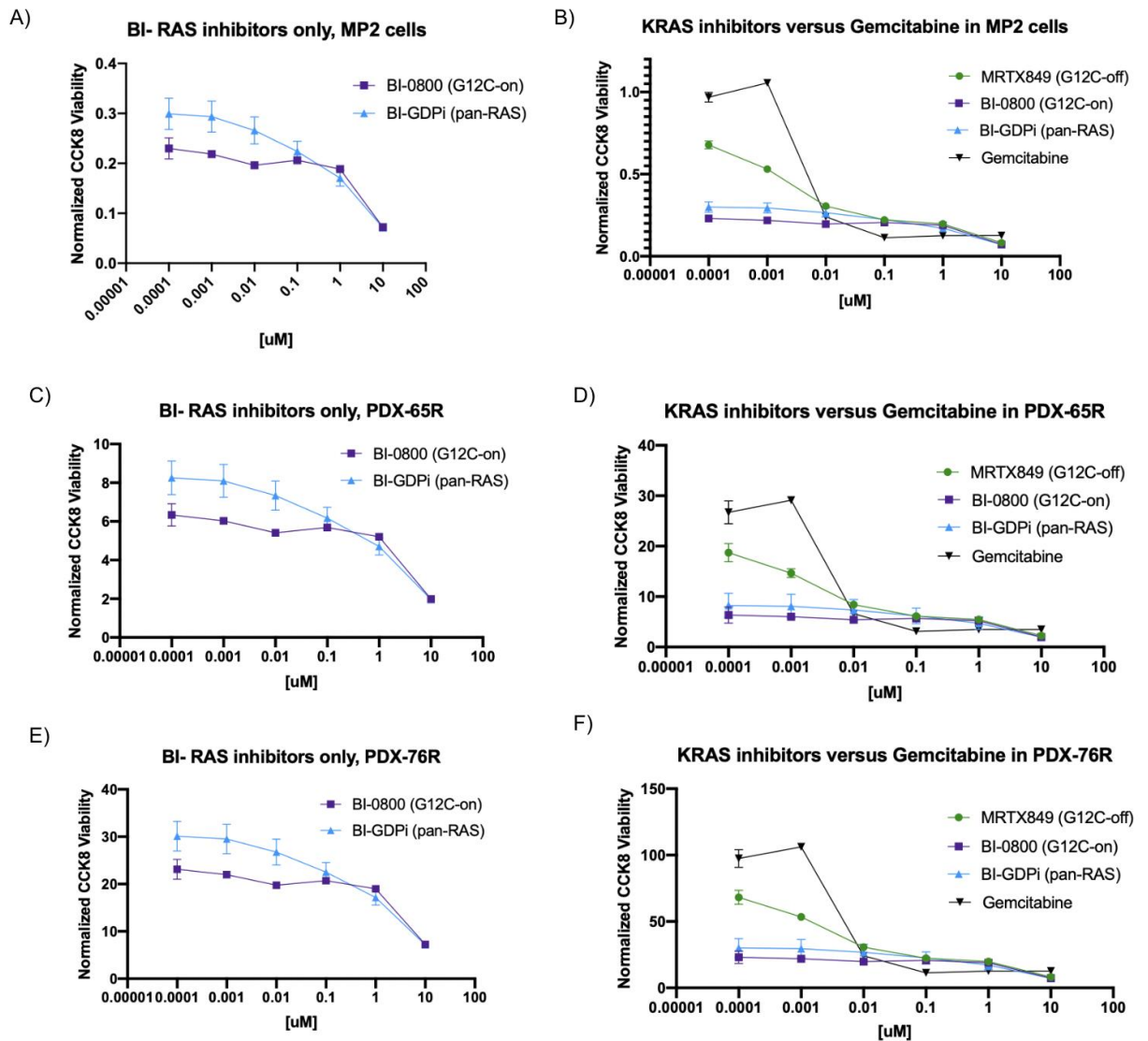
Figure 25: Mutation-specific inhibition is more effective than pan-RAS inhibition in acute G12C* context.

A) MiaPaca-2 (G12C*) responses to BI agents, depicting lower cell viability, measured by CCK8 assay, achieved by BI-0800 over the pan-RAS inhibitor.

B) Comparative MiaPaca-2 (G12C*) responses to BI agents, benchmarked against standard-of-care Gemcitabine, and G12Ci Mirati competitor drug, MRTX849. Cell viability measured by CCK8 assay.

C-D) Same as **(A)** and **(B)** for NCI-G12C* PDX-65R.

E-F) Same as **(A-D)** for NCI-G12C* PDX-76R.

Preliminary Characterization of PDO responses to KRAS G12D* inhibitors.

Given the prevalence of the $KRAS^{G12D}$ mutation in PDAC lesions (>40%), deciphering mechanisms underlying resistance to G12Di is paramount to the success of these agents in the

clinic. Recent work in *KRAS*^G12D* animal models has shown that ablating *KRAS* reduces, but does not fully abolish the tumorigenic capacity of PDAC cells[187]. These reports suggest that resistance to KRAS G12D inhibition may be innate to these tumors, and that innovating effective combinatorial regimens will be of the utmost importance in these PDAC cases. Indeed, in my own assays, I find that in both G12D* PDO samples and G12D* PDAC cell lines, total cell death is certainly not achieved, as viability at any dose administration of G12Di remains at or above 50% in all samples (**Figure 26**), where a G12C inhibitor positive control (MRTX849) yielded toxicity-associated PDO death at doses where the G12D inhibitor remained ineffectual on cell survival. It is important to note that the samples tested here were positive for KRAS G12D* variant allele fraction (VAF) by ddPCR in over 95% of cells.
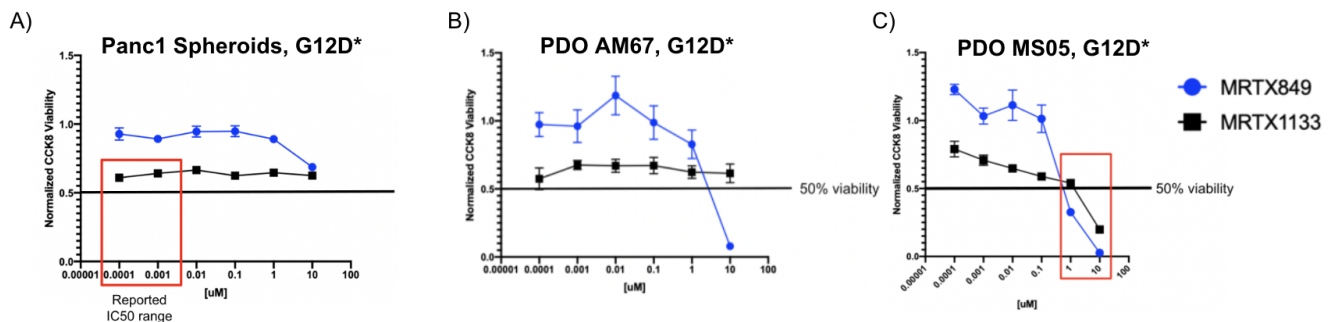
Figure 26: Characterization of response of KRAS G12D-mutant PDAC samples to commercial G12D* inhibitors.
Cataloging responses of G12D* models (1 PDAC cell line grown in 3D (**A**), 2 PDO lines (**B, C**) to KRAS G12D inhibitor MRTX1133 (black squares). G12C inhibitor MRTX849 (blue circles) used as positive control. X-axis represents uM doses of inhibitors administered, y-axis represents CCK8 viability measurements normalized to untreated controls in this assay.

Chapter 3 Discussion

While I will not be able to harvest post-treatment cells for sequencing or profiling before this dissertation is due, what characteristics possessed by the 50% of tumor cells alive at should-be intolerable G12Di and G12Ci doses is certainly an area for future study that the Maitra Lab has a vested interest in pursuing. Previous studies by Sivakumar et al to understand the "master regulators" of KRAS in pancreatic cancers suggest that differences in Hedgehog, Notch, and Cell Cycle signaling pathways may be the most predominating programs determining cellular responses to manipulation of oncogenic KRAS signaling[188]. However, whether the same pathways that govern how tumors behave as a function of an oncogenic RAS mutation, versus

what "salvage pathways" are employed when oncogenic RAS is inhibited in the acute treatment setting is very much so a robustly-developing research area.

The "same" needs apply for determining what mechanisms arise after longterm treatment with any KRAS inhibitor, weighing those molecular programs against the responses induced by acute treatment administration, and identifying useful strategies to anticipate the extent of the biological havoc treatment-induced adaptations will wreak in a patient. Whether PDOs, and patient tumors, for that matter, harbor sneaky mutations that are recalcitrant to inhibition of any kind, or whether they may have evolved mutations in actionable genomic regions will be critical to discern, if not just for the sake of scientific inquiry but for the eventual implementation of data-driven treatment plans in the clinical setting.

Conclusions and Final Thoughts

I have put off concluding for weeks, as I've tried to level with the task of neatly and succinctly summarizing the work presented in this dissertation. I've struggled, as each of these chapters, I feel, very much tell their own story and inform the scientific community of ways we can come to understand pancreatic ductal adenocarcinoma, and how we can employ various methods, analyses, hypotheses, and interpretations to make sense of it all. I have tried to illustrate, also, the value of orthogonal validation, wanting to emphasize that in science, there is certainly more than one way to do something, and the only way to arrive at Ground Truth is to demonstrate something in no short of a million different ways.

I came to graduate school as an Evolutionary Biologist, and now reflect on how the fundamental laws underlying ecosystem biology and species evolution are alive and well in pancreatic tumors. The methods that Cancer Biologists (me, included) employ to characterize tumor heterogeneity, measure clonal outgrowth, and identify resistant cells- these can all be likened to the same ways ecologists think about population growth, edge communities, and resource scarcity or geographic location driving speciation. PDAC lesions are every bit as much their own ecosystem as they are a part of a larger biological entity, and I have done my best to understand how their population dynamics ebb and flow as these cells cope with the survival challenges imposed by treatment regimens, surgeries, immune systems, and the myriad other strategies humans leverage to kill them off. This is a lethal malignancy that I've spent my time studying- the adaptive measures PDAC tumors will take to improve their chances of survival, against what we'd think are all odds, are nothing short of an evolutionary marvel.

I began by questioning the assumptions of what we, as a PDAC community, understood about the features determining how PDAC behaves. In Chapter 1, I discussed the underlying heterogeneity, indeed the occult polyclonality, that single cell technologies at multiple levels of

95

biological organization have enabled us to discover and systematically interrogate. Pancreatic cancer cell lines, the most commonly used unit of study for PDAC research, are not so isogenic as we (used again Royally) had asserted they are. Whether we were using the correct "normal controls" to benchmark our studies, if amplification or deletion events of large swaths of the genome have endowed certain groups of cells in culture with an evolutionary advantage, if chromatin recoiling as a function of a matrigel scaffold determines the response to a therapeutic agent in silico or if and how PDAC organoids change in time are topics that had not been fully divulged prior to this dissertation. The findings discussed in Chapter 1 may have broad implications for future work, as researchers may now understand the importance of fully characterizing any of their study models prior to assuming the contextual applicability of their own studies. Further, the results described in Chapter 1 may (hopefully) provide a "roadmap" of the level of granularity required to meaningfully profile PDAC lesions in the clinic, in our efforts to provide Precision Medicine-based treatment strategies to patients.

In Chapter 2, I moved into the realm of exploring how agnostic, multimodal characterization of a model system can lead to discovery of novel treatment combinations in PDAC. In striving to address the gap of knowledge left by the long history of clinical HDACi failures, we identified a resistance mechanism that, while not only previously unreported, could be targeted in a combinatorial approach to achieve tumor cell death. I cannot envision AP1 inhibitors being brought to clinic on account of HDACi-based trials in PDAC being all but absconded in recent years. However, parsing apart one of the many "why's" of PDAC treatment failure goes beyond an academic exercise, and instead exemplifies how multiple levels of biological activity are co-opted into promoting post-treatment tumor growth.

Finally, in my last chapter, I sought to understand, and possibly anticipate, how PDAC lesions will respond to the inhibition of the "holy grail" of cancer genes: KRAS. That PDAC patients harbor different KRAS mutations and have different response capabilities to KRASi was an inevitability

the research community would have to confront eventually. While the earlier literature on the subject seemed to suggest that knocking out KRAS would bring tumors to their metaphorical knees, we soon learned by way of clinical trial results and more accurate preclinical modeling methods that tumors will upregulate any number of survival pathways when the Big Red KRAS Button gets pushed. These pathways include but are not limited to autophagy, SOS1 and RTK signaling, and tumors often combine a multitude of pathways to avoid death by KRASi. By inhibiting cancer's so-called "heart", we've managed to seemingly give a pancreatic tumor the ability to grow at least seven new heads in addition to activating a second heart it kept handy in a storage closet. I know, science is no place for metaphor, but in this case, you get the point. By studying differential responses to KRAS G12C and G12D inhibitors, I've shown that while nearly all cells in a cultured population harbor a KRAS mutation, only about half of them (at best) are completely incapacitated by inhibiting KRAS. The other half of the tumor cells have, perhaps, evolved beyond their KRAS activating mutation and have sought greener genetic pastures, instead favoring reliance on pathways and mutations that make them biologically stronger than an individual KRAS mutation ever could alone. By forcing a resistant phenotype to KRAS G12C inhibitors, I've also shown that treatment resistance, at unfathomably high doses of drug administration, can be achieved in organoid models. These early studies might suggest that proliferation of the surviving 50% of cells after baseline treatment administration is an altogether possible reality, and characterization of those remaining cellular stalwarts ought to be of top priority to anticipate tumor outgrowth after an initial lesion regression. For this reason, a shift towards conducting followup patient biopsies in the clinic, to catalog the dynamic changes and growth of tumor cells, ought to be implemented. Initiatives like Break Through Cancer have begun to sort this out, but there is a long way to go on the clinical front in order to achieve meaningful, durable responses that are mindful of ever-evolving resistance dynamics.

In my time as a graduate student, I have watched the 5-year survival rate of pancreatic cancer patients be nudged from 8% to 11%. This is a significant improvement, but we have so much

farther to go. With the advancement of technologies and study platforms, the sophistication of targeted compounds, the multidisciplinary approaches being taken by physicians and scientists, et cetera, I am confident that the 5-year survival rate of pancreatic cancer patients will continue to increase. If there's anything I've learned, it's that the easiest pancreatic cancer patient to treat is one who has not yet developed a pancreatic tumor. These are patients who, while they may have a low grade IPMN or a small cyst, have not developed a jungle of oncogenic driver mutations, nor have their tissues been tried and tested with vicious chemotherapeutics. These are patients with a low prevalence of a KRAS mutation, perhaps a TP53 mutation, and (hopefully) little else. If we are to see an improvement in pancreatic cancer survival, I believe that this pre-cancer cohort is the one that would benefit the most from targeted KRAS inhibitors, and where I would most like to see these compounds tested. If i were granted unlimited time and resources in the Maitra Lab, these are the future directions I would like most to explore, and that I hope are expanded upon by researchers who come after me. This is currently not the focus of ongoing RAS-centric studies, and I must admit that I have grown weary of chasing down the rabbit-holes of acquired RAS resistance. Understanding how to best treat late-stage patients is, of course, a hugely important endeavor and one that I take very seriously. However, RAS biology and resistance becomes very complicated very quickly, and tumor cells have, as I've tried to show in this dissertation, a near-unlimited repertoire of strategies to keep on living in the face of RAS-induced adversity. By inhibiting RAS in its "toddler stage", while pancreata have detectable precursor lesions instead of "matured" RAS-driven tumors, I think we stand a much better chance of both decreasing the incidence of pancreatic cancers and continuing to improve PDAC survival rates.

References

1. Bengtsson, A., R. Andersson, and D. Ansari. 2020. 'The actual 5-year survivors of pancreatic ductal adenocarcinoma based on real-world data', Sci Rep, 10: 16425.

2. Li, Q., Z. Feng, R. Miao, X. Liu, C. Liu, and Z. Liu. 2022. 'Prognosis and survival analysis of patients with pancreatic cancer: retrospective experience of a single institution', World J Surg Oncol, 20: 11.

3. Sarantis, P., E. Koustas, A. Papadimitropoulou, A. G. Papavassiliou, and M. V. Karamouzis. 2020. 'Pancreatic ductal adenocarcinoma: Treatment hurdles, tumor microenvironment and immunotherapy', World J Gastrointest Oncol, 12: 173-81.

4. Park, W., A. Chawla, and E. M. O'Reilly. 2021. 'Pancreatic Cancer: A Review', JAMA, 326: 851-62.

5. Cid-Arregui, A., and V. Juarez. 2015. 'Perspectives in the treatment of pancreatic adenocarcinoma', World J Gastroenterol, 21: 9297-316.

6. Catalano, M., R. Conca, R. Petrioli, M. Ramello, and G. Roviello. 2020. 'FOLFOX vs FOLFIRI as Second-line of Therapy After Progression to Gemcitabine/Nab-paclitaxel in Patients with Metastatic Pancreatic Cancer', Cancer Manag Res, 12: 10271-78.

7. Kunzmann, V., J. T. Siveke, H. Algul, E. Goekkurt, G. Siegler, U. Martens, D. Waldschmidt, U. Pelzer, M. Fuchs, F. Kullmann, S. Boeck, T. J. Ettrich, S. Held, R. Keller, I. Klein, C. T. Germer, H. Stein, H. Friess, M. Bahra, R. Jakobs, I. Hartlapp, V. Heinemann, Group German Pancreatic Cancer Working, and Neolap investigators. 2021. 'Nab-paclitaxel plus gemcitabine versus nab-paclitaxel plus gemcitabine followed by FOLFIRINOX induction chemotherapy in

locally advanced pancreatic cancer (NEOLAP-AIO-PAK-0113): a multicentre, randomised, phase 2 trial', Lancet Gastroenterol Hepatol, 6: 128-38.

8. Conroy, T., P. Hammel, M. Hebbar, M. Ben Abdelghani, A. C. Wei, J. L. Raoul, L. Chone, E. Francois, P. Artru, J. J. Biagi, T. Lecomte, E. Assenat, R. Faroux, M. Ychou, J. Volet, A. Sauvanet, G. Breysacher, F. Di Fiore, C. Cripps, P. Kavan, P. Texereau, K. Bouhier-Leporrier, F. Khemissa-Akouz, J. L. Legoux, B. Juzyna, S. Gourgou, C. J. O'Callaghan, C. Jouffroy-Zeller, P. Rat, D. Malka, F. Castan, J. B. Bachet, Group Canadian Cancer Trials, and G. I. Prodige Group the Unicancer. 2018. 'FOLFIRINOX or Gemcitabine as Adjuvant Therapy for Pancreatic Cancer', N Engl J Med, 379: 2395-406.

9. Rawla, P., T. Sunkara, and V. Gaduputi. 2019. 'Epidemiology of Pancreatic Cancer: Global Trends, Etiology and Risk Factors', World J Oncol, 10: 10-27.

10. Distler, M., D. Aust, J. Weitz, C. Pilarsky, and R. Grutzmann. 2014. 'Precursor lesions for sporadic pancreatic cancer: PanIN, IPMN, and MCN', Biomed Res Int, 2014: 474905.

11. Ferreira, R. M. M., R. Sancho, H. A. Messal, E. Nye, B. Spencer-Dene, R. K. Stone, G. Stamp, I. Rosewell, A. Quaglia, and A. Behrens. 2017. 'Duct- and Acinar-Derived Pancreatic Ductal Adenocarcinomas Show Distinct Tumor Progression and Marker Expression', Cell Rep, 21: 966-78

12. Iacobuzio-Donahue, C. A., V. E. Velculescu, C. L. Wolfgang, and R. H. Hruban. 2012. 'Genetic basis of pancreas cancer development and progression: insights from whole-exome and whole-genome sequencing', Clin Cancer Res, 18: 4257-65.

13. Kanda, M., H. Matthaei, J. Wu, S. M. Hong, J. Yu, M. Borges, R. H. Hruban, A. Maitra, K. Kinzler, B. Vogelstein, and M. Goggins. 2012. 'Presence of somatic mutations in most early-stage pancreatic intraepithelial neoplasia', Gastroenterology, 142: 730-33 e9.

14. Singh, K., M. Pruski, R. Bland, M. Younes, S. Guha, N. Thosani, A. Maitra, B. D. Cash, F. McAllister, C. D. Logsdon, J. T. Chang, and J. M. Bailey-Lundberg. 2021. 'Kras mutation rate precisely orchestrates ductal derived pancreatic intraepithelial neoplasia and pancreatic cancer', Lab Invest, 101: 177-92.

15. Hingorani, S. R., L. Wang, A. S. Multani, C. Combs, T. B. Deramaudt, R. H. Hruban, A. K. Rustgi, S. Chang, and D. A. Tuveson. 2005. 'Trp53R172H and KrasG12D cooperate to promote chromosomal instability and widely metastatic pancreatic ductal adenocarcinoma in mice', Cancer Cell, 7: 469-83.

16. Qiu, W., F. Sahin, C. A. Iacobuzio-Donahue, D. Garcia-Carracedo, W. M. Wang, C. Y. Kuo, D. Chen, D. E. Arking, A. M. Lowy, R. H. Hruban, H. E. Remotti, and G. H. Su. 2011. 'Disruption of p16 and activation of Kras in pancreas increase ductal adenocarcinoma formation and metastasis in vivo', Oncotarget, 2: 862-73.

17. Hosein, A. N., G. Dangol, T. Okumura, J. Roszik, K. Rajapakshe, M. Siemann, M. Zaid, B. Ghosh, M. Monberg, P. A. Guerrero, A. Singhi, C. L. Haymaker, H. Clevers, L. Abou-Elkacem, S. M. Woermann, and A. Maitra. 2022. 'Loss of Rnf43 Accelerates Kras-Mediated Neoplasia and Remodels the Tumor Immune Microenvironment in Pancreatic Adenocarcinoma', Gastroenterology, 162: 1303-18 e18.

18. Patra, K. C., Y. Kato, Y. Mizukami, S. Widholz, M. Boukhali, I. Revenco, E. A. Grossman, F. Ji, R. I. Sadreyev, A. S. Liss, R. A. Screaton, K. Sakamoto, D. P. Ryan, M. Mino-Kenudson, C. F. Castillo, D. K. Nomura, W. Haas, and N. Bardeesy. 2018. 'Mutant GNAS drives pancreatic

tumourigenesis by inducing PKA-mediated SIK suppression and reprogramming lipid metabolism', Nat Cell Biol, 20: 811-22

19. Noe, M., N. Niknafs, C. G. Fischer, W. M. Hackeng, V. Beleva Guthrie, W. Hosoda, M. Debeljak, E. Papp, V. Adleff, J. R. White, C. Luchini, A. Pea, A. Scarpa, G. Butturini, G. Zamboni, P. Castelli, S. M. Hong, S. Yachida, N. Hiraoka, A. J. Gill, J. S. Samra, G. J. A. Offerhaus, A. Hoorens, J. Verheij, C. Jansen, N. V. Adsay, W. Jiang, J. Winter, J. Albores-Saavedra, B. Terris, E. D. Thompson, N. J. Roberts, R. H. Hruban, R. Karchin, R. B. Scharpf, L. A. A. Brosens, V. E. Velculescu, and L. D. Wood. 2020. 'Genomic characterization of malignant progression in neoplastic pancreatic cysts', Nat Commun, 11: 4085.

20. Maitra, A., and R. H. Hruban. 2008. 'Pancreatic cancer', Annu Rev Pathol, 3: 157-88

21. Iacobuzio-Donahue, C. A., B. Fu, S. Yachida, M. Luo, H. Abe, C. M. Henderson, F. Vilardell, Z. Wang, J. W. Keller, P. Banerjee, J. M. Herman, J. L. Cameron, C. J. Yeo, M. K. Halushka, J. R. Eshleman, M. Raben, A. P. Klein, R. H. Hruban, M. Hidalgo, and D. Laheru. 2009. 'DPC4 gene status of the primary carcinoma correlates with patterns of failure in patients with pancreatic cancer', J Clin Oncol, 27: 1806-13.

22. Wang, J., C. G. Mullighan, J. Easton, S. Roberts, S. L. Heatley, J. Ma, M. C. Rusch, K. Chen, C. C. Harris, L. Ding, L. Holmfeldt, D. Payne-Turner, X. Fan, L. Wei, D. Zhao, J. C. Obenauer, C. Naeve, E. R. Mardis, R. K. Wilson, J. R. Downing, and J. Zhang. 2011. 'CREST maps somatic structural variation in cancer genomes with base-pair resolution', Nat Methods, 8: 652-4.

23. Murakami, T., Y. Hiroshima, R. Matsuyama, Y. Homma, R. M. Hoffman, and I. Endo. 2019. 'Role of the tumor microenvironment in pancreatic cancer', Ann Gastroenterol Surg, 3: 130-37.

24. Waldman, A. D., J. M. Fritz, and M. J. Lenardo. 2020. 'A guide to cancer immunotherapy: from T cell basic science to clinical practice', Nat Rev Immunol, 20: 651-68.

25. Garcia Garcia, C. J., Y. Huang, N. R. Fuentes, M. C. Turner, M. E. Monberg, D. Lin, N. D. Nguyen, T. N. Fujimoto, J. Zhao, J. J. Lee, V. Bernard, M. Yu, A. M. Delahoussaye, I. J. Sacarello, E. G. Caggiano, J. L. Phan, A. Deorukhkar, J. M. Molkentine, D. Saur, A. Maitra, and C. M. Taniguchi. 2022. 'Stromal HIF2 Regulates Immune Suppression in the Pancreatic Cancer Microenvironment', Gastroenterology.

26. Ho, W. J., E. M. Jaffee, and L. Zheng. 2020. 'The tumour microenvironment in pancreatic cancer - clinical challenges and opportunities', Nat Rev Clin Oncol, 17: 527-40.

27. Yang, J., Q. Zhang, J. Wang, Y. Lou, Z. Hong, S. Wei, K. Sun, J. Wang, Y. Chen, J. Sheng, W. Su, X. Bai, and T. Liang. 2022. 'Dynamic profiling of immune microenvironment during pancreatic cancer development suggests early intervention and combination strategy of immunotherapy', EBioMedicine, 78: 103958.

28. Brouwer, T. P., A. L. Vahrmeijer, and Nfcc de Miranda. 2021. 'Immunotherapy for pancreatic cancer: chasing the light at the end of the tunnel', Cell Oncol (Dordr), 44: 261-78.

29. Lee, J. S., and E. Ruppin. 2019. 'Multiomics Prediction of Response Rates to Therapies to Inhibit Programmed Cell Death 1 and Programmed Cell Death 1 Ligand 1', JAMA Oncol, 5: 1614-18.

30. Ohlund, D., A. Handly-Santana, G. Biffi, E. Elyada, A. S. Almeida, M. Ponz-Sarvise, V. Corbo, T. E. Oni, S. A. Hearn, E. J. Lee, Chio, II, C. I. Hwang, H. Tiriac, L. A. Baker, D. D. Engle, C. Feig, A. Kultti, M. Egeblad, D. T. Fearon, J. M. Crawford, H. Clevers, Y. Park, and D. A. Tuveson. 2017. 'Distinct populations of inflammatory fibroblasts and myofibroblasts in pancreatic cancer', J Exp Med, 214: 579-96.

31. Elyada, E., M. Bolisetty, P. Laise, W. F. Flynn, E. T. Courtois, R. A. Burkhart, J. A. Teinor, P. Belleau, G. Biffi, M. S. Lucito, S. Sivajothi, T. D. Armstrong, D. D. Engle, K. H. Yu, Y. Hao, C. L. Wolfgang, Y. Park, J. Preall, E. M. Jaffee, A. Califano, P. Robson, and D. A. Tuveson. 2019. 'Cross-Species Single-Cell Analysis of Pancreatic Ductal Adenocarcinoma Reveals Antigen-Presenting Cancer-Associated Fibroblasts', Cancer Discov, 9: 1102-23.

32. Ozdemir, B. C., et al. (2014). "Depletion of carcinoma-associated fibroblasts and fibrosis induces immunosuppression and accelerates pancreas cancer with reduced survival." Cancer Cell 25(6): 719-734.

33. Jiang, H., R. J. Torphy, K. Steiger, H. Hongo, A. J. Ritchie, M. Kriegsmann, D. Horst, S. E. Umetsu, N. M. Joseph, K. McGregor, M. J. Pishvaian, E. M. Blais, B. Lu, M. Li, M. Hollingsworth, C. Stashko, K. Volmar, J. J. Yeh, V. M. Weaver, Z. J. Wang, M. A. Tempero, W. Weichert, and E. A. Collisson. 2020. 'Pancreatic ductal adenocarcinoma progression is restrained by stromal matrix', J Clin Invest, 130: 4704-09.

34. Jiang, B., L. Zhou, J. Lu, Y. Wang, C. Liu, L. You, and J. Guo. 2020. 'Stroma-Targeting Therapy in Pancreatic Cancer: One Coin With Two Sides?', Front Oncol, 10: 576399.

35. Chen, K., Q. Wang, M. Li, H. Guo, W. Liu, F. Wang, X. Tian, and Y. Yang. 2021. 'Single-cell RNA-seq reveals dynamic change in tumor microenvironment during pancreatic ductal

adenocarcinoma malignant progression', EBioMedicine, 66: 103315.

36. Raghavan, S., P. S. Winter, A. W. Navia, H. L. Williams, A. DenAdel, K. E. Lowder, J. Galvez-Reyes, R. L. Kalekar, N. Mulugeta, K. S. Kapner, M. S. Raghavan, A. A. Borah, N. Liu, S. A. Vayrynen, A. D. Costa, R. W. S. Ng, J. Wang, E. K. Hill, D. Y. Ragon, L. K. Brais, A. M. Jaeger, L. F. Spurr, Y. Y. Li, A. D. Cherniack, M. A. Booker, E. F. Cohen, M. Y. Tolstorukov, I. Wakiro, A. Rotem, B. E. Johnson, J. M. McFarland, E. T. Sicinska, T. E. Jacks, R. J. Sullivan, G. I. Shapiro, T. E. Clancy, K. Perez, D. A. Rubinson, K. Ng, J. M. Cleary, L. Crawford, S. R. Manalis, J. A. Nowak, B. M. Wolpin, W. C. Hahn, A. J. Aguirre, and A. K. Shalek. 2021. 'Microenvironment drives cell state, plasticity, and drug response in pancreatic cancer', Cell, 184: 6119-37 e26.

37. Bechard, M. E., R. Smalling, A. Hayashi, Y. Zhong, A. E. Word, S. L. Campbell, A. V. Tran, V. L. Weiss, C. Iacobuzio-Donahue, K. E. Wellen, and O. G. McDonald. 2020. 'Pancreatic cancers suppress negative feedback of glucose transport to reprogram chromatin for metastasis', Nat Commun, 11: 4055.

38. Kamyabi, N., V. Bernard, and A. Maitra. 2019. 'Liquid biopsies in pancreatic cancer', Expert Rev Anticancer Ther, 19: 869-78.

39. Aung, K. L., S. E. Fischer, R. E. Denroche, G. H. Jang, A. Dodd, S. Creighton, B. Southwood, S. B. Liang, D. Chadwick, A. Zhang, G. M. O'Kane, H. Albaba, S. Moura, R. C. Grant, J. K. Miller, F. Mbabaali, D. Pasternack, I. M. Lungu, J. M. S. Bartlett, S. Ghai, M. Lemire, S. Holter, A. A. Connor, R. A. Moffitt, J. J. Yeh, L. Timms, P. M. Krzyzanowski, N. Dhani, D. Hedley, F. Notta, J. M. Wilson, M. J. Moore, S. Gallinger, and J. J. Knox. 2018. 'Genomics-Driven Precision Medicine for Advanced Pancreatic Cancer: Early Results from the

COMPASS Trial', Clin Cancer Res, 24: 1344-54.

40. Waddell, N., M. Pajic, A. M. Patch, D. K. Chang, K. S. Kassahn, P. Bailey, A. L. Johns, D. Miller, K. Nones, K. Quek, M. C. Quinn, A. J. Robertson, M. Z. Fadlullah, T. J. Bruxner, A. N. Christ, I. Harliwong, S. Idrisoglu, S. Manning, C. Nourse, E. Nourbakhsh, S. Wani, P. J. Wilson, E. Markham, N. Cloonan, M. J. Anderson, J. L. Fink, O. Holmes, S. H. Kazakoff, C. Leonard, F. Newell, B. Poudel, S. Song, D. Taylor, N. Waddell, S. Wood, Q. Xu, J. Wu, M. Pinese, M. J. Cowley, H. C. Lee, M. D. Jones, A. M. Nagrial, J. Humphris, L. A. Chantrill, V. Chin, A. M. Steinmann, A. Mawson, E. S. Humphrey, E. K. Colvin, A. Chou, C. J. Scarlett, A. V. Pinho, M. Giry-Laterriere, I. Rooman, J. S. Samra, J. G. Kench, J. A. Pettitt, N. D. Merrett, C. Toon, K. Epari, N. Q. Nguyen, A. Barbour, N. Zeps, N. B. Jamieson, J. S. Graham, S. P. Niclou, R. Bjerkvig, R. Grutzmann, D. Aust, R. H. Hruban, A. Maitra, C. A. Iacobuzio-Donahue, C. L. Wolfgang, R. A. Morgan, R. T. Lawlor, V. Corbo, C. Bassi, M. Falconi, G. Zamboni, G. Tortora, M. A. Tempero, Initiative Australian Pancreatic Cancer Genome, A. J. Gill, J. R. Eshleman, C. Pilarsky, A. Scarpa, E. A. Musgrove, J. V. Pearson, A. V. Biankin, and S. M. Grimmond. 2015. 'Whole genomes redefine the mutational landscape of pancreatic cancer', Nature, 518: 495-501.

41. Cancer Genome Atlas Research Network. Electronic address, andrew aguirre dfci harvard edu, and Network Cancer Genome Atlas Research. 2017. 'Integrated Genomic Characterization of Pancreatic Ductal Adenocarcinoma', Cancer Cell, 32: 185-203 e13.

42. Connor, A. A., R. E. Denroche, G. H. Jang, M. Lemire, A. Zhang, M. Chan-Seng-Yue, G. Wilson, R. C. Grant, D. Merico, I. Lungu, J. M. S. Bartlett, D. Chadwick, S. B. Liang, J. Eagles, F. Mbabaali, J. K. Miller, P. Krzyzanowski, H. Armstrong, X. Luo, L. G. T. Jorgensen, J. M. Romero, P. Bavi, S. E. Fischer, S. Serra, S. Hafezi-Bakhtiari, D. Caglar, M. H. A. Roehrl, S. Cleary, M. A. Hollingsworth, G. M. Petersen, S. Thayer, C. H. L. Law, S. Nanji, T. Golan, A. L.

Smith, A. Borgida, A. Dodd, D. Hedley, B. G. Wouters, G. M. O'Kane, J. M. Wilson, G. Zogopoulos, F. Notta, J. J. Knox, and S. Gallinger. 2019. 'Integration of Genomic and Transcriptional Features in Pancreatic Cancer Reveals Increased Cell Cycle Progression in Metastases', Cancer Cell, 35: 267-82 e7.

43. Makohon-Moore, A. P., M. Zhang, J. G. Reiter, I. Bozic, B. Allen, D. Kundu, K. Chatterjee, F. Wong, Y. Jiao, Z. A. Kohutek, J. Hong, M. Attiyeh, B. Javier, L. D. Wood, R. H. Hruban, M. A. Nowak, N. Papadopoulos, K. W. Kinzler, B. Vogelstein, and C. A. Iacobuzio-Donahue. 2017. 'Limited heterogeneity of known driver gene mutations among the metastases of individual patients with pancreatic cancer', Nat Genet, 49: 358-66.

44. Eslami, S. Z., L. E. Cortes-Hernandez, and C. Alix-Panabieres. 2020. 'The Metastatic Cascade as the Basis for Liquid Biopsy Development', Front Oncol, 10: 1055.

45. McDonald, O. G., X. Li, T. Saunders, R. Tryggvadottir, S. J. Mentch, M. O. Warmoes, A. E. Word, A. Carrer, T. H. Salz, S. Natsume, K. M. Stauffer, A. Makohon-Moore, Y. Zhong, H. Wu, K. E. Wellen, J. W. Locasale, C. A. Iacobuzio-Donahue, and A. P. Feinberg. 2017. 'Epigenomic reprogramming during pancreatic cancer progression links anabolic glucose metabolism to distant metastasis', Nat Genet, 49: 367-76.

46. Torres, C., and P. J. Grippo. 2018. 'Pancreatic cancer subtypes: a roadmap for precision medicine', Ann Med, 50: 277-87.

47. Aguirre, A. J., J. A. Nowak, N. D. Camarda, R. A. Moffitt, A. A. Ghazani, M. Hazar-Rethinam, S. Raghavan, J. Kim, L. K. Brais, D. Ragon, M. W. Welch, E. Reilly, D. McCabe, L. Marini, K. Anderka, K. Helvie, N. Oliver, A. Babic, A. Da Silva, B. Nadres, E. E. Van Seventer, H. A. Shahzade, J. P. St Pierre, K. P. Burke, T. Clancy, J. M. Cleary, L. A. Doyle, K. Jajoo, N.

J. McCleary, J. A. Meyerhardt, J. E. Murphy, K. Ng, A. K. Patel, K. Perez, M. H. Rosenthal, D. A. Rubinson, M. Ryou, G. I. Shapiro, E. Sicinska, S. G. Silverman, R. J. Nagy, R. B. Lanman, D. Knoerzer, D. J. Welsch, M. B. Yurgelun, C. S. Fuchs, L. A. Garraway, G. Getz, J. L. Hornick, B. E. Johnson, M. H. Kulke, R. J. Mayer, J. W. Miller, P. B. Shyn, D. A. Tuveson, N. Wagle, J. J. Yeh, W. C. Hahn, R. B. Corcoran, S. L. Carter, and B. M. Wolpin. 2018. 'Real-time Genomic Characterization of Advanced Pancreatic Cancer to Enable Precision Medicine', Cancer Discov, 8: 1096-111.

48. Collisson, E. A., A. Sadanandam, P. Olson, W. J. Gibb, M. Truitt, S. Gu, J. Cooc, J. Weinkle, G. E. Kim, L. Jakkula, H. S. Feiler, A. H. Ko, A. B. Olshen, K. L. Danenberg, M. A. Tempero, P. T. Spellman, D. Hanahan, and J. W. Gray. 2011. 'Subtypes of pancreatic ductal adenocarcinoma and their differing responses to therapy', Nat Med, 17: 500-3.

49. Moffitt, R. A., R. Marayati, E. L. Flate, K. E. Volmar, S. G. Loeza, K. A. Hoadley, N. U. Rashid, L. A. Williams, S. C. Eaton, A. H. Chung, J. K. Smyla, J. M. Anderson, H. J. Kim, D. J. Bentrem, M. S. Talamonti, C. A. Iacobuzio-Donahue, M. A. Hollingsworth, and J. J. Yeh. 2015. 'Virtual microdissection identifies distinct tumor- and stroma-specific subtypes of pancreatic ductal adenocarcinoma', Nat Genet, 47: 1168-78.

50. Bailey, P., D. K. Chang, K. Nones, A. L. Johns, A. M. Patch, M. C. Gingras, D. K. Miller, A. N. Christ, T. J. Bruxner, M. C. Quinn, C. Nourse, L. C. Murtaugh, I. Harliwong, S. Idrisoglu, S. Manning, E. Nourbakhsh, S. Wani, L. Fink, O. Holmes, V. Chin, M. J. Anderson, S. Kazakoff, C. Leonard, F. Newell, N. Waddell, S. Wood, Q. Xu, P. J. Wilson, N. Cloonan, K. S. Kassahn, D. Taylor, K. Quek, A. Robertson, L. Pantano, L. Mincarelli, L. N. Sanchez, L. Evers, J. Wu, M. Pinese, M. J. Cowley, M. D. Jones, E. K. Colvin, A. M. Nagrial, E. S. Humphrey, L. A. Chantrill, A. Mawson, J. Humphris, A. Chou, M. Pajic, C. J. Scarlett, A. V. Pinho, M. Giry-Laterriere, I. Rooman, J. S. Samra, J. G. Kench, J. A. Lovell, N. D. Merrett, C. W. Toon, K. Epari, N. Q.

Nguyen, A. Barbour, N. Zeps, K. Moran-Jones, N. B. Jamieson, J. S. Graham, F. Duthie, K. Oien, J. Hair, R. Grutzmann, A. Maitra, C. A. Iacobuzio-Donahue, C. L. Wolfgang, R. A. Morgan, R. T. Lawlor, V. Corbo, C. Bassi, B. Rusev, P. Capelli, R. Salvia, G. Tortora, D. Mukhopadhyay, G. M. Petersen, Initiative Australian Pancreatic Cancer Genome, D. M. Munzy, W. E. Fisher, S. A. Karim, J. R. Eshleman, R. H. Hruban, C. Pilarsky, J. P. Morton, O. J. Sansom, A. Scarpa, E. A. Musgrove, U. M. Bailey, O. Hofmann, R. L. Sutherland, D. A. Wheeler, A. J. Gill, R. A. Gibbs, J. V. Pearson, N. Waddell, A. V. Biankin, and S. M. Grimmond. 2016. 'Genomic analyses identify molecular subtypes of pancreatic cancer', Nature, 531: 47-52.

51. O'Kane, G. M., B. T. Grunwald, G. H. Jang, M. Masoomian, S. Picardo, R. C. Grant, R. E. Denroche, A. Zhang, Y. Wang, B. Lam, P. M. Krzyzanowski, I. M. Lungu, J. M. S. Bartlett, M. Peralta, F. Vyas, R. Khokha, J. Biagi, D. Chadwick, S. Ramotar, S. Hutchinson, A. Dodd, J. M. Wilson, F. Notta, G. Zogopoulos, S. Gallinger, J. J. Knox, and S. E. Fischer. 2020. 'GATA6 Expression Distinguishes Classical and Basal-like Subtypes in Advanced Pancreatic Cancer', Clin Cancer Res, 26: 4901-10.

52. Keck, K. M., and L. F. Pemberton. 2012. 'Histone chaperones link histone nuclear import and chromatin assembly', Biochim Biophys Acta, 1819: 277-89.

53. Marino-Ramirez, L., M. G. Kann, B. A. Shoemaker, and D. Landsman. 2005. 'Histone structure and nucleosome stability', Expert Rev Proteomics, 2: 719-29.

54. Bannister, A. J., and T. Kouzarides. 2011. 'Regulation of chromatin by histone modifications', Cell Res, 21: 381-95.

55. Hull, E. E., M. R. Montgomery, and K. J. Leyva. 2016. 'HDAC Inhibitors as Epigenetic Regulators of the Immune System: Impacts on Cancer Therapy and Inflammatory Diseases',

Biomed Res Int, 2016: 8797206.

56. Ververis, K., A. Hiong, T. C. Karagiannis, and P. V. Licciardi. 2013. 'Histone deacetylase inhibitors (HDACIs): multitargeted anticancer agents', Biologics, 7: 47-60.

57. Li, G., Y. Tian, and W. G. Zhu. 2020. 'The Roles of Histone Deacetylases and Their Inhibitors in Cancer Therapy', Front Cell Dev Biol, 8: 576946.

58. Burrell, R. A., and C. Swanton. 2014. 'Tumour heterogeneity and the evolution of polyclonal drug resistance', Mol Oncol, 8: 1095-111.

59. Gillies, R. J., D. Verduzco, and R. A. Gatenby. 2012. 'Evolutionary dynamics of carcinogenesis and why targeted therapy does not work', Nat Rev Cancer, 12: 487-93.

60. Merlo, L. M., J. W. Pepper, B. J. Reid, and C. C. Maley. 2006. 'Cancer as an evolutionary and ecological process', Nat Rev Cancer, 6: 924-35.

61. Gerlinger, M., S. Horswell, J. Larkin, A. J. Rowan, M. P. Salm, I. Varela, R. Fisher, N. McGranahan, N. Matthews, C. R. Santos, P. Martinez, B. Phillimore, S. Begum, A. Rabinowitz, B. Spencer-Dene, S. Gulati, P. A. Bates, G. Stamp, L. Pickering, M. Gore, D. L. Nicol, S. Hazell, P. A. Futreal, A. Stewart, and C. Swanton. 2014. 'Genomic architecture and evolution of clear cell renal cell carcinomas defined by multiregion sequencing', Nat Genet, 46: 225-33.

62. Han, J., R. A. DePinho, and A. Maitra. 2021. 'Single-cell RNA sequencing in pancreatic cancer', Nat Rev Gastroenterol Hepatol, 18: 451-52.

63. Lee, J. J., V. Bernard, A. Semaan, M. E. Monberg, J. Huang, B. M. Stephens, D. Lin, K. I. Rajapakshe, B. R. Weston, M. S. Bhutani, C. L. Haymaker, C. Bernatchez, C. M. Taniguchi, A. Maitra, and P. A. Guerrero. 2021. 'Elucidation of Tumor-Stromal Heterogeneity and the Ligand-Receptor Interactome by Single-Cell Transcriptomics in Real-world Pancreatic Cancer Biopsies', Clin Cancer Res, 27: 5912-21.

64. McDonald, O. G., X. Li, T. Saunders, R. Tryggvadottir, S. J. Mentch, M. O. Warmoes, A. E. Word, A. Carrer, T. H. Salz, S. Natsume, K. M. Stauffer, A. Makohon-Moore, Y. Zhong, H. Wu, K. E. Wellen, J. W. Locasale, C. A. Iacobuzio-Donahue, and A. P. Feinberg. 2017. 'Epigenomic reprogramming during pancreatic cancer progression links anabolic glucose metabolism to distant metastasis', *Nat Genet*, 49: 367-76.

65. Cancer Genome Atlas Research Network (2017). "Integrated Genomic Characterization of Pancreatic Ductal Adenocarcinoma." Cancer Cell **32**(2): 185-203.e113.

66. Harada, T., C. Chelala, V. Bhakta, T. Chaplin, K. Caulee, P. Baril, B. D. Young, and N. R. Lemoine. 2008. 'Genome-wide DNA copy number analysis in pancreatic cancer using high-density single nucleotide polymorphism arrays', *Oncogene*, 27: 1951-60.

67. Ruggeri, B., S. Y. Zhang, J. Caamano, M. DiRado, S. D. Flynn, and A. J. Klein-Szanto. 1992. 'Human pancreatic carcinomas and cell lines reveal frequent and multiple alterations in the p53 and Rb-1 tumor-suppressor genes', Oncogene, 7: 1503-11.

68. Liu, Y., Y. Mi, T. Mueller, S. Kreibich, E. G. Williams, A. Van Drogen, C. Borel, M. Frank, P. L. Germain, I. Bludau, M. Mehnert, M. Seifert, M. Emmenlauer, I. Sorg, F. Bezrukov, F. S. Bena, H. Zhou, C. Dehio, G. Testa, J. Saez-Rodriguez, S. E. Antonarakis, W. D. Hardt, and R. Aebersold. 2019. 'Multi-omic measurements of heterogeneity in HeLa cells across laboratories',

Nat Biotechnol, 37: 314-22.

69. Ben-David, U., B. Siranosian, G. Ha, H. Tang, Y. Oren, K. Hinohara, C. A. Strathdee, J. Dempster, N. J. Lyons, R. Burns, A. Nag, G. Kugener, B. Cimini, P. Tsvetkov, Y. E. Maruvka, R. O'Rourke, A. Garrity, A. A. Tubelli, P. Bandopadhayay, A. Tsherniak, F. Vazquez, B. Wong, C. Birger, M. Ghandi, A. R. Thorner, J. A. Bittker, M. Meyerson, G. Getz, R. Beroukhim, and T. R. Golub. 2018. 'Genetic and transcriptional evolution alters cancer cell line drug response', Nature, 560: 325-30.

70. Aung, K. L., S. E. Fischer, R. E. Denroche, G. H. Jang, A. Dodd, S. Creighton, B. Southwood, S. B. Liang, D. Chadwick, A. Zhang, G. M. O'Kane, H. Albaba, S. Moura, R. C. Grant, J. K. Miller, F. Mbabaali, D. Pasternack, I. M. Lungu, J. M. S. Bartlett, S. Ghai, M. Lemire, S. Holter, A. A. Connor, R. A. Moffitt, J. J. Yeh, L. Timms, P. M. Krzyzanowski, N. Dhani, D. Hedley, F. Notta, J. M. Wilson, M. J. Moore, S. Gallinger, and J. J. Knox. 2018. 'Genomics-Driven Precision Medicine for Advanced Pancreatic Cancer: Early Results from the COMPASS Trial', Clin Cancer Res, 24: 1344-54.

71. Raghavan, S., P. S. Winter, A. W. Navia, H. L. Williams, A. DenAdel, K. E. Lowder, J. Galvez-Reyes, R. L. Kalekar, N. Mulugeta, K. S. Kapner, M. S. Raghavan, A. A. Borah, N. Liu, S. A. Vayrynen, A. D. Costa, R. W. S. Ng, J. Wang, E. K. Hill, D. Y. Ragon, L. K. Brais, A. M. Jaeger, L. F. Spurr, Y. Y. Li, A. D. Cherniack, M. A. Booker, E. F. Cohen, M. Y. Tolstorukov, I. Wakiro, A. Rotem, B. E. Johnson, J. M. McFarland, E. T. Sicinska, T. E. Jacks, R. J. Sullivan, G. I. Shapiro, T. E. Clancy, K. Perez, D. A. Rubinson, K. Ng, J. M. Cleary, L. Crawford, S. R. Manalis, J. A. Nowak, B. M. Wolpin, W. C. Hahn, A. J. Aguirre, and A. K. Shalek. 2021. 'Microenvironment drives cell state, plasticity, and drug response in pancreatic cancer', Cell, 184: 6119-37 e26.

72. Marchesi, F., P. Monti, B. E. Leone, A. Zerbi, A. Vecchi, L. Piemonti, A. Mantovani, and P. Allavena. 2004. 'Increased survival, proliferation, and migration in metastatic human pancreatic tumor cells expressing functional CXCR4', *Cancer Res*, 64: 8420-7.

73. Fredebohm, J., M. Boettcher, C. Eisen, M. M. Gaida, A. Heller, S. Keleg, J. Tost, K. M. Greulich-Bode, A. Hotz-Wagenblatt, M. Lathrop, N. A. Giese, and J. D. Hoheisel. 2012. 'Establishment and characterization of a highly tumourigenic and cancer stem cell enriched pancreatic cancer cell line as a well defined model system', PLoS One, 7: e48503.

74. Huang, L., A. Holtzinger, I. Jagan, M. BeGora, I. Lohse, N. Ngai, C. Nostro, R. Wang, L. B. Muthuswamy, H. C. Crawford, C. Arrowsmith, S. E. Kalloger, D. J. Renouf, A. A. Connor, S. Cleary, D. F. Schaeffer, M. Roehrl, M. S. Tsao, S. Gallinger, G. Keller, and S. K. Muthuswamy. 2015. 'Ductal pancreatic cancer modeling and drug screening using human pluripotent stem cell- and patient-derived tumor organoids', Nat Med, 21: 1364-71.

75. Semaan, A., V. Bernard, J. J. Lee, J. W. Wong, J. Huang, D. B. Swartzlander, B. M. Stephens, M. E. Monberg, B. R. Weston, M. S. Bhutani, K. Chang, P. A. Scheet, A. Maitra, Y. A. Jakubek, and P. A. Guerrero. 2021. 'Defining the Comprehensive Genomic Landscapes of Pancreatic Ductal Adenocarcinoma Using Real-World Endoscopic Aspiration Samples', *Clin Cancer Res*, 27: 1082-93.

76. Van der Auwera, G. A., M. O. Carneiro, C. Hartl, R. Poplin, G. Del Angel, A. Levy-Moonshine, T. Jordan, K. Shakir, D. Roazen, J. Thibault, E. Banks, K. V. Garimella, D. Altshuler, S. Gabriel, and M. A. DePristo. 2013. 'From FastQ data to high confidence variant calls: the Genome Analysis Toolkit best practices pipeline', Curr Protoc Bioinformatics, 43: 11 10 1-11 10 33.

77. Butler, A., P. Hoffman, P. Smibert, E. Papalexi, and R. Satija. 2018. 'Integrating single-cell transcriptomic data across different conditions, technologies, and species', Nat Biotechnol, 36:

411-20.

78. Castillo, J., V. Bernard, F. A. San Lucas, K. Allenson, M. Capello, D. U. Kim, P. Gascoyne, F. C. Mulu, B. M. Stephens, J. Huang, H. Wang, A. A. Momin, R. O. Jacamo, M. Katz, R. Wolff, M. Javle, G. Varadhachary, Wistuba, II, S. Hanash, A. Maitra, and H. Alvarez. 2018. 'Surfaceome profiling enables isolation of cancer-specific exosomal cargo in liquid biopsies from pancreatic cancer patients', Ann Oncol, 29: 223-29.

79. Korotkevich, Gennady, Vladimir Sukhov, Nikolay Budin, Boris Shpak, Maxim N. Artyomov, and Alexey Sergushichev. 2021. 'Fast gene set enrichment analysis', *bioRxiv*: 060012.

80. Setty, M., V. Kiseliovas, J. Levine, A. Gayoso, L. Mazutis, and D. Pe'er. 2019. 'Characterization of cell fate probabilities in single-cell data with Palantir', Nat Biotechnol, 37: 451-60.

81. Lafon, S., Y. Keller, and R. R. Coifman. 2006. 'Data fusion and multicue data matching by diffusion maps', *IEEE Trans Pattern Anal Mach Intell*, 28: 1784-97.

82. Azizi, E., A. J. Carr, G. Plitas, A. E. Cornish, C. Konopacki, S. Prabhakaran, J. Nainys, K. Wu, V. Kiseliovas, M. Setty, K. Choi, R. M. Fromme, P. Dao, P. T. McKenney, R. C. Wasti, K. Kadaveru, L. Mazutis, A. Y. Rudensky, and D. Pe'er. 2018. 'Single-Cell Map of Diverse Immune Phenotypes in the Breast Tumor Microenvironment', Cell, 174: 1293-308 e36.

83. Mayer, C., C. Hafemeister, R. C. Bandler, R. Machold, R. Batista Brito, X. Jaglin, K. Allaway, A. Butler, G. Fishell, and R. Satija. 2018. 'Developmental diversification of cortical inhibitory interneurons', Nature, 555: 457-62.

84. Haghverdi, L., M. Buttner, F. A. Wolf, F. Buettner, and F. J. Theis. 2016. 'Diffusion pseudotime robustly reconstructs lineage branching', *Nat Methods*, 13: 845-8.

85. McInnes, Leland, John Healy, and James Melville. 2018. 'Umap: Uniform manifold approximation and projection for dimension reduction', arXiv preprint arXiv:1802.03426.

86. Sinha, A., D. Cherba, H. Bartlam, E. Lenkiewicz, L. Evers, M. T. Barrett, and B. B. Haab. 2014. 'Mesenchymal-like pancreatic cancer cells harbor specific genomic alterations more frequently than their epithelial-like counterparts', *Mol Oncol*, 8: 1253-65.

87. Lee, K. M., H. Yasuda, M. A. Hollingsworth, and M. M. Ouellette. 2005. 'Notch 2-positive progenitors with the intrinsic ability to give rise to pancreatic ductal cells', Lab Invest, 85: 1003-12.

88. Kim, T., I. R. Chen, Y. Lin, A. Y. Wang, J. Y. H. Yang, and P. Yang. 2019. 'Impact of similarity metrics on single-cell RNA-seq data clustering', *Brief Bioinform*, 20: 2316-26.

89. Chen, S. H., Y. Zhang, R. D. Van Horn, T. Yin, S. Buchanan, V. Yadav, I. Mochalkin, S. S. Wong, Y. G. Yue, L. Huber, I. Conti, J. R. Henry, J. J. Starling, G. D. Plowman, and S. B. Peng. 2016. 'Oncogenic BRAF Deletions That Function as Homodimers and Are Sensitive to Inhibition by RAF Dimer Inhibitor LY3009120', *Cancer Discov*, 6: 300-15.

90. Furukawa, T., W. P. Duguid, L. Rosenberg, J. Viallet, D. A. Galloway, and M. S. Tsao. 1996. 'Long-term culture and immortalization of epithelial cells from normal adult human pancreatic ducts transfected by the E6E7 gene of human papilloma virus 16', Am J Pathol, 148: 1763-70.

91. Marcotte, R., K. R. Brown, F. Suarez, A. Sayad, K. Karamboulas, P. M. Krzyzanowski, F. Sircoulomb, M. Medrano, Y. Fedyshyn, J. L. Y. Koh, D. van Dyk, B. Fedyshyn, M. Luhova, G. C. Brito, F. J. Vizeacoumar, F. S. Vizeacoumar, A. Datti, D. Kasimer, A. Buzina, P. Mero, C. Misquitta, J. Normand, M. Haider, T. Ketela, J. L. Wrana, R. Rottapel, B. G. Neel, and J. Moffat. 2012. 'Essential gene profiles in breast, pancreatic, and ovarian cancer cells', Cancer Discov, 2: 172-89.

92. Radulovich, Nikolina, Jia-ying Qian, and Ming-Sound Tsao. 2008. 'Human Pancreatic Duct Epithelial Cell Model for KRAS Transformation.' in, Methods in Enzymology (Academic Press).
93. Furukawa, T. 2015. 'Impacts of activation of the mitogen-activated protein kinase pathway in pancreatic cancer', Front Oncol, 5: 23.

94. Li, D., J. Zhu, P. F. Firozi, J. L. Abbruzzese, D. B. Evans, K. Cleary, H. Friess, and S. Sen. 2003. 'Overexpression of oncogenic STK15/BTAK/Aurora A kinase in human pancreatic cancer', Clin Cancer Res, 9: 991-7.

95. Yoshida, K., and Y. Miki. 2004. 'Role of BRCA1 and BRCA2 as regulators of DNA repair, transcription, and cell cycle in response to DNA damage', Cancer Sci, 95: 866-71.

96. Nguyen, L., W. M. Martens J, A. Van Hoeck, and E. Cuppen. 2020. 'Pan-cancer landscape of homologous recombination deficiency', Nat Commun, 11: 5584.

97. Cavo, M., D. Delle Cave, E. D'Amone, G. Gigli, E. Lonardo, and L. L. Del Mercato. 2020. 'A synergic approach to enhance long-term culture and manipulation of MiaPaCa-2 pancreatic cancer spheroids', Sci Rep, 10: 10192.

98. Shirk, A. J., and R. Kuver. 2005. 'Epidermal growth factor mediates detachment from and invasion through collagen I and Matrigel in Capan-1 pancreatic cancer cells', BMC Gastroenterol, 5: 12.

99. Tickle T, Tirosh I, Georgescu C, Brown M, Haas B (2019). inferCNV of the Trinity CTAT Project.. Klarman Cell Observatory, Broad Institute of MIT and Harvard, Cambridge, MA, USA. https://github.com/broadinstitute/inferCNV.

100. Macaulay, I. C., W. Haerty, P. Kumar, Y. I. Li, T. X. Hu, M. J. Teng, M. Goolam, N. Saurat, P. Coupland, L. M. Shirley, M. Smith, N. Van der Aa, R. Banerjee, P. D. Ellis, M. A. Quail, H. P. Swerdlow, M. Zernicka-Goetz, F. J. Livesey, C. P. Ponting, and T. Voet. 2015. 'G&T-seq: parallel sequencing of single-cell genomes and transcriptomes', Nat Methods, 12: 519-22.

101. Dey, S. S., L. Kester, B. Spanjaard, M. Bienko, and A. van Oudenaarden. 2015. 'Integrated genome and transcriptome sequencing of the same cell', Nat Biotechnol, 33: 285-89.

102. Han, K. Y., K. T. Kim, J. G. Joung, D. S. Son, Y. J. Kim, A. Jo, H. J. Jeon, H. S. Moon, C. E. Yoo, W. Chung, H. H. Eum, S. Kim, H. K. Kim, J. E. Lee, M. J. Ahn, H. O. Lee, D. Park, and W. Y. Park. 2018. 'SIDR: simultaneous isolation and parallel sequencing of genomic DNA and total RNA from single cells', Genome Res, 28: 75-87.

103. Campbell, K. R., A. Steif, E. Laks, H. Zahn, D. Lai, A. McPherson, H. Farahani, F. Kabeer, C. O'Flanagan, J. Biele, J. Brimhall, B. Wang, P. Walters, Imaxt Consortium, A. Bouchard-Cote, S. Aparicio, and S. P. Shah. 2019. 'clonealign: statistical integration of independent single-cell RNA and DNA sequencing data from human cancers', Genome Biol, 20: 54.

104. Birnbaum, D. J., P. Finetti, A. Lopresti, M. Gilabert, F. Poizat, J. L. Raoul, J. R. Delpero, V. Moutardier, D. Birnbaum, E. Mamessier, and F. Bertucci. 2017. 'A 25-gene classifier predicts overall survival in resectable pancreatic cancer', BMC Med, 15: 170.

105. Chen, R., S. Pan, N. A. Ottenhof, R. F. de Wilde, C. L. Wolfgang, Z. Lane, J. Post, M. P. Bronner, J. K. Willmann, A. Maitra, and T. A. Brentnall. 2012. 'Stromal galectin-1 expression is associated with long-term survival in resectable pancreatic ductal adenocarcinoma', Cancer Biol Ther, 13: 899-907.

106. Chen, R., D. W. Dawson, S. Pan, N. A. Ottenhof, R. F. de Wilde, C. L. Wolfgang, D. H. May, D. A. Crispin, L. A. Lai, A. R. Lay, M. Waghray, S. Wang, M. W. McIntosh, D. M. Simeone, A. Maitra, and T. A. Brentnall. 2015. 'Proteins associated with pancreatic cancer survival in patients with resectable pancreatic ductal adenocarcinoma', Lab Invest, 95: 43-55.

107. Feng, Y., L. Gao, G. Cui, and Y. Cao. 2020. 'LncRNA NEAT1 facilitates pancreatic cancer growth and metastasis through stabilizing ELF3 mRNA', Am J Cancer Res, 10: 237-48.

108. Torres, C., and P. J. Grippo. 2018. 'Pancreatic cancer subtypes: a roadmap for precision medicine', Ann Med, 50: 277-87.

109. Zeeberg, K., R. A. Cardone, M. R. Greco, M. Saccomano, A. Nohr-Nielsen, F. Alves, S. F. Pedersen, and S. J. Reshkin. 2016. 'Assessment of different 3D culture systems to study tumor phenotype and chemosensitivity in pancreatic ductal adenocarcinoma', Int J Oncol, 49: 243-52.

110. Lazzari, G., V. Nicolas, M. Matsusaki, M. Akashi, P. Couvreur, and S. Mura. 2018. 'Multicellular spheroid based on a triple co-culture: A novel 3D model to mimic pancreatic tumor

complexity', Acta Biomater, 78: 296-307.

111. Longati, P., X. Jia, J. Eimer, A. Wagman, M. R. Witt, S. Rehnmark, C. Verbeke, R. Toftgard, M. Lohr, and R. L. Heuchel. 2013. '3D pancreatic carcinoma spheroids induce a matrix-rich, chemoresistant phenotype offering a better model for drug testing', BMC Cancer, 13: 95.

112. Loessner, D., K. S. Stok, M. P. Lutolf, D. W. Hutmacher, J. A. Clements, and S. C. Rizzi. 2010. 'Bioengineered 3D platform to explore cell-ECM interactions and drug resistance of epithelial ovarian cancer cells', Biomaterials, 31: 8494-506.

113. Riedl, A., M. Schlederer, K. Pudelko, M. Stadler, S. Walter, D. Unterleuthner, C. Unger, N. Kramer, M. Hengstschlager, L. Kenner, D. Pfeiffer, G. Krupitza, and H. Dolznig. 2017. 'Comparison of cancer cells in 2D vs 3D culture reveals differences in AKT-mTOR-S6K signaling and drug responses', J Cell Sci, 130: 203-18.

114. Stuart, T., A. Srivastava, S. Madad, C. A. Lareau, and R. Satija. 2021. 'Single-cell chromatin state analysis with Signac', Nat Methods, 18: 1333-41.

115. Papa, L., et al. (2014). "SOD1, an unexpected novel target for cancer therapy." Genes Cancer 5(1-2): 15-21.

116. Huang, Y. H., et al. (2020). "ID1 Mediates Escape from TGFbeta Tumor Suppression in Pancreatic Cancer." Cancer Discov 10(1): 142-157.

117. Masoud, R., et al. (2020). "Targeting Mitochondrial Complex I Overcomes Chemoresistance in High OXPHOS Pancreatic Cancer." Cell Rep Med 1(8): 100143.

118. Zhang, Y., et al. (1998). "Smad3 and Smad4 cooperate with c-Jun/c-Fos to mediate TGF-beta-induced transcription." Nature 394(6696): 909-913.

119. Jacob, F., R. D. Salinas, D. Y. Zhang, P. T. T. Nguyen, J. G. Schnoll, S. Z. H. Wong, R. Thokala, S. Sheikh, D. Saxena, S. Prokop, D. A. Liu, X. Qian, D. Petrov, T. Lucas, H. I. Chen, J. F. Dorsey, K. M. Christian, Z. A. Binder, M. Nasrallah, S. Brem, D. M. O'Rourke, G. L. Ming, and H. Song. 2020. 'A Patient-Derived Glioblastoma Organoid Model and Biobank Recapitulates Inter- and Intra-tumoral Heterogeneity', Cell, 180: 188-204 e22.

120. Ganesh, K., C. Wu, K. P. O'Rourke, B. C. Szeglin, Y. Zheng, C. G. Sauve, M. Adileh, I. Wasserman, M. R. Marco, A. S. Kim, M. Shady, F. Sanchez-Vega, W. R. Karthaus, H. H. Won, S. H. Choi, R. Pelossof, A. Barlas, P. Ntiamoah, E. Pappou, A. Elghouayel, J. S. Strong, C. T. Chen, J. W. Harris, M. R. Weiser, G. M. Nash, J. G. Guillem, I. H. Wei, R. N. Kolesnick, H. Veeraraghavan, E. J. Ortiz, I. Petkovska, A. Cercek, K. O. Manova-Todorova, L. B. Saltz, J. A. Lavery, R. P. DeMatteo, J. Massague, P. B. Paty, R. Yaeger, X. Chen, S. Patil, H. Clevers, M. F. Berger, S. W. Lowe, J. Shia, P. B. Romesser, L. E. Dow, J. Garcia-Aguilar, C. L. Sawyers, and J. J. Smith. 2019. 'A rectal cancer organoid platform to study individual responses to chemoradiation', Nat Med, 25: 1607-14.

121. Ooft, S. N., F. Weeber, K. K. Dijkstra, C. M. McLean, S. Kaing, E. van Werkhoven, L. Schipper, L. Hoes, D. J. Vis, J. van de Haar, W. Prevoo, P. Snaebjornsson, D. van der Velden, M. Klein, M. Chalabi, H. Boot, M. van Leerdam, H. J. Bloemendal, L. V. Beerepoot, L. Wessels, E. Cuppen, H. Clevers, and E. E. Voest. 2019. 'Patient-derived organoids can predict response

to chemotherapy in metastatic colorectal cancer patients', Sci Transl Med, 11.

122. Topham, J. T., J. M. Karasinska, M. K. C. Lee, V. Csizmok, L. M. Williamson, G. H. Jang, R. E. Denroche, E. S. Tsang, S. E. Kalloger, H. L. Wong, G. M. O'Kane, R. A. Moore, A. J. Mungall, F. Notta, J. M. Loree, J. M. Wilson, O. Bathe, P. A. Tang, R. Goodwin, J. J. Knox, S. Gallinger, J. Laskin, M. A. Marra, S. J. M. Jones, D. J. Renouf, and D. F. Schaeffer. 2021. 'Subtype-Discordant Pancreatic Ductal Adenocarcinoma Tumors Show Intermediate Clinical and Molecular Characteristics', Clin Cancer Res, 27: 150-57.

123. Porter, R. L., N. K. C. Magnus, V. Thapar, R. Morris, A. Szabolcs, A. Neyaz, A. S. Kulkarni, E. Tai, A. Chougule, A. Hillis, G. Golczer, H. Guo, T. Yamada, T. Kurokawa, C. Yashaswini, M. Ligorio, K. D. Vo, L. Nieman, A. S. Liss, V. Deshpande, M. S. Lawrence, S. Maheswaran, C. Fernandez-Del Castillo, T. S. Hong, D. P. Ryan, P. J. O'Dwyer, J. A. Drebin, C. R. Ferrone, D. A. Haber, and D. T. Ting. 2019. 'Epithelial to mesenchymal plasticity and differential response to therapies in pancreatic ductal adenocarcinoma', Proc Natl Acad Sci U S A.

124. Minussi, Darlan C., Michael D. Nicholson, Hanghui Ye, Alexander Davis, Kaile Wang, Toby Baker, Maxime Tarabichi, Emi Sei, Haowei Du, Mashiat Rabbani, Cheng Peng, Min Hu, Shanshan Bai, Yu-wei Lin, Aislyn Schalck, Asha Multani, Jin Ma, Thomas O. McDonald, Anna Casasent, Angelica Barrera, Hui Chen, Bora Lim, Banu Arun, Funda Meric-Bernstam, Peter Van Loo, Franziska Michor, and Nicholas E. Navin. 2021. 'Breast tumours maintain a reservoir of subclonal diversity during expansion', Nature.

125. Cox, A. D., and C. J. Der. 2021. 'Filling in the GAPs in understanding RAS', Science, 374: 152-53.

126. Mao, Zhongwei, Hongying Xiao, Panpan Shen, Yu Yang, Jing Xue, Yunyun Yang, Yanguo Shang, Lilan Zhang, Xin Li, Yuying Zhang, Yanan Du, Chun-Chi Chen, Rey-Ting Guo, and Yonghui Zhang. 2022. 'KRAS(G12D) can be targeted by potent inhibitors via formation of salt bridge', Cell Discovery, 8: 5

127. Wang, Xiaolun, Shelley Allen, James F. Blake, Vickie Bowcut, David M. Briere, Andrew Calinisan, Joshua R. Dahlke, Jay B. Fell, John P. Fischer, Robin J. Gunn, Jill Hallin, Jade Laguer, J. David Lawson, James Medwid, Brad Newhouse, Phong Nguyen, Jacob M. O'Leary, Peter Olson, Spencer Pajk, Lisa Rahbaek, Mareli Rodriguez, Christopher R. Smith, Tony P. Tang, Nicole C. Thomas, Darin Vanderpool, Guy P. Vigers, James G. Christensen, and Matthew A. Marx. 2022. 'Identification of MRTX1133, a Noncovalent, Potent, and Selective KRASG12D Inhibitor', Journal of Medicinal Chemistry, 65: 3123-33.

128. Pishvaian, M. J., R. J. Bender, D. Halverson, L. Rahib, A. E. Hendifar, S. Mikhail, V. Chung, V. J. Picozzi, D. Sohal, E. M. Blais, K. Mason, E. E. Lyons, L. M. Matrisian, J. R. Brody, S. Madhavan, and E. F. Petricoin, 3rd. 2018. 'Molecular Profiling of Patients with Pancreatic Cancer: Initial Results from the Know Your Tumor Initiative', Clin Cancer Res, 24: 5018-27.

129. Reiter, J. G., A. P. Makohon-Moore, J. M. Gerold, I. Bozic, K. Chatterjee, C. A. Iacobuzio-Donahue, B. Vogelstein, and M. A. Nowak. 2017. 'Reconstructing metastatic seeding patterns of human cancers', Nat Commun, 8: 14114.

130. Ryan, David P., Theodore S. Hong, and Nabeel Bardeesy. 2014. 'Pancreatic Adenocarcinoma', New England Journal of Medicine, 371: 1039-49.

131. Seth, Sahil, Chieh-Yuan Li, I. Lin Ho, Denise Corti, Sara Loponte, Luigi Sapio, Edoardo Del Poggetto, Er-Yen Yen, Frederick Scott Robinson, Michael Peoples, Tatiana Karpinets,

Angela Kay Deem, Tapsi Kumar, Xingzhi Song, Shan Jiang, Ya'an Kang, Jason Fleming, Michael Kim, Jianhua Zhang, Anirban Maitra, Timothy Paul Heffernan, Virginia Giuliani, Giannicola Genovese, Andrew Futreal, Giulio Francesco Draetta, Alessandro Carugo, and Andrea Viale. 2019. 'Pre-existing Functional Heterogeneity of Tumorigenic Compartment as the Origin of Chemoresistance in Pancreatic Tumors', Cell Reports, 26: 1518-32.e9.

132. Beatty, G. L., G. Werba, C. A. Lyssiotis, and D. M. Simeone. 2021. 'The biological underpinnings of therapeutic resistance in pancreatic cancer', Genes Dev, 35: 940-62.

133. Juiz, Natalia Anahi, Juan Iovanna, and Nelson Dusetti. 2019. 'Pancreatic Cancer Heterogeneity Can Be Explained Beyond the Genome', Frontiers in Oncology, 9.

134. Bernard, V., A. Semaan, J. Huang, F. A. San Lucas, F. C. Mulu, B. M. Stephens, P. A. Guerrero, Y. Huang, J. Zhao, N. Kamyabi, S. Sen, P. A. Scheet, C. M. Taniguchi, M. P. Kim, C. W. Tzeng, M. H. Katz, A. D. Singhi, A. Maitra, and H. A. Alvarez. 2019. 'Single-Cell Transcriptomics of Pancreatic Cancer Precursors Demonstrates Epithelial and Microenvironmental Heterogeneity as an Early Event in Neoplastic Progression', Clin Cancer Res, 25: 2194-205.

135. Wolff, R. A., A. Wang-Gillam, H. Alvarez, H. Tiriac, D. Engle, S. Hou, A. F. Groff, A. San Lucas, V. Bernard, K. Allenson, J. Castillo, D. Kim, F. Mulu, J. Huang, B. Stephens, Wistuba, II, M. Katz, G. Varadhachary, Y. Park, J. Hicks, A. Chinnaiyan, L. Scampavia, T. Spicer, C. Gerhardinger, A. Maitra, D. Tuveson, J. Rinn, G. Lizee, C. Yee, and A. J. Levine. 2018. 'Dynamic changes during the treatment of pancreatic cancer', Oncotarget, 9: 14764-90.

136. Schreyer, Daniel, John P. Neoptolemos, Simon T. Barry, and Peter Bailey. 2022. 'Deconstructing Pancreatic Cancer Using Next Generation-Omic Technologies–From Discovery

to Knowledge-Guided Platforms for Better Patient Management', Frontiers in Cell and Developmental Biology, 9..

137. Heinz, S., C. E. Romanoski, C. Benner, and C. K. Glass. 2015. 'The selection and function of cell type-specific enhancers', Nat Rev Mol Cell Biol, 16: 144-54.

138. Lomberk, G., Y. Blum, R. Nicolle, A. Nair, K. S. Gaonkar, L. Marisa, A. Mathison, Z. Sun, H. Yan, N. Elarouci, L. Armenoult, M. Ayadi, T. Ordog, J. H. Lee, G. Oliver, E. Klee, V. Moutardier, O. Gayet, B. Bian, P. Duconseil, M. Gilabert, M. Bigonnet, S. Garcia, O. Turrini, J. R. Delpero, M. Giovannini, P. Grandval, M. Gasmi, V. Secq, A. De Reynies, N. Dusetti, J. Iovanna, and R. Urrutia. 2018. 'Distinct epigenetic landscapes underlie the pathobiology of pancreatic cancer subtypes', Nat Commun, 9: 1978.

139. McDonald, Oliver G., Xin Li, Tyler Saunders, Rakel Tryggvadottir, Samantha J. Mentch, Marc O. Warmoes, Anna E. Word, Alessandro Carrer, Tal H. Salz, Sonoko Natsume, Kimberly M. Stauffer, Alvin Makohon-Moore, Yi Zhong, Hao Wu, Kathryn E. Wellen, Jason W. Locasale, Christine A. Iacobuzio-Donahue, and Andrew P. Feinberg. 2017. 'Epigenomic reprogramming during pancreatic cancer progression links anabolic glucose metabolism to distant metastasis', Nature Genetics, 49: 367-76.

140. Marks, P. A. 2007. 'Discovery and development of SAHA as an anticancer agent', Oncogene, 26: 1351-56.

141. Xu, W. S., R. B. Parmigiani, and P. A. Marks. 2007. 'Histone deacetylase inhibitors: molecular mechanisms of action', Oncogene, 26: 5541-52.

142. Manzotti, G., A. Ciarrocchi, and V. Sancisi. 2019. 'Inhibition of BET Proteins and Histone Deacetylase (HDACs): Crossing Roads in Cancer Therapy', Cancers (Basel), 11.

143. Wawruszak, A., L. Borkiewicz, E. Okon, W. Kukula-Koch, S. Afshan, and M. Halasa. 2021. 'Vorinostat (SAHA) and Breast Cancer: An Overview', Cancers (Basel), 13.

144. Woods, D. M., A. L. Sodre, A. Villagra, A. Sarnaik, E. M. Sotomayor, and J. Weber. 2015. 'HDAC Inhibition Upregulates PD-1 Ligands in Melanoma and Augments Immunotherapy with PD-1 Blockade', Cancer Immunol Res, 3: 1375-85.

145. Park, J., D. Eisenbarth, W. Choi, H. Kim, C. Choi, D. Lee, and D. S. Lim. 2020. 'YAP and AP-1 Cooperate to Initiate Pancreatic Cancer Development from Ductal Cells in Mice', Cancer Res, 80: 4768-79.

146. LaFave, Lindsay M., and Jason D. Buenrostro. 2021. 'Unlocking PDAC initiation with AP-1', Nature Cancer, 2: 14-15.

147. Shin, S., T. Asano, Y. Yao, R. Zhang, F. X. Claret, M. Korc, K. Sabapathy, D. G. Menter, J. L. Abbruzzese, and S. A. G. Reddy. 2009. 'Activator protein-1 has an essential role in pancreatic cancer cells and is regulated by a novel Akt-mediated mechanism', Mol Cancer Res, 7: 745-54.

148. Tu, Mengyu, Lukas Klein, Elisa Espinet, Theodoros Georgomanolis, Florian Wegwitz, Xiaojuan Li, Laura Urbach, Adi Danieli-Mackay, Stefan Küffer, Kamil Bojarczuk, Athanasia Mizi, Ufuk Günesdogan, Björn Chapuy, Zuguang Gu, Albrecht Neesse, Uday Kishore, Philipp Ströbel, Elisabeth Hessmann, Stephan A. Hahn, Andreas Trumpp, Argyris Papantonis, Volker Ellenrieder, and Shiv K. Singh. 2021. 'TNF-α-producing macrophages determine subtype

identity and prognosis via AP1 enhancer reprogramming in pancreatic cancer', Nature Cancer, 2: 1185-203.

149. Li, Y., Y. He, J. Peng, Z. Su, Z. Li, B. Zhang, J. Ma, M. Zhuo, D. Zou, X. Liu, X. Liu, W. Wang, D. Huang, M. Xu, J. Wang, H. Deng, J. Xue, W. Xie, X. Lan, M. Chen, Y. Zhao, W. Wu, and C. J. David. 2021. 'Mutant Kras co-opts a proto-oncogenic enhancer network in inflammation-induced metaplastic progenitor cells to initiate pancreatic cancer', Nat Cancer, 2: 49-65.

150. Wang, Y., G. H. Wan, Y. M. Wu, H. S. Wang, H. F. Wang, G. Zhang, L. L. Lu, Z. Q. Li, K. Y. Chan, Y. Zhou, S. H. Cai, Y. F. Qi, and J. Du. 2018. 'AP-1 confers resistance to anti-cancer therapy by activating XIAP', Oncotarget, 9: 14124-37.

151. Nguyen, A. H., I. A. Elliott, N. Wu, C. Matsumura, M. Vogelauer, N. Attar, A. Dann, R. Ghukasyan, P. A. Toste, S. G. Patel, J. L. Williams, L. Li, D. W. Dawson, C. Radu, S. K. Kurdistani, and T. R. Donahue. 2017. 'Histone deacetylase inhibitors provoke a tumor supportive phenotype in pancreatic cancer associated fibroblasts', Oncotarget, 8: 19074-88.

152. Awad, M. M., S. Liu, Rybkin, II, K. C. Arbour, J. Dilly, V. W. Zhu, M. L. Johnson, R. S. Heist, T. Patil, G. J. Riely, J. O. Jacobson, X. Yang, N. S. Persky, D. E. Root, K. E. Lowder, H. Feng, S. S. Zhang, K. M. Haigis, Y. P. Hung, L. M. Sholl, B. M. Wolpin, J. Wiese, J. Christiansen, J. Lee, A. B. Schrock, L. P. Lim, K. Garg, M. Li, L. D. Engstrom, L. Waters, J. D. Lawson, P. Olson, P. Lito, S. I. Ou, J. G. Christensen, P. A. Janne, and A. J. Aguirre. 2021. 'Acquired Resistance to KRAS(G12C) Inhibition in Cancer', N Engl J Med, 384: 2382-93.

153. Stuart, T., A. Butler, P. Hoffman, C. Hafemeister, E. Papalexi, W. M. Mauck, 3rd, Y. Hao, M. Stoeckius, P. Smibert, and R. Satija. 2019. 'Comprehensive Integration of Single-Cell Data',

Cell, 177: 1888-902 e21.

154. Tiriac, H., P. Belleau, D. D. Engle, D. Plenker, A. Deschenes, T. D. D. Somerville, F. E. M. Froeling, R. A. Burkhart, R. E. Denroche, G. H. Jang, K. Miyabayashi, C. M. Young, H. Patel, M. Ma, J. F. LaComb, R. L. D. Palmaira, A. A. Javed, J. C. Huynh, M. Johnson, K. Arora, N. Robine, M. Shah, R. Sanghvi, A. B. Goetz, C. Y. Lowder, L. Martello, E. Driehuis, N. LeComte, G. Askan, C. A. Iacobuzio-Donahue, H. Clevers, L. D. Wood, R. H. Hruban, E. Thompson, A. J. Aguirre, B. M. Wolpin, A. Sasson, J. Kim, M. Wu, J. C. Bucobo, P. Allen, D. V. Sejpal, W. Nealon, J. D. Sullivan, J. M. Winter, P. A. Gimotty, J. L. Grem, D. J. DiMaio, J. M. Buscaglia, P. M. Grandgenett, J. R. Brody, M. A. Hollingsworth, G. M. O'Kane, F. Notta, E. Kim, J. M. Crawford, C. Devoe, A. Ocean, C. L. Wolfgang, K. H. Yu, E. Li, C. R. Vakoc, B. Hubert, S. E. Fischer, J. M. Wilson, R. Moffitt, J. Knox, A. Krasnitz, S. Gallinger, and D. A. Tuveson. 2018. 'Organoid Profiling Identifies Common Responders to Chemotherapy in Pancreatic Cancer', Cancer Discov, 8: 1112-29.

155. Raimondi, G., A. Mato-Berciano, S. Pascual-Sabater, M. Rovira-Rigau, M. Cuatrecasas, C. Fondevila, S. Sanchez-Cabus, H. Begthel, S. F. Boj, H. Clevers, and C. Fillat. 2020. 'Patient-derived pancreatic tumour organoids identify therapeutic responses to oncolytic adenoviruses', EBioMedicine, 56: 102786.

156. Wu, Zuoqiao, Mary Nicoll, and Robert J. Ingham. 2021. 'AP-1 family transcription factors: a diverse family of proteins that regulate varied cellular activities in classical hodgkin lymphoma and ALK+ ALCL', Experimental Hematology & Oncology, 10: 4.
157. Seo, J., D. D. Kocak, L. C. Bartelt, C. A. Williams, A. Barrera, C. A. Gersbach, and T. E. Reddy. 2021. 'AP-1 subunits converge promiscuously at enhancers to potentiate transcription', Genome Res, 31: 538-50.

158. Zhang, L., and Q. Nie. 2021. 'scMC learns biological variation through the alignment of multiple single-cell genomics datasets', Genome Biol, 22: 10.

159. Borcherding, N, and J. Andrews. 2021. "escape: Easy single cell analysis platform for enrichment." R package version 1.0.1.

160. Subramanian, A., P. Tamayo, V. K. Mootha, S. Mukherjee, B. L. Ebert, M. A. Gillette, A. Paulovich, S. L. Pomeroy, T. R. Golub, E. S. Lander, and J. P. Mesirov. 2005. 'Gene set enrichment analysis: a knowledge-based approach for interpreting genome-wide expression profiles', Proc Natl Acad Sci U S A, 102: 15545-50.

161. Chinenov, Y., and T. K. Kerppola. 2001. 'Close encounters of many kinds: Fos-Jun interactions that mediate transcription regulatory specificity', Oncogene, 20: 2438-52.

162. Fu, S. L., A. Waha, and P. K. Vogt. 2000. 'Identification and characterization of genes upregulated in cells transformed by v-Jun', Oncogene, 19: 3537-45.

163. Aikawa, Yukihiko, Kimiko Morimoto, Tetsuya Yamamoto, Hisaaki Chaki, Akira Hashiramoto, Hirokazu Narita, Shuichi Hirono, and Shunichi Shiozawa. 2008. 'Treatment of arthritis with a selective inhibitor of c-Fos/activator protein-1', Nature Biotechnology, 26: 817-23.

164. Makino, Hiroto, Shoji Seki, Yasuhito Yahara, Shunichi Shiozawa, Yukihiko Aikawa, Hiraku Motomura, Makiko Nogami, Kenta Watanabe, Takeshi Sainoh, Hisakatsu Ito, Noriyuki Tsumaki, Yoshiharu Kawaguchi, Mitsuaki Yamazaki, and Tomoatsu Kimura. 2017. 'A selective inhibition of c-Fos/activator protein-1 as a potential therapeutic target for intervertebral disc degeneration and associated pain', Scientific Reports, 7: 16983.

165. Truong, A. S., M. Zhou, B. Krishnan, T. Utsumi, U. Manocha, K. G. Stewart, W. Beck, T. L. Rose, M. I. Milowsky, X. He, C. C. Smith, L. M. Bixby, C. M. Perou, S. E. Wobker, S. T. Bailey, B. G. Vincent, and W. Y. Kim. 2021. 'Entinostat induces antitumor immune responses through immune editing of tumor neoantigens', J Clin Invest, 131.

166. Palma, G., F. Khurshid, K. Lu, B. Woodward, and H. Husain. 2021. 'Selective KRAS G12C inhibitors in non-small cell lung cancer: chemistry, concurrent pathway alterations, and clinical outcomes', NPJ Precis Oncol, 5: 98.

167. Nakajima, E. C., N. Drezner, X. Li, P. S. Mishra-Kalyani, Y. Liu, H. Zhao, Y. Bi, J. Liu, A. Rahman, E. Wearne, I. Ojofeitimi, L. T. Hotaki, D. Spillman, R. Pazdur, J. A. Beaver, and H. Singh. 2022. 'FDA Approval Summary: Sotorasib for KRAS G12C-Mutated Metastatic NSCLC', Clin Cancer Res, 28: 1482-86.

168. Bryant, K. L., C. A. Stalnecker, D. Zeitouni, J. E. Klomp, S. Peng, A. P. Tikunov, V. Gunda, M. Pierobon, A. M. Waters, S. D. George, G. Tomar, B. Papke, G. A. Hobbs, L. Yan, T. K. Hayes, J. N. Diehl, G. D. Goode, N. V. Chaika, Y. Wang, G. F. Zhang, A. K. Witkiewicz, E. S. Knudsen, E. F. Petricoin, 3rd, P. K. Singh, J. M. Macdonald, N. L. Tran, C. A. Lyssiotis, H. Ying, A. C. Kimmelman, A. D. Cox, and C. J. Der. 2019. 'Combination of ERK and autophagy inhibition as a treatment approach for pancreatic cancer', Nat Med, 25: 628-40.

169. Kinsey, C. G., S. A. Camolotto, A. M. Boespflug, K. P. Guillen, M. Foth, A. Truong, S. S. Schuman, J. E. Shea, M. T. Seipp, J. T. Yap, L. D. Burrell, D. H. Lum, J. R. Whisenant, G. W. Gilcrease, 3rd, C. C. Cavalieri, K. M. Rehbein, S. L. Cutler, K. E. Affolter, A. L. Welm, B. E. Welm, C. L. Scaife, E. L. Snyder, and M. McMahon. 2019. 'Protective autophagy elicited by RAF-->MEK-->ERK inhibition suggests a treatment strategy for RAS-driven cancers', Nat Med,

25: 620-27.

170. Gort, Eelke, Melissa Lynne Johnson, Jimmy J. Hwang, Shubham Pant, Ulrich Dünzinger, Kathrin Riemann, Thomas Kitzing, and Pasi A. Janne. 2020. 'A phase I, open-label, dose-escalation trial of BI 1701963 as monotherapy and in combination with trametinib in patients with KRAS mutated advanced or metastatic solid tumors', Journal of Clinical Oncology, 38: TPS3651-TPS51.

171. Hofmann, M. H., M. Gmachl, J. Ramharter, F. Savarese, D. Gerlach, J. R. Marszalek, M. P. Sanderson, D. Kessler, F. Trapani, H. Arnhof, K. Rumpel, D. A. Botesteanu, P. Ettmayer, T. Gerstberger, C. Kofink, T. Wunberg, A. Zoephel, S. C. Fu, J. L. Teh, J. Bottcher, N. Pototschnig, F. Schachinger, K. Schipany, S. Lieb, C. P. Vellano, J. C. O'Connell, R. L. Mendes, J. Moll, M. Petronczki, T. P. Heffernan, M. Pearson, D. B. McConnell, and N. Kraut. 2021. 'BI-3406, a Potent and Selective SOS1-KRAS Interaction Inhibitor, Is Effective in KRAS-Driven Cancers through Combined MEK Inhibition', Cancer Discov, 11: 142-57.

172. Kessler, D., D. Gerlach, N. Kraut, and D. B. McConnell. 2021. 'Targeting Son of Sevenless 1: The pacemaker of KRAS', Curr Opin Chem Biol, 62: 109-18.

173. Savarese, F., M. Gmachl, L. Federico, F. Trapani, D. Gerlach, J. Daniele, N. Feng, C. A. Bristow, A. Machado, J. Huang, D. Rudolph, I. Waizenegger, J. Ramharter, C. P. Vellano, M. Petronczki, J. R. Marszalek, T. P. Heffernan, D. B. McConnell, N. Kraut, and M. Hofmann. 2020. '51 Poster Discussion - Vertical pathway inhibition with a SOS1::KRAS inhibitor enhances the efficacy of KRAS G12C inhibitors, delays feedback resistance and demonstrates durable response', European Journal of Cancer, 138: S22.

174. Hofmann, Marco H., Hengyu Lu, Ulrich Duenzinger, Daniel Gerlach, Francesca Trapani, Annette A. Machado, Joseph R. Daniele, Irene Waizenegger, Michael Gmachl, Dorothea Rudolph, Christopher P. Vellano, Marcelo Marotti, Vitomir Vucenovic, Timothy P. Heffernan, Joseph R. Marszalek, Mark P. Petronczki, and Norbert Kraut. 2021. 'Abstract CT210: Trial in Process: Phase 1 studies of BI 1701963, a SOS1::KRAS Inhibitor, in combination with MEK inhibitors, irreversible KRASG12C inhibitors or irinotecan', Cancer Research, 81: CT210-CT10.

175. Huang, L., et al. (2015). "Ductal pancreatic cancer modeling and drug screening using human pluripotent stem cell- and patient-derived tumor organoids." Nat Med 21(11): 1364-1371.

176. Viale, A., P. Pettazzoni, C. A. Lyssiotis, H. Ying, N. Sanchez, M. Marchesini, A. Carugo, T. Green, S. Seth, V. Giuliani, M. Kost-Alimova, F. Muller, S. Colla, L. Nezi, G. Genovese, A. K. Deem, A. Kapoor, W. Yao, E. Brunetto, Y. Kang, M. Yuan, J. M. Asara, Y. A. Wang, T. P. Heffernan, A. C. Kimmelman, H. Wang, J. B. Fleming, L. C. Cantley, R. A. DePinho, and G. F. Draetta. 2014. 'Oncogene ablation-resistant pancreatic cancer cells depend on mitochondrial function', Nature, 514: 628-32.

177. Ying, H., A. C. Kimmelman, C. A. Lyssiotis, S. Hua, G. C. Chu, E. Fletcher-Sananikone, J. W. Locasale, J. Son, H. Zhang, J. L. Coloff, H. Yan, W. Wang, S. Chen, A. Viale, H. Zheng, J. H. Paik, C. Lim, A. R. Guimaraes, E. S. Martin, J. Chang, A. F. Hezel, S. R. Perry, J. Hu, B. Gan, Y. Xiao, J. M. Asara, R. Weissleder, Y. A. Wang, L. Chin, L. C. Cantley, and R. A. DePinho. 2012. 'Oncogenic Kras maintains pancreatic tumors through regulation of anabolic glucose metabolism', Cell, 149: 656-70.

178. Collins, M. A., F. Bednar, Y. Zhang, J. C. Brisset, S. Galban, C. J. Galban, S. Rakshit, K. S. Flannagan, N. V. Adsay, and M. Pasca di Magliano. 2012. 'Oncogenic Kras is required for

both the initiation and maintenance of pancreatic cancer in mice', J Clin Invest, 122: 639-53.

179. Ostrem, J. M., U. Peters, M. L. Sos, J. A. Wells, and K. M. Shokat. 2013. 'K-Ras(G12C) inhibitors allosterically control GTP affinity and effector interactions', Nature, 503: 548-51.

180. Hallin, J., L. D. Engstrom, L. Hargis, A. Calinisan, R. Aranda, D. M. Briere, N. Sudhakar, V. Bowcut, B. R. Baer, J. A. Ballard, M. R. Burkard, J. B. Fell, J. P. Fischer, G. P. Vigers, Y. Xue, S. Gatto, J. Fernandez-Banet, A. Pavlicek, K. Velastagui, R. C. Chao, J. Barton, M. Pierobon, E. Baldelli, E. F. Patricoin, 3rd, D. P. Cassidy, M. A. Marx, Rybkin, II, M. L. Johnson, S. I. Ou, P. Lito, K. P. Papadopoulos, P. A. Janne, P. Olson, and J. G. Christensen. 2020. 'The KRAS(G12C) Inhibitor MRTX849 Provides Insight toward Therapeutic Susceptibility of KRAS-Mutant Cancers in Mouse Models and Patients', Cancer Discov, 10: 54-71.

181. Canon, J., K. Rex, A. Y. Saiki, C. Mohr, K. Cooke, D. Bagal, K. Gaida, T. Holt, C. G. Knutson, N. Koppada, B. A. Lanman, J. Werner, A. S. Rapaport, T. San Miguel, R. Ortiz, T. Osgood, J. R. Sun, X. Zhu, J. D. McCarter, L. P. Volak, B. E. Houk, M. G. Fakih, B. H. O'Neil, T. J. Price, G. S. Falchook, J. Desai, J. Kuo, R. Govindan, D. S. Hong, W. Ouyang, H. Henary, T. Arvedson, V. J. Cee, and J. R. Lipford. 2019. 'The clinical KRAS(G12C) inhibitor AMG 510 drives anti-tumour immunity', Nature, 575: 217-23.

182. Hong, D. S., M. G. Fakih, J. H. Strickler, J. Desai, G. A. Durm, G. I. Shapiro, G. S. Falchook, T. J. Price, A. Sacher, C. S. Denlinger, Y. J. Bang, G. K. Dy, J. C. Krauss, Y. Kuboki, J. C. Kuo, A. L. Coveler, K. Park, T. W. Kim, F. Barlesi, P. N. Munster, S. S. Ramalingam, T. F. Burns, F. Meric-Bernstam, H. Henary, J. Ngang, G. Ngarmchamnanrith, J. Kim, B. E. Houk, J. Canon, J. R. Lipford, G. Friberg, P. Lito, R. Govindan, and B. T. Li. 2020. 'KRAS(G12C) Inhibition with Sotorasib in Advanced Solid Tumors', N Engl J Med, 383: 1207-17.

183. Riely GJ, Ou SI, Rybkin I, Spira AI, Papadopoulos KP, Sabari JK, et al. 99O_PR - KRYSTAL-1: Activity and Preliminary Pharmacodynamic (PD) Analysis of Adagrasib (MRTX849) in Patients (Pts) With Advanced Non-Small- Cell Lung Cancer (NSCLC) Harboring KRASG12C Mutation. Journal of Thoracic Oncology 2021;16 (suppl_4): S748-S802.

184. Janne PA, Rybkin I, Spira AI, Riely GJ, Papadopoulos KP, Sabari JK, et al. KRYSTAL-1: Activity and Safety of Adagrasib (MRTX849) in Advanced/Metastatic Non–Small-Cell Lung Cancer (NSCLC) Harboring KRAS G12C Mutation. EORTC-NCI-AACR Symposium 2020;Abstract LBA3. Presented October 25, 2020.

185. Zhao, Y., Y. R. Murciano-Goroff, J. Y. Xue, A. Ang, J. Lucas, T. T. Mai, A. F. Da Cruz Paula, A. Y. Saiki, D. Mohn, P. Achanta, A. E. Sisk, K. S. Arora, R. S. Roy, D. Kim, C. Li, L. P. Lim, M. Li, A. Bahr, B. R. Loomis, E. de Stanchina, J. S. Reis-Filho, B. Weigelt, M. Berger, G. Riely, K. C. Arbour, J. R. Lipford, B. T. Li, and P. Lito. 2021. 'Diverse alterations associated with resistance to KRAS(G12C) inhibition', Nature, 599: 679-83.

186. Hou, P., A. Kapoor, Q. Zhang, J. Li, C. J. Wu, J. Li, Z. Lan, M. Tang, X. Ma, J. J. Ackroyd, R. Kalluri, J. Zhang, S. Jiang, D. J. Spring, Y. A. Wang, and R. A. DePinho. 2020. 'Tumor Microenvironment Remodeling Enables Bypass of Oncogenic KRAS Dependency in Pancreatic Cancer', Cancer Discov, 10: 1058-77.

187. Ischenko, I., S. D'Amico, M. Rao, J. Li, M. J. Hayman, S. Powers, O. Petrenko, and N. C. Reich. 2021. 'KRAS drives immune evasion in a genetic model of pancreatic cancer', Nat Commun, 12: 1482.

188. Sivakumar, S., I. de Santiago, L. Chlon, and F. Markowetz. 2017. 'Master Regulators of Oncogenic KRAS Response in Pancreatic Cancer: An Integrative Network Biology Analysis', PLoS Med, 14: e1002223.

Vita

Maria Elizabeth Monberg was born in Evanston, IL, to parents Nadina Cezara Monberg and Michael Peter Rudolf Monberg. She graduated from Mars Area High School in Mars, PA, and matriculated to the University of Michigan - Ann Arbor, in 2014. At UofM, Maria pursued dual degrees in Biology and Evolutionary Anthropology, conducting research through the Undergraduate Research Opportunities Program (studying the effects of toxicants on placental development and pregnancy outcomes) and writing senior capstone theses in Biological Anthropology (effects of temperature and exercise on bone acquisition in mammals) and Ecosystem Biology (mechanisms of carbon cycling in freshwater ecosystems). In summer 2017, Maria interned in the Translational Biomarkers Department of Merck Research Laboratories, orthotopically modeling STING agonists in murine pancreatic and breast cancers using bioluminescent reporter imaging systems. Maria received her Bachelors in Science degrees in December 2017, and joined Tempus Labs in Chicago IL as a junior data analyst of clinical oncology data, working with breast, lung, and pancreatic cancer special cases. Maria joined the University of Texas MD Anderson Cancer Center UTHealth Graduate School of Biomedical Sciences in August of 2018, formally becoming a student of Cancer Biology in January 2019.